Triplet-Triplet Energy Transfer in Organic Synthesis: Efforts toward a Chiral Lewis Acid Catalyzed De Mayo Reaction and Investigations of a Photoactive Ruthenium(polypyridyl)-NHC Complex

by

James William Pearson

A thesis submitted in partial fulfillment of the requirements for the degree of

Master of Science

Department of Chemistry

University of Alberta

Abstract

The fundamentals of energy transfer catalysis and its application in [2+2] photocycloadditions are thoroughly discussed.

The De Mayo reaction is a UV light-promoted [2+2] photocycloaddition between enolic β-diketones and olefins that has been used to form α-substituted 1,5-diketones. Its introduction has enabled the assembly of complex macrocyclic scaffolds and been used as a key step in the synthesis of natural products. To address limitations imposed by direct UV light excitation the development of a visible-light variant(s) De Mayo reaction is essential. Herein, a report detailing a co-catalyzed system deploying the low-cost organic dye 4CzIPN in combination with a Lewis acid enables [2+2] photocycloaddition between β-diketones and styrenes to occur. Attempts toward an enantioselective De Mayo reaction via a chiral Lewis acid is also reported.

In an effort to explore potential intramolecular energy transfer strategies the asymmetric imidazolium salt $[Ru(dmbpy)_2(bpip)](PF_6)_3$ (bpip = 1-benzyl-3-isopropyl-1*H*-imidazo[4,5-*f*][1,10]phenanthrolinium), was prepared by a 4-step synthetic route. The isotopomer labelled with ^{13}C at the C2 position of the bpip ligand was prepared from 1,10-phenanthroline-5,6-diamine and triethyl orthoformate-(*formyl*-^{13}C). Deprotonation of the imidazolium salt at low temperatures in acetonitrile using KO^{t}Bu and KHMDS were monitored by NMR to investigate the formation of the free N-heterocyclic carbene.

Acknowledgements

First, I would like to thank my supervisor, Prof. Steve Bergens, for his guidance and support during my degree and for providing me with interesting ideas to pursue as projects.

I would also like to thank the members of the Bergens Research Group, Dr. Riley Endean, Dr. Loorthuraja Rasu, Octavio Martinez Perez, Jinkin Lui, and Emily Majaesic for great conversations, helpful advice, and for demonstrating excellent lab stewardship towards myself.

Additional thanks goes out to all of my friends and relatives who have supported me with encouragement and kind listening for these past three years.

Finally, I would like to thank my mother, Yvonne Pearson, whose unwavering support, love and pride have ben instrumental in keeping me grounded and motivated during the most trying of times.

Table of Contents

List of Tables

Chapter 2

List of Figures

Chapter 1

Chapter 2

Chapter 3

List of Schemes

Chapter 1

Chapter 2

Chapter 3

Chapter 4

List of Symbols and Abbreviations

Ar	Aryl
Bn	Benzyl
Bpm	Bis(para-phosphophenyl)
bpy	2,2'-bipyridine
bpz	2,2'-bipyrazine
CDCB	carbozoyl dicyanobenzenes
CFL	Compact fluorescent light
CT	Charge transfer
Cz	Carbazole
DCM	Dichloromethane
DMAc	Dimethylacetamide
ddp	2,4-Diamino-4,6-Dihydroxypyrimidine
dF(CF_3)ppy	3,5-difluoro-2-[5-(trifluoromethyl)-2-pyridinyl]
dmbpy	4,4'-dimethyl-2,2'-dipyridyl
DMF	Dimethylformamide
DMSO	Dimethyl sulfoxide
dppm	Bis(diphenylphosphino)methane
dtbbpy	4,4'-di-tert-butyl-2,2’-dipyridyl
ee	Enantiomeric excess
EnT	Triplet-triplet energy transfer
E_T	Excited triplet energy
$E_{1/2}$	Half wave potential
HOMO	Highest occupied molecular orbital
ISC	Intersystem crossing
iPr	*Iso*-propyl
KHMDS	Potassium bis(trimethylsilyl)amide
LA	Lewis acid

LUMO	Lowest unoccupied molecular orbital
Mes-Acr^{+}	9-mesityl-10-methylacridinium
MLCT	Metal-to-ligand charge transfer
MV	Methyl viologen
NHC	N-Heterocyclic Carbene
OAc	Acetyloxy
OTf	Triflate
PC	Photocatalyst
Ph	Phenyl
phen	1,10-phenanthroline
ppy	2-phenylpyridine
p-Tol	Para-toluene
r.t	Room temperature
SCE	Standard calomel electrode
SET	Single electron transfer
S_0	Ground state
S_1	First excited singlet state
tBu	*Tert*-butyl
tBu-PyBox	2,6-Bis((S)-4-(tert-butyl)-4,5-dihydrooxazol-2-yl)pyridine
TBS	*Tert*-butyldimethylsilyl
TLC	Thin layer chromatography
TMS	Trimethylsilyl
Ts	Tosyl
TW	Terrawatt
T_1	First triplet excited state
4CzIPN	2,4,5,6-Tetra(9H-carbazol-9-yl)isophthalonitrile

Chapter 1: Introduction

1.1 Introduction - Why Photocatalysis?

Recently, the U.S Energy Information Administration (EIA) announced that the world's global energy consumption, 17 trillion watts (TW), is projected to rise 50% by 2050, with the growing global industrial sector as the major contributor to this increase.[1] So far, fossil fuels have served as the primary source of energy for industrial processes, accounting for 80% of the inputs.[2,3] The chemical sector represents the largest industrial energy consumer, requiring 14% and 8% of total demand for crude oil and natural gas, respectively.[4] The energy-intensive chemical processes that both consume and convert these fossil fuels into vital chemical products are responsible for 5.5% of the global anthropogenic CO_2 emissions.[5,6] Consequently, in 2016, atmospheric levels of CO_2 surpassed 400 ppm, nearly doubling the levels observed prior to the industrial revolution, and placing the earth on a 2 °C warming trajectory by 2050.[4,7] In addition to the threat of global warming, reserves of fossil fuels are in progressive decline.[8,9] To circumvent such issues, and meet the future energy demands in a sustainable manner, effort toward replacing fossil fuels with renewable and environmentally friendly energy sources is under continuous investigation.

In this context, sunlight is widely regarded as a hopeful candidate, as it represents an inexpensive, non-polluting, abundant, and endlessly renewable source of clean energy. The sun consistently provides earth with 120 000 TW of electromagnetic radiation (in the form of ultraviolet (UV), visible and infrared light). It is proposed that converting 10% of this solar energy, by covering 0.16% of earth's landmass, would amount to 20 TW of power, thereby exceeding the 14 TW of energy currently supplied by fossil fuels.[10] Thus, development of

efficient systems to harness solar energy for important chemical processes has emerged as one of the prominent focuses of the scientific community.[11-13]

The idea of connecting solar energy and environmental sustainability is not a recent epiphany of the twenty-first century. The earliest known articulation of this idea was at the 8th International Congress of Applied Chemistry in 1912 given by Italian chemist Giacomo Ciamician. Ciamician proposed that the ability to harvest solar energy could offer means for a more environmentally responsible chemical industry. Speculating that it would replace energy intensive chemical processes with clean, cost-effective, and environmentally friendly photochemical transformations[14]:

On the arid lands there will spring up industrial colonies without smoke and without smokestacks; forests of glass tubes will extend over the plains and glass buildings will rise everywhere; inside of these will take place the photochemical processes that hitherto have been guarded secret of the plants, but that will have been mastered by human industry which will know how to make them bear even more abundant fruit than nature, for nature is not in a hurry and mankind is. And if in a distant future the supply of coal becomes completely exhausted, civilization will not be checked by that, for life and civilization will continue as long as the sun shines!

Considering this long-standing vision, significant progress over the past several decades has been made toward efficient conversion of solar energy into electricity and chemical fuels,[15-18] however, the use of photochemical transformations in organic synthesis has remained relatively limited in scope.[19-22]

Conventional photochemical organic reactions (pericyclic, atom abstraction, and isomerization reactions) are typically carried out through direct excitation of organic substrates with ultraviolet (UV) light.[19] UV light is required as most organic compounds predominantly absorb photons within this region. This inherent photophysical property presents several issues that impede sustainable light-driven synthesis. Firstly, UV light only accounts for 3% of the solar radiation that penetrates the earth's atmosphere, with visible and infrared light constituting the remaining 44% and 53%, respectively.[23] Consequentially, this has slowed implementation of large-scale industrial photochemical synthesis, as specialized photoreactors are required.[20,24] In addition to the substantial cost, scale, and poor versatility of these reactors, the energy inputs required to generate UV light ultimately increases the environmental footprint of the process.[24] Moreover, similarity in energy between UV photons and C-C σ-bonds typical results in poor selectivity, and functional group tolerance.[25] Thus limiting its application toward production of important synthetic targets often bearing diverse functionalities contained within a complex scaffold.[26] If Ciamician's vision is to be realized, further development of more selective and efficient photochemical reactions is a requirement.

To address the limitations of UV excitation, there has recently been significant progress in the past decade in the area of visible-light photocatalysis.[27] The same transition metal complexes that convert sunlight into useful electrochemical potential have proven to be effective photocatalysts in unique and useful organic reactions under very mild conditions.[28,29] In general, upon photoexcitation with visible light, the photocatalyst 'activates' an organic substrate in a chemoselective manner to form a useful reactive intermediate and in turn returns the photocatalyst to its ground state, thereby closing the catalytic cycle. Ultimately, these revelations in visible-light mediated photocatalysis have enabled the discovery of a vast array of novel

transformations, previously unknown or considered impossible using traditional methods.[27] Considering the abundance of visible-light provided by the sun, these novel transformations represent promising strides toward a more sustainable chemical industry, originally envisioned by Ciamician.

1.2 Mechanisms of Photocatalysis: Electron vs Energy Transfer Catalysis

Many of the common photocatalysts employed within visible light mediated photocatalysis are polypyridyl complexes of ruthenium,[27-29] iridium,[30] and recently copper[31-33] and gold[34] (Figure 1-1). The most studied and widely employed being $Ru(bpy)_3^{2+}$ (bpy = 2,2'-bipyridine). The ability of these complexes to function as visible light photocatalysts has been the subject of intensive study within inorganic and materials chemistry. Specifically, $Ru(bpy)_3^{2+}$ and related analogues have functioned as successful photocatalysts for the splitting of water into hydrogen and oxygen,[35] and the reduction of CO_2.[36] Moreover, they have been deployed within dye-sensitized solar cells[37] and organic light-emitting diodes[38] and photodynamic therapy,[39] as well as polymerization initiators.[40]

Within the context of organic synthesis these complexes function as excellent photocatalyst for several important reasons. Firstly, these metal polypyridyl complexes absorb photons within the visible region of the electromagnetic spectrum.[41] Absorption of visible light generates a relatively long-lived excited state, for example $Ru(bpy)_3^{2+}$ exhibits an excited state lifetime of 1100 ns.[42] The long-lived excited state is critical as it enables these photocatalyst to engage in bimolecular quenching pathways with organic substrates.[43] These complexes are also easily tuneable, as modification to the polypyridyl ligand scaffold can alter their photophysical properties.[44] This is an important function as organic reactions often require precise conditions for productive activity to occur. Furthermore, the use of $Ru(bpy)_3^{2+}$ and related analogues as

photocatalysts has enabled reactions to occur under extremely mild conditions, typically at room temperature, with a commercial light source (CFL or LEDs) as an irradiation source.[26-30] This offers a significant advantage over the specialized equipment for processes that require high-energy UV light.

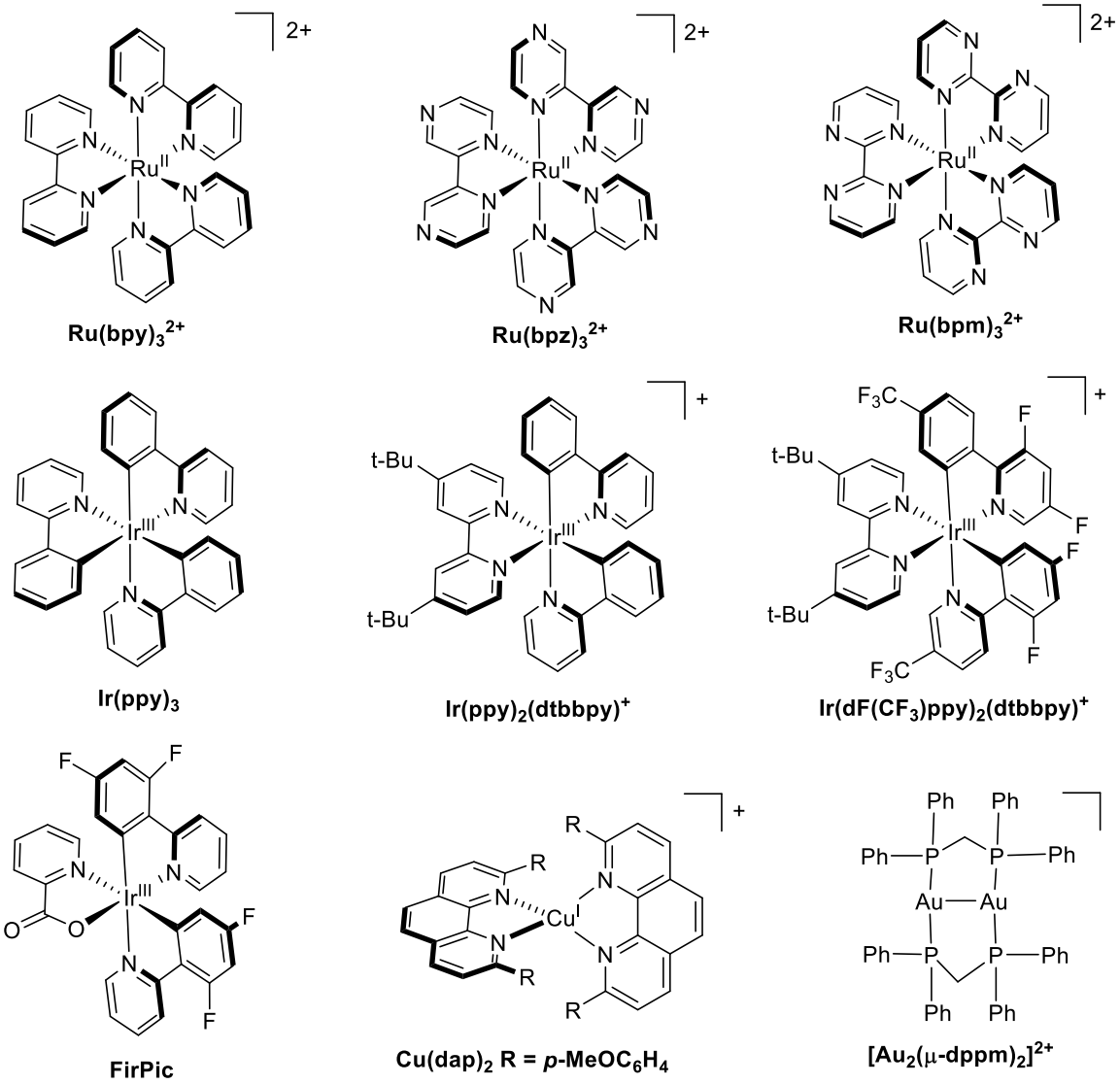

Figure 1-1. Chemical Structures of commonly used transition metal photocatalysts.

As mentioned above, visible-light-mediated photocatalysis proceeds via 'activation' of an organic substrate from an excited state photocatalyst. This 'activation' can occur through two distinct mechanisms: single electron transfer (SET) also known as photoredox and photosensitization via triplet-triplet energy transfer (EnT). Excited states of photocatalysts can

engage in either mechanism, so for the purpose of distinguishing these pathways, SET and EnT will be discussed within the context of the well-defined $Ru(bpy)_3^{2+}$ (Figure 1-2).[45]

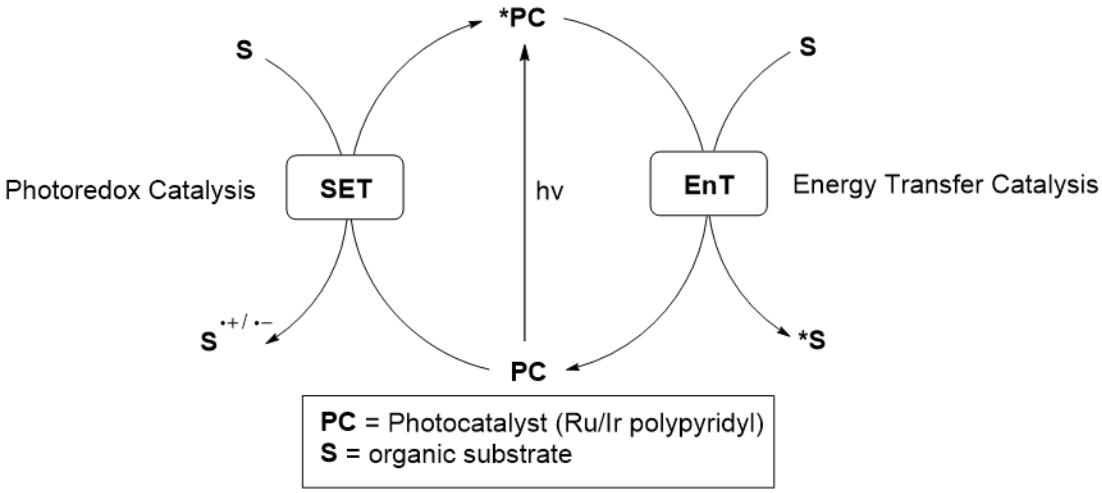

Figure 1-2. Upon irradiation with visible light, excited photocatalysts can participate in either photoredox or photosensitization via SET or EnT, respectively.

1.2.1 Photochemistry of $Ru(bpy)_3^{2+}$

Upon absorption of a photon within the visible region (~450 nm), $Ru(bpy)_3^{2+}$ undergoes metal-to-ligand charge transfer (MLCT), whereby an electron within the metal-centered t_{2g} orbitals is excited into a π* orbital of the bipyridine ligand (Figure 1-3).[41,46] This transition essentially results in an oxidized Ru(III) metal center and single-electron reduction of the ligand framework.[47] The singlet excited state (S_1) can either decay back into its ground state (S_0) (fluorescence) or it can undergo intersystem crossing (ISC) to produce the lowest-energy triplet excited state, T_1. Slow non-radiative decay and emission (phosphorescence) to return to S_0 is spin-forbidden results in a relatively long-lived T_1 excited state $*Ru(bpy)_3^{2+}$.[42] It is this long-lived T_1 species that enables $Ru(bpy)_3^{2+}$ and related complexes to engage in either SET or EnT with a suitable organic substrate.[29]

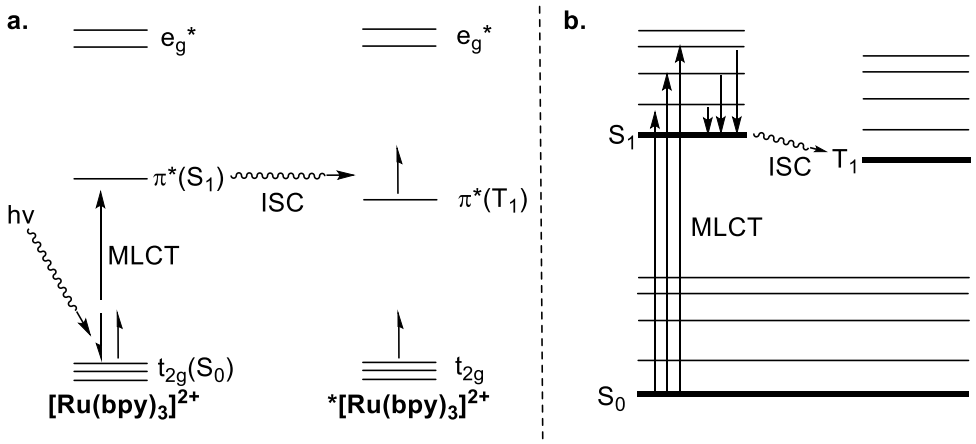

Figure 1-3. (a) MO diagram of $Ru(bpy)_3^{2+}$ photoexcitation process. (b) Simplified Jablonski diagram of $Ru(bpy)_3^{2+}$ representing MLCT as excitation from S_0 to S_1 followed by ISC to form long-lived T_1 species.

1.2.2 Single Electron Transfer

Single electron transfer from the T_1 state of the excited photocatalyst to an organic substrate hinges on the photoexcited species' ability to act as both a stronger reductant and oxidant than its ground state counterpart. This dichotomic nature is exemplified in the standard half reaction reduction potentials for $Ru(bpy)_3^{2+}$.

For example, written in the direction from the oxidized to the reduced species the half reaction $Ru(bpy)_3^{3+} + e^- \rightarrow {}^*Ru(bpy)_3^{2+}$ has a reduction potential of $E_{1/2}^{III/*II} = -0.81$ V vs the saturated calomel electrode (SCE).[48] When compared to the same half reaction reduction potential of the ground state ($E_{1/2}^{III/II} = 1.29$ V vs SCE), it is clear $^*Ru(bpy)_3^{2+}$ is a significantly more potent electron donor (reductant) than its S_0 counterpart, $Ru(bpy)_3^{2+}$. Simultaneously, the reduction potential of the excited state, $E_{1/2}^{*II/I} = 0.77$ V vs SCE ($^*Ru(bpy)_3^{2+} + e^- \rightarrow Ru(bpy)_3^{+}$), indicates that the T_1 species is also a much stronger electron acceptor (oxidant) than the ground state ($E_{1/2}^{II/I} = -1.33$ V vs SCE).[49]

The dual nature of the T_1 species, acting as both oxidant and reductant, is understood via molecular orbital diagram of *$Ru(bpy)_3^{2+}$ (Figure 1-4). As stated previously, photoexcitation of $Ru(bpy)_3^{2+}$ produces a higher-energy electron that occupies the π* orbital of the ligand framework, which can be expelled from the π* network to a suitable acceptor (**A**) when operating as a reductant (Pathway 1). At the same time, excitation produces a lower-energy hole in the t_{2g} orbital, and when serving as an oxidant (Pathway 2), this lower-energy hole can accept an electron from a suitable donor (**D**).[29] The resulting oxidized $Ru(bpy)_3^{3+}$ or reduced $Ru(bpy)_3^{+}$ species are a powerful oxidant ($E_{1/2}^{III/II}$ = 1.29 V vs SCE) and reducant ($E_{1/2}^{II/I}$ = -1.33 V vs SCE), respectively. A second SET between either $Ru(bpy)_3^{3+}$ and **D** or $Ru(bpy)_3^{+}$ and **A** restores the ground state $Ru(bpy)_3^{2+}$. These photophysical properties enable *$Ru(bpy)_3^{2+}$ to participate in either an oxidative or reductive quenching cycle (Scheme 1-1).

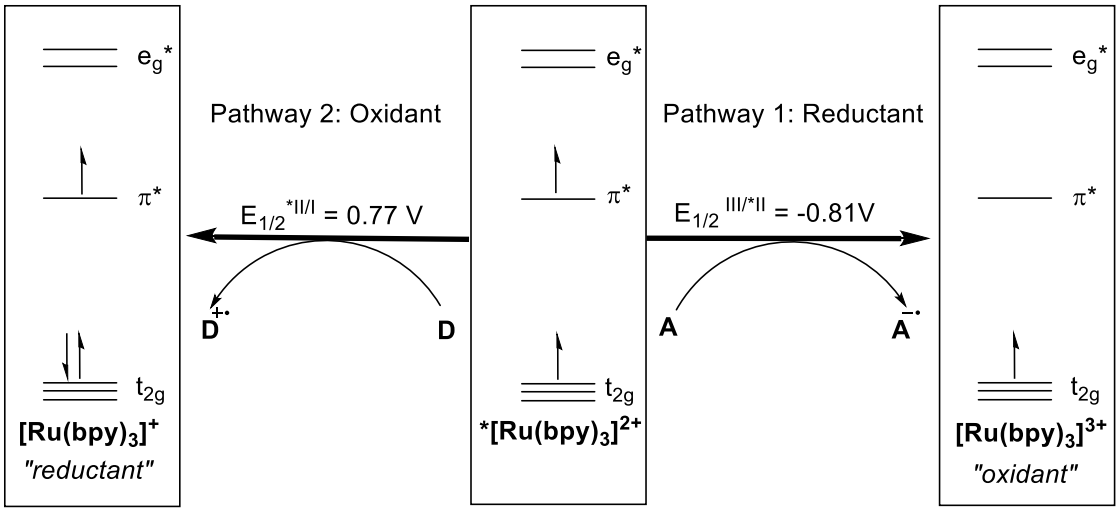

Figure 1-4. Excited redox potentials enable *$Ru(bpy)_3^{2+}$ to simultaneously act as a stronger oxidant or reductant than its ground-state.

In an oxidative quenching cycle, **A** is reduced by *$Ru(bpy)_3^{2+}$ to give the radical anion of **A** and the oxidized species $Ru(bpy)_3^{3+}$. Suitable electron acceptors , also referred to as oxidative quenchers, of *$Ru(bpy)_3^{2+}$ are viologens, polyhalomethanes, dinitro- and dicyanobenzenes, and

aryldiazonium salts.[26-30] $Ru(bpy)_3^{3+}$ accepts an electron from **D** to generate the radical cation of **D** and the catalytic cycle is completed by returning the photocatalyst to its ground-state.

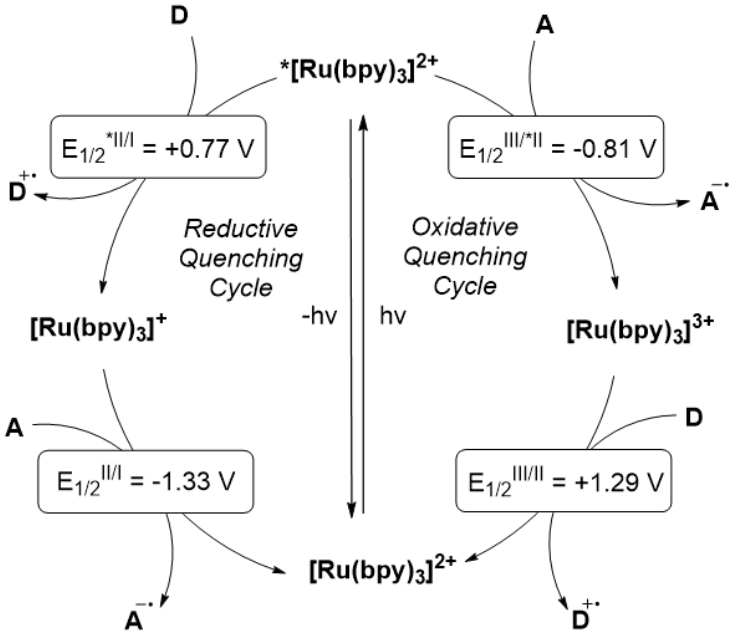

Scheme 1-1. Oxidative and Reductive quenching cycles via SET of $Ru(bpy)_3^{2+}$.

Conversely, in a reductive quenching cycle, $*Ru(bpy)_3^{2+}$ accepts an electron from **D** to generate the reduced $Ru(bpy)_3^{+}$ species. Typical reductive quenchers (electron donors) are tertiary amines.[26-30] Subsequently, $Ru(bpy)_3^{+}$ donates an electron to **A**, thereby forming the ground state $Ru(bpy)_3^{2+}$ species and closing the catalytic cycle.

Organic transformations exploiting SET is known as photoredox catalysis. In 2008, Yoon and MacMillan were first to demonstrate the use of $Ru(bpy)_3^{2+}$ as a photoredox catalyst for the [2+2] cycloaddition[26] and α-alkylation of aldehydes,[27] respectively. Since these discoveries, the field of photoredox catalysis has exploded, resulting in numerous developments of novel bond formations employing a variety of photocatalysts (Figure 1-1). More in-depth discussions of its mechanism and applications have the been the subject of several reviews.[28-30]

1.2.3 Energy Transfer

Apart from engaging in SET, the T_1 species may also participate in an energy transfer pathway EnT, also known as photosensitization. EnT is formally defined as: "the photophysical process in which an excited state of one molecular entity (the donor, D) is deactivated to a lower-lying state by transferring energy to a second molecular entity (the acceptor), which is thereby raised to a higher energy state."[50-58] By this definition, the photocatalyst operates as the donor, which upon photoexcitation transfers its triplet excited state energy to a respective organic substrate (**A**). Using $Ru(bpy)_3^{2+}$ as an example, decay of $*Ru(bpy)_3^{2+}$ from T_1 to S_0 promotes another molecule from its ground state to its lowest-energy triplet state ($S_0 \rightarrow T_1$), thereby closing the photocatalytic cycle and indirectly sensitizing the acceptor molecule (Scheme 1-2).[29,51]

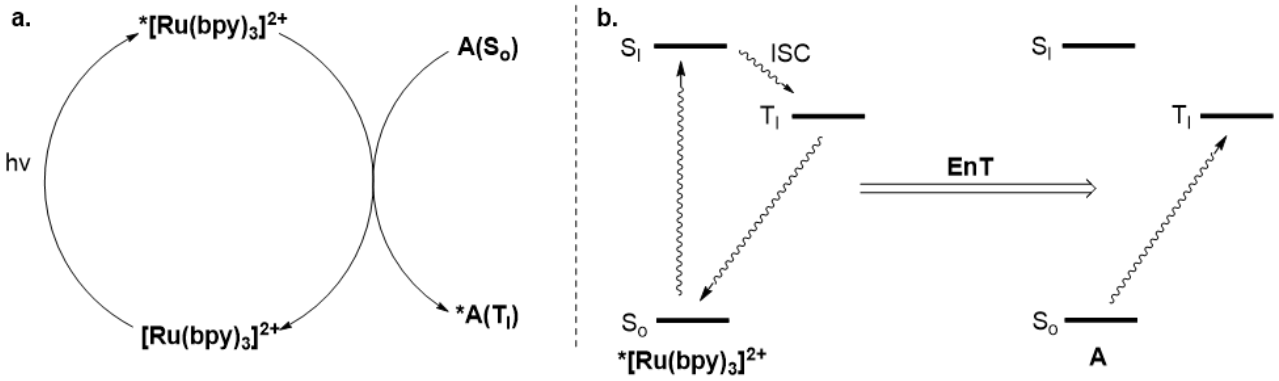

Scheme 1-2. Simplified interpretation of EnT. (a) In a catalytic cycle $*Ru(bpy)_3^{2+}$ promotes organic substrate acceptor (**A**) from ground-state to triplet-state via EnT. (b) EnT represented in Jablonski diagram depicting decay of $*Ru(bpy)_3^{2+}$ induces S_0 to T_1 transition in **A**.

Relative to photoredox catalysis, organic transformations employing EnT only account for a small number of reactions.[51,52] However, many organic molecules have redox potentials that are not accessible with current photocatalysts, and therefore cannot be activated via SET processes (oxidative or reductive quenching). EnT is not constrained by redox potentials, thereby providing access to these previously inert substrates via photosensitization to produce their more reactive triplet energy state.[52]

1.3 Fundamentals of Energy Transfer Catalysis

As stated previously, EnT catalysis proceeds via transfer of T_1 excited state energy between the photoexcited photocatalyst (the donor, **D***) and ground-state substrate (acceptor, **A**). There are two proposed mechanisms: Förster[53] and Dexter[54] energy transfer. The basis for these mechanisms are Coulombic (Förster) and exchange (Dexter) interactions found within quantum mechanics (Figure 1-5).[55] Dexter energy transfer is the predominant mechanism used to explain EnT in visible-light-mediated photocatalysis.[51,56]

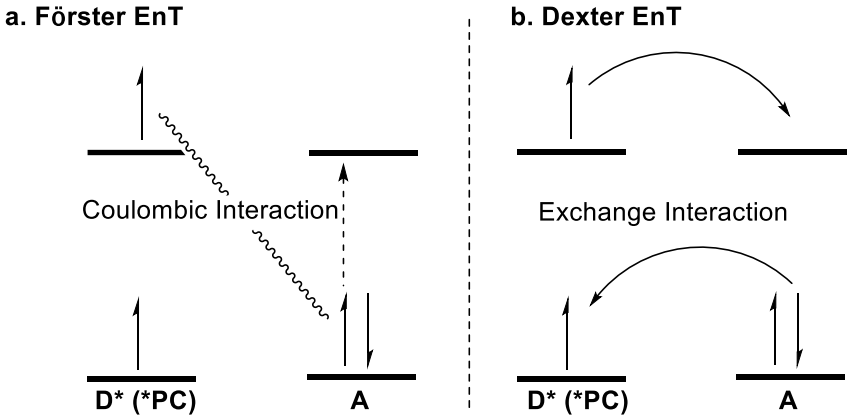

Figure 1-5. Distinguishing two mechanisms of EnT. (a) Forster EnT proceeding via Coulombic interaction. (b) Dexter EnT, **D*** and **A** undergo an exchange interaction.

1.3.1 Dexter Energy Transfer

Dexter Energy Transfer, proposed by D.L. Dexter in 1953, involves the simultaneous intermolecular exchange of excited and ground-state electrons between **D*** and **A**, respectively (Figure 1-5b).[54] In solution, intermolecular electron exchange proceeds via the sequence of events depicted in Scheme 1-3. Isolated molecules of **D*** and **A** diffuse through solution toward each other to form a solvent-caged encounter complex **[D*+A]**.[51,56] Collision within the encounter complex forms the collision complex **[D*-A]**. Orbital overlap due to collision places **D*** and **A** close enough in space for EnT to occur.[59,60] Due to the reversibility of each step in the

mechanism,[54] dissociation of the collision complex followed by subsequent diffusion of the encounter complex out of the solvent cage releases the EnT products **D** and **A***. Given that EnT depends on the lifetime of T_1, each step in the mechanism is in simultaneous competition with phosphorescence or fluorescence.[55]

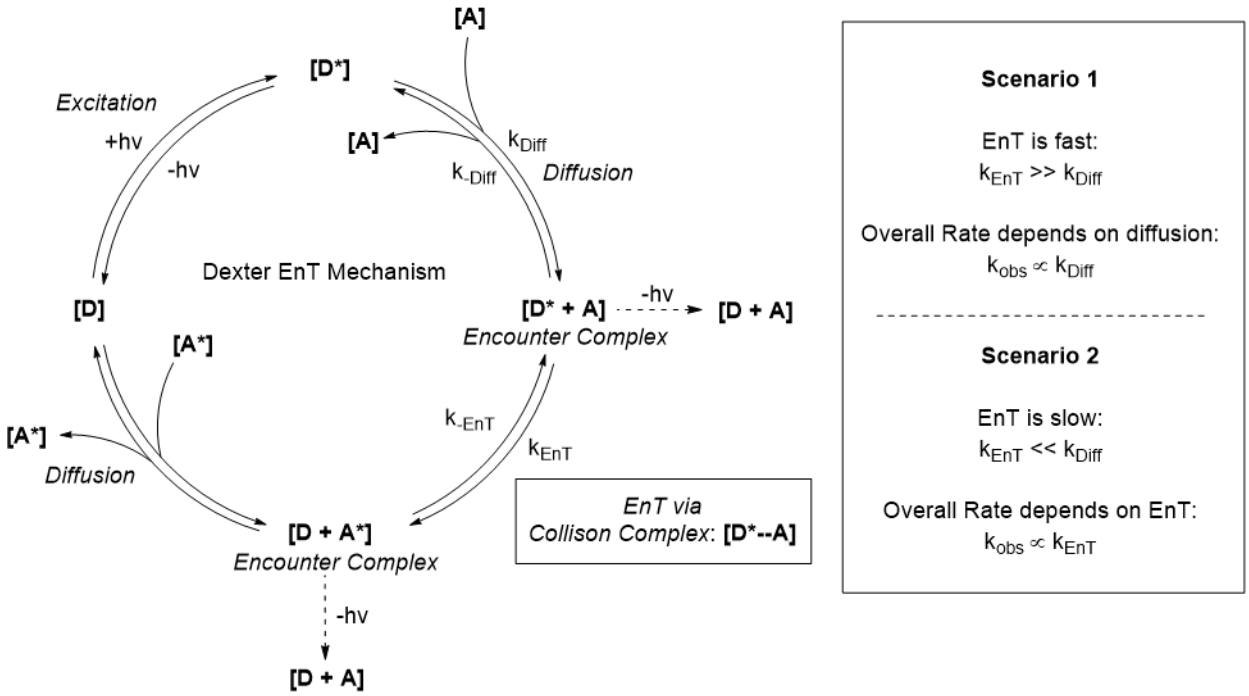

Scheme 1-3. Dexter EnT mechanism in solution. **D*** and **A** diffuse through solution and form an encounter complex. EnT between **D*** and **A** is facilitated through a collision complex. The EnT products are released by diffusion out of solvent cage. The mechanism is either controlled by rate of diffusion (k_{Diff}) or rate of EnT (k_{EnT}).

The overall rate of Dexter EnT, k_{obs}, depends on both the diffusion rate to form the encounter complex (k_{Diff}) and the rate at which EnT occurs (k_{EnT}) during the lifetime of the encounter complex.[51] This gives rise to two kinetic possibilities: (1) if $k_{EnT} >>> k_{Diff}$, then k_{obs} will be proportional to the rate of diffusion in solution, thereby dependent on solvent vicosity and temperature, or (2) if $k_{Diff} >>> k_{EnT}$, solvent effects are negligible as k_{EnT} becomes the rate-limiting step.[54,61]

The rate for EnT (k_{EnT}) can be defined by the following equation[54]:

$$k_{EnT} = K \cdot J \cdot e^{\frac{-2R_{DA}}{L}}$$

where K is the steric repulsion between the **D** and **A** in the collision complex.[62] R_{DA}/L defines the distance between **D** and **A** which indicates k_{EnT} decays exponentially as distance increases. J measures the number of T_1-S_o transitions of **D*** that can induce a coupled S_o-T_1 transition in the ground-state of **A**.[51] Simply put, J is proportional to the number of EnT events that occurs within the collision complex, and thus governs the rate of EnT.

Measuring J is often experimentally cumbersome. Instead, the difference in T_1 energies (E_T) between **D*** and **A*** ($\Delta E_T = E_T(A) - E_T(D)$) is used to predict the efficiency of EnT (Figure 1-6).[63,64] When $\Delta E_T < 0$ (exergonic EnT), J is assumed to be large, transitions to populate the acceptor's T_1 state (or higher excited states) from **D*** is highly favoured.[52] Likewise, when $\Delta E_T > 0$ (endergonic EnT), only transitions from higher energy T_1 vibrational or rotational levels of **D*** are possible.[56] Under these conditions EnT follows Botlzmann/Arrhenius-type kinetics and efficiencies diminish as ΔE_T becomes more positive.[56,62] Most Dexter EnT-mediated organic

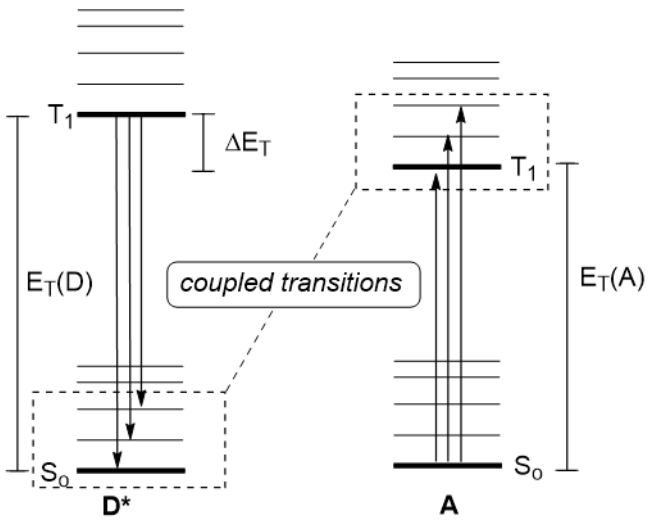

Figure 1-6. A Jablonski scheme depicting the energy gap, ΔE_T, between T_1 states of **D*** and **A**. ΔE_T serves as an approximation of the spectral overlap, J, between the two species. When $\Delta E_T < 0$, EnT is exergonic; when $\Delta E_T > 0$, EnT is endergonic.

reactions, specifically the reactions discussed in the following section, proceed under exergonic EnT conditions, whereby E_T(D) (photocatalyst) > E_T(A) (organic substrate).[51,52, 65]

To summarize, photocatalyzed organic transformations that proceed via Dexter EnT requires intimate physical contact between the excited photocatalyst (**D***) and substrate (**A**) to facilitate intermolecular exchange of excited and ground-state electrons. The efficiency of EnT (governed by J) can be approximated by the difference in E_T between photocatalyst and acceptor.

1.3.2 Experimental determination and overview of E_T

E_T can be measured through several spectroscopic techniques. The most reliable method is observation of the longest-wavelength band from phosphorescence spectra.[51] In this technique, spectra are recorded at cryogenic temperatures to ensure the spectral resolution required to accurately assign the T_1-S_o transition, thereby determining E_T.[64] Other spectral methods include singlet-triplet absorption spectra and luminescence quenching; however, these methods are often experimentally tedious and require difficult deconvolution methods to obtain E_T.[64] In cases where obtaining experimental data is difficult, DFT has become viable alternative. Despite criticism for its reliability toward excited state energies, DFT methods such as B3LYP, M06-2X in conjunction with 6-311+(2d,p) basis sets have produced accurate E_T for a series of organic molecules.[66] As a result of numerous spectroscopic investigations, a vast number of excited state energies for organic molecules and photocatalyst have been determined, summarized in Figure 1-7.[37,42, 67-69] From these E_T values shown in Figure 1-7 a direct relationship between molecules with increased π-conjugation and decreased E_T is observed, however, no obvious correlation has yet to be drawn between substituent properties and E_T.[51]

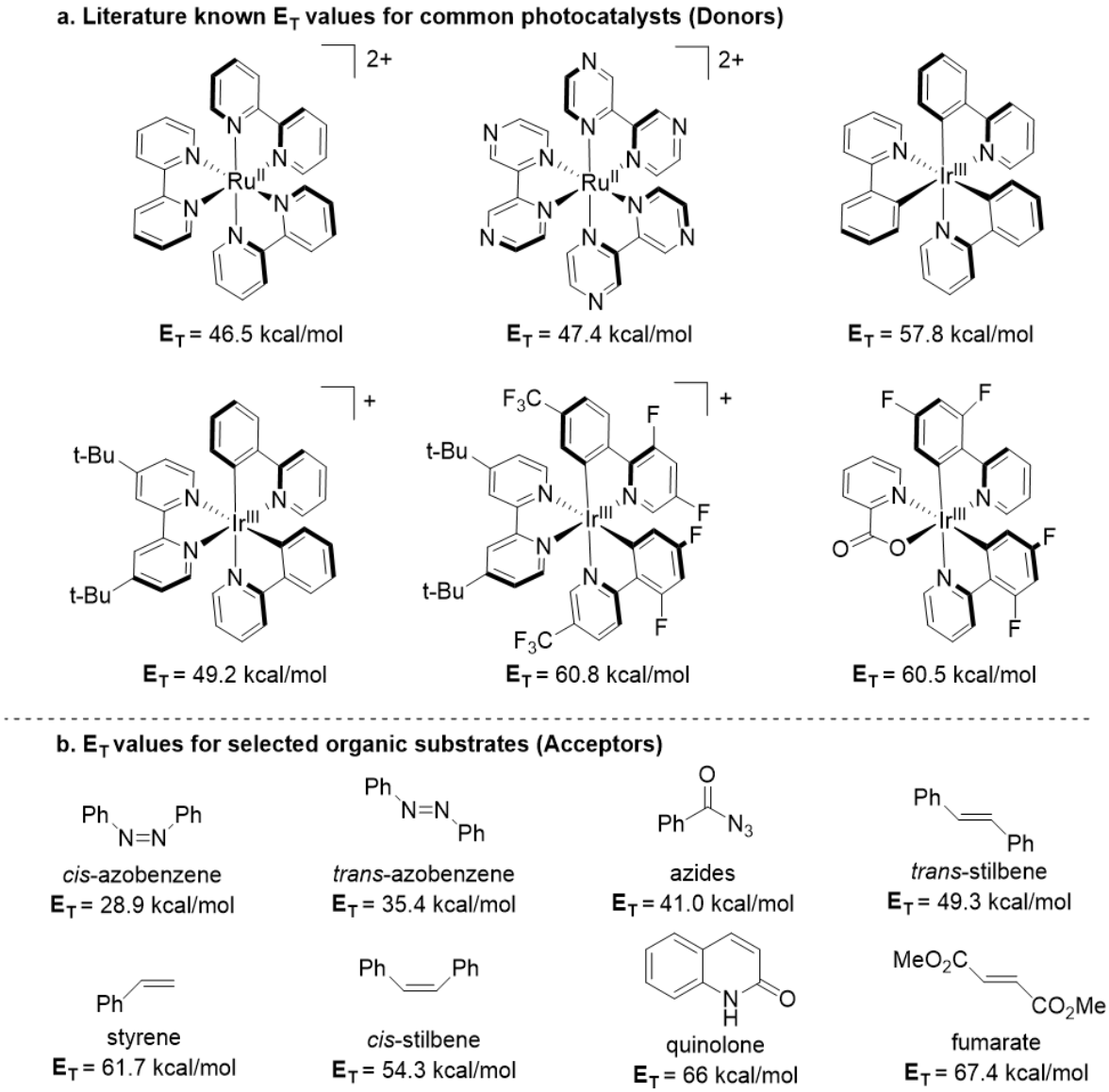

Figure 1-7. All E_T values were collected using phosphorescence spectra and are quoted relative to their respective ground state singlet energies (S_0).[51]

1.4 Applications of EnT Catalysis in Organic Synthesis

Alongside photoredox catalysis, EnT catalysis has seen significant developments in several areas of organic synthesis. Namely, areas such as cyclization reactions, photoisomerizations, bond dissociations and sensitization of metal complexes have drastically benefited. In the

interest of the work discussed in this dissertation (made clear in Section 1.5 and chapter 2), this section will highlight a few of the advances made in EnT catalysis toward [2+2] photocycloadditions. Several recent reviews provide a more in-depth discussion of EnT catalysis applications in organic synthesis.[51,52]

1.4.1 [2+2] Photocycloadditions

Cyclobutanes represent an important structural class of molecules as they are present in many biologically-active natural products. Conventional [2+2] photocycloaddition via the direct excitation of alkenes with UV light, to form their T_1 state has been a powerful tool for constructing these important motifs.[70-72] However, the use of UV light in [2+2] cycloadditions often leads to competitive side reactions, which results in poor product selectivity and hinders wider application.[25] To overcome the limitations, a suitable photocatalyst promotes an alkene, **1**, to its T_1 state via Dexter EnT (Scheme 1-4a). Promotion of the alkene to the T_1 state technically generates a relatively long-lived diradical species **1(T_1)** that can undergo addition with another ground-state alkene **2** to give the diradical intermediate **4**. Subsequent ISC of **4** and ring closure leads to the formation of the cyclobutane product **3** (Scheme 1-4b).[73-74]

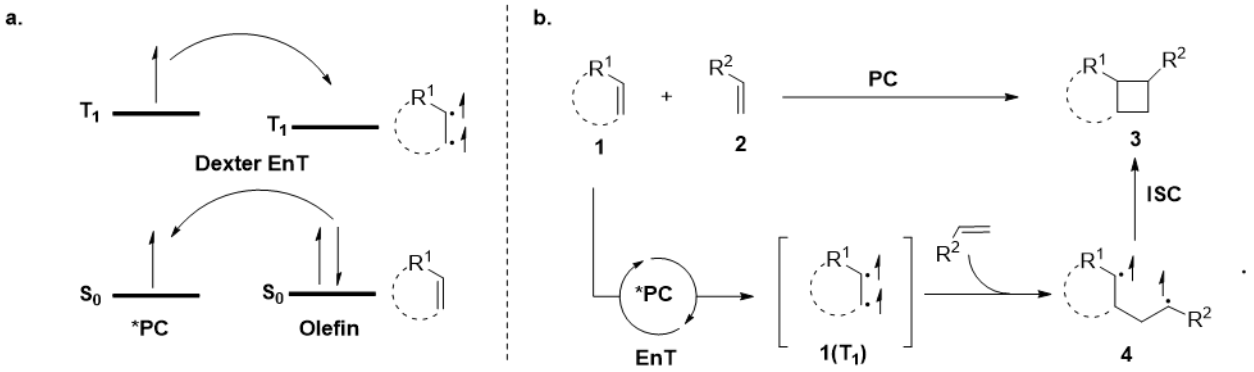

Scheme 1-4. (a) Dexter EnT between photocatalyst (PC) and olefin generates a diradical species of olefin. (b) [2+2] Photocycloaddition between olefins via Dexter EnT catalysis.

1.4.2 Racemic [2+2] Photocycloadditions

The earliest known example of EnT-mediated [2+2] photocycloaddition is the intramolecular cyclization of the substituted norbornadiene **5**. First reported by Kutal and coworkers in 1986, this pathway utilizes $[Ru(bpy)_3]Cl_2$ as the photocatalyst, which upon photoexcitation with visible light undergoes EnT with **5** to form its T_1 state (Scheme 1-5).[76] This facilitates intramolecular [2+2] cyclization to yield the corresponding quadricyclane isomer **6**. The incompatible redox potentials of **5** ($E_{1/2}^{+1/0}$ = 1.82 V vs SCE, $E_{1/2}^{0/-1}$ = -1.39 V vs SCE) with the photocatalyst indicates that this transformation cannot proceed via an oxidative or reductive SET mechanism. Additionally, successful formation of **6** by direct excitation with UV light further corroborates that this reaction transpires via the excited state of **5**; therefore, supporting the claim of an EnT mechanism between $[Ru(bpy)_3]Cl_2$ and **5**.[29,76]

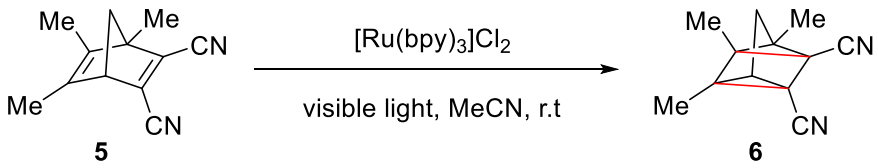

5 **6**

Scheme 1-5. First example of EnT catalysis. Intramolecular [2+2] photocycloaddition of norbornadiene.

One of the first major advances in visible-light-mediated catalysis was accomplished by Yoon and co-workers, who demonstrated an EnT pathway for the intramolecular [2+2] photocycloaddition of dienes **7** (Scheme 1-6).[77] Previous efforts from this group utilized a SET mechanism to accomplish this reaction, but was limited to electron-rich styrene deriatives.[78] Given that the E_T of unsubstituted styrenes is approximately 55 - 60 kcal/mol, $[Ir(dF(CF_3)ppy)_2(dtbbpy)](PF_6)$ (**[Ir]**, E_T = 61.8 kcal/mol) was required to initiate an exergonic EnT with electron-neutral and -deficient styrene derivatives to form the diradical intermediates **7(T_1)**.[77] These diradicals subsequently undergo [2+2] intramolecular cyclization to produce cyclobutane products **8** in high yields with excellent regio- and diastereoselectivity. A SET is

ruled out on the basis that the Ir catalyst ($E_{1/2}^{*III/II}$ = 1.21 vs SCE) is not a strong enough oxidant to remove electrons from **7** ($E_{1/2}^{red}$ = 1.42 V vs SCE).[69,77] In addition, the more oxidizing photocatalysts $Ru(bpy)_3^{2+}$ and $Ru(bpz)_3^{2+}$ possessing lower E_T (46.8 kcal/mol and 47.4 kcal/mol, respectively)[43] could not catalyze the transformation, which further supports the proposed EnT mechanism. Cyclization of electron-deficient styrene **9** demonstrates orthogonal reactivity capabilities of EnT pathways. Under a SET pathway the resulting [4+2] product **11** is formed, however, EnT from $[Ir(dF(CF_3)ppy)_2(dtbbpy)](PF_6)$ exclusively forms the [2+2] cyclobutane product **10**.

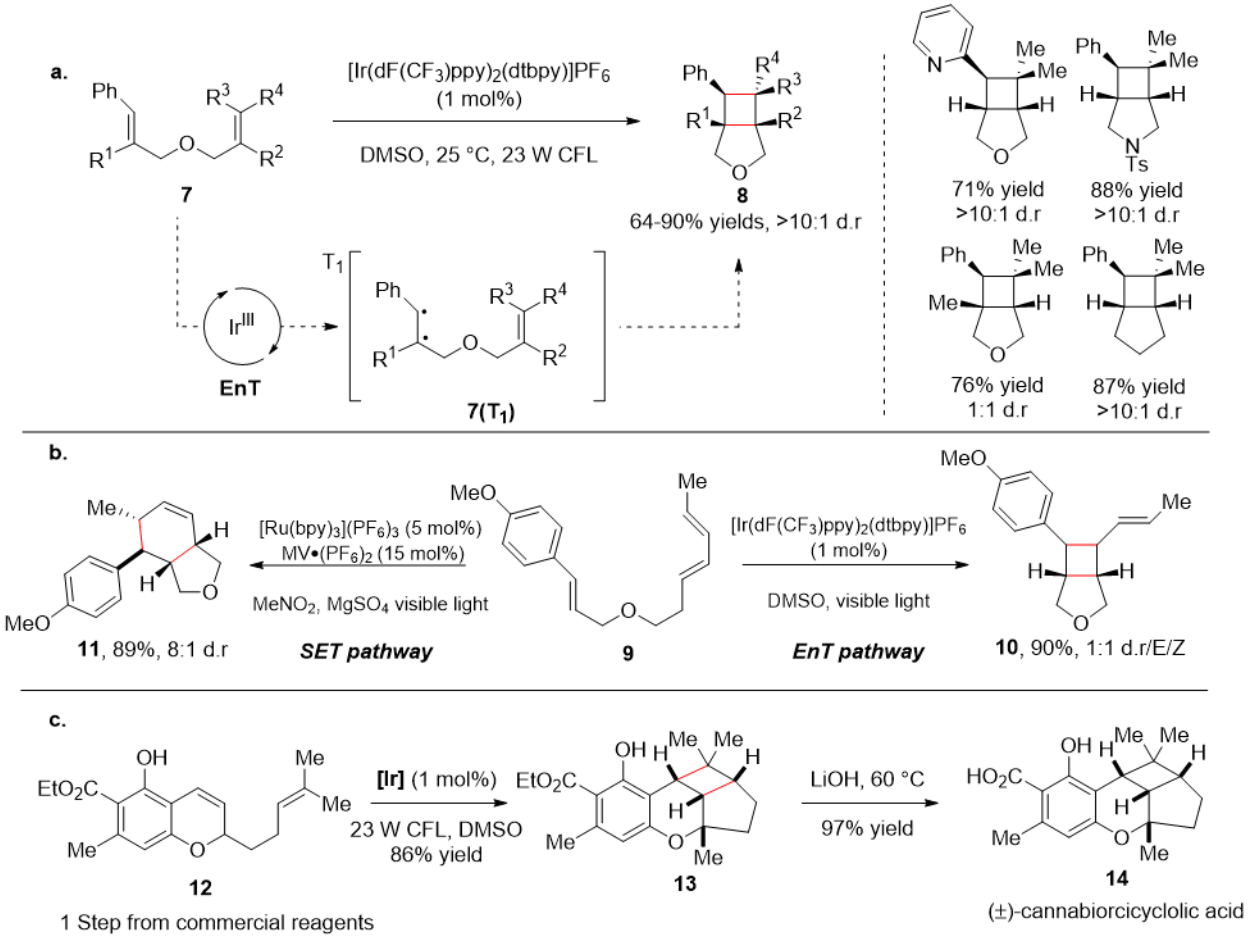

Scheme 1-6. (a) Intramolecular [2+2] photocycloaddition of styrenes by EnT process. (b) Orthogonal reaction pathways available by employing SET or EnT conditions. (c) EnT in natural product synthesis.

Apart from improved functional-group tolerance and substrate diversity, the synthetic utility of this methodology was elegantly demonstrated in a three-step synthesis of (±)-cannabiorcicyclolic acid **14**.[77]

The work conducted by Yoon stands as a landmark achievement in EnT catalysis enabling discovery of analogous and novel [2+2] photocycloadditions. In 2012, Cibulka and coworkers reported that similar [2+2] transformations could be efficiently achieved (10 minutes) under metal-free conditions by employing flavin derivatives as an organic photocatalyst.[79,80] Yoon and coworkers extended this methodology beyond styrenes to 1,3-dienes **15**, whereby under similar conditions these substrates underwent intramolecular [2+2] photocycloadditions (Scheme 1-7).[81] The authors were able to employ this extension as a key step in the synthesis of the natural product (±)-epiraikovenal.

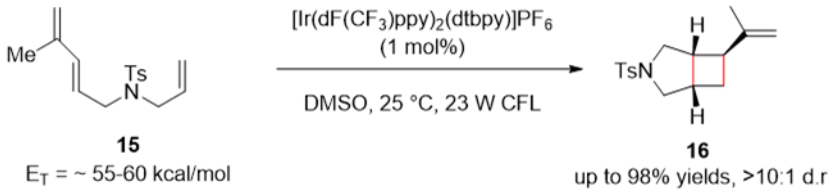

Scheme 1-7. Intramolecular [2+2] photocycloaddition of 1,3-dienes.

The previously mentioned studies highlight the versatility of EnT mediated intramolecular [2+2] photocycloaddition of dienes, however, efforts toward intermolecular [2+2] photocycloaddition of acyclic dienes proved more challenging.[52] In a similar fashion to the intramolecular [2+2] EnT strategies, Wu and coworkers were the first to report an intermolecular process that enabled the highly diastereoselective [2+2] photodimerization of chalcones and cinnamic acid derivatives **15** (Scheme 1-8).[82] Experimental investigations concluded that the photocatalyst, $Ir(ppy)_3$, was engaged in an exergonic EnT mechanism with the chosen substrates. Analogously to intramolecular cycloaddition, the photoexcited $Ir(ppy)_3$ catalyst transfers its T_1

energy (E_T = 57.9 kcal/mol) to ground state **17** (E_T = 49.2 kcal/mol) to yield the T_1 diradical **17(T_1)**. Upon generation, **17(T_1)** couples with **17** to form a 1,4-diradical species **18**, which after ISC rapidly forms the cyclobutane product **19** with high diastereoselective yields.

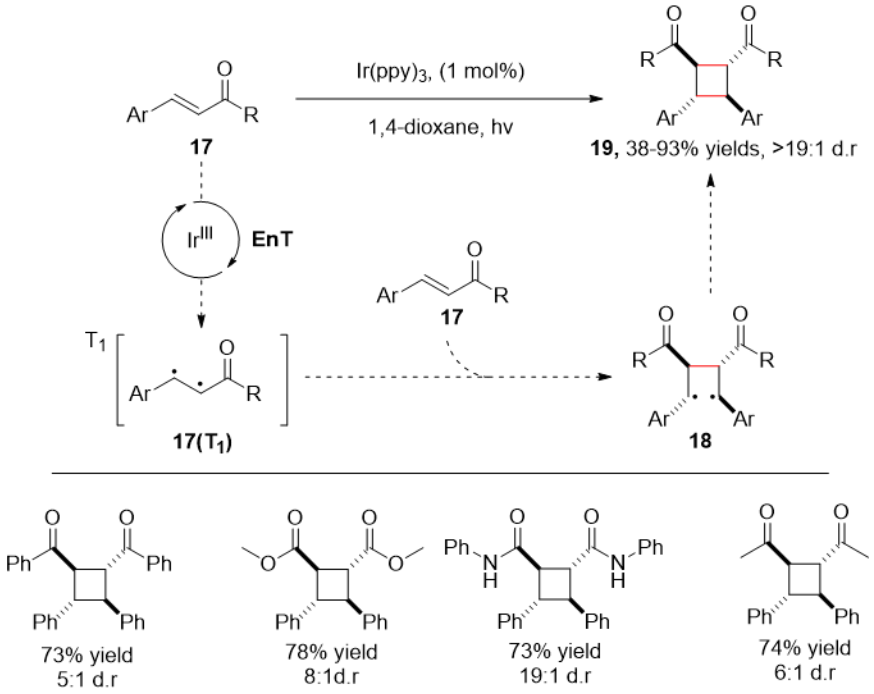

Scheme 1-8. EnT mediated [2+2] photodimerization of chalcones.

Building on the previous discovery, Wang and Lu also reported the intermolecular [2+2] photocyclization of 1,4-dihydropyridines with olefins to construct polysubstituted 2-azabicyclo[4.2.0]octanes **22** (Scheme 1-9).[83]

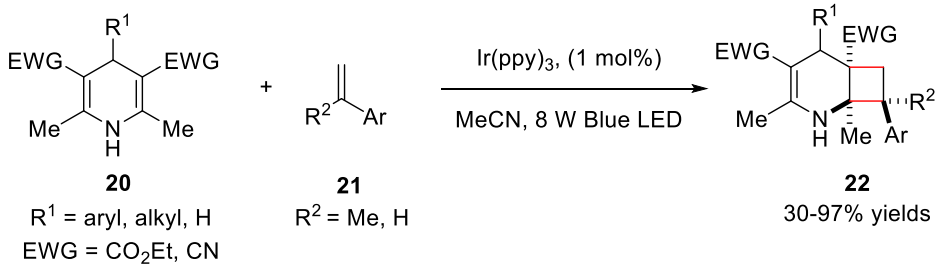

Scheme 1-9. 1,4-Dihydropyridens and olefins undergo [2+2] cycloaddiation via EnT process.

1.4.3 Asymmetric [2+2] Photocycloadditions

The previous examples demonstrate that EnT mediated [2+2] photocycloadditions can be used to produce cyclobutanes with good diastereoselectivity. Asymmetric [2+2] photocycloadditions remains an area with rich synthetic potential.[51] In a recent landmark study, Yoon and coworkers disclosed an asymmetric EnT visible-light-mediated process that promoted enantioselective intermolecular [2+2] photocycloaddition of 2'-hydroxychalcones (**23**) with styrenic olefins and dienes (**24**) via a chiral Lewis acid catalyst (Scheme 1-10).[84,85] The report demonstrates that coordination of **23** with a chiral scandium catalyst (**[Sc]**, generated *in-situ*) to form chiral complex **26**. Formation of **26** dramatically lowers the E_T (33 kcal/mol) when compared to uncoordinated **23** (54 kcal/mol).

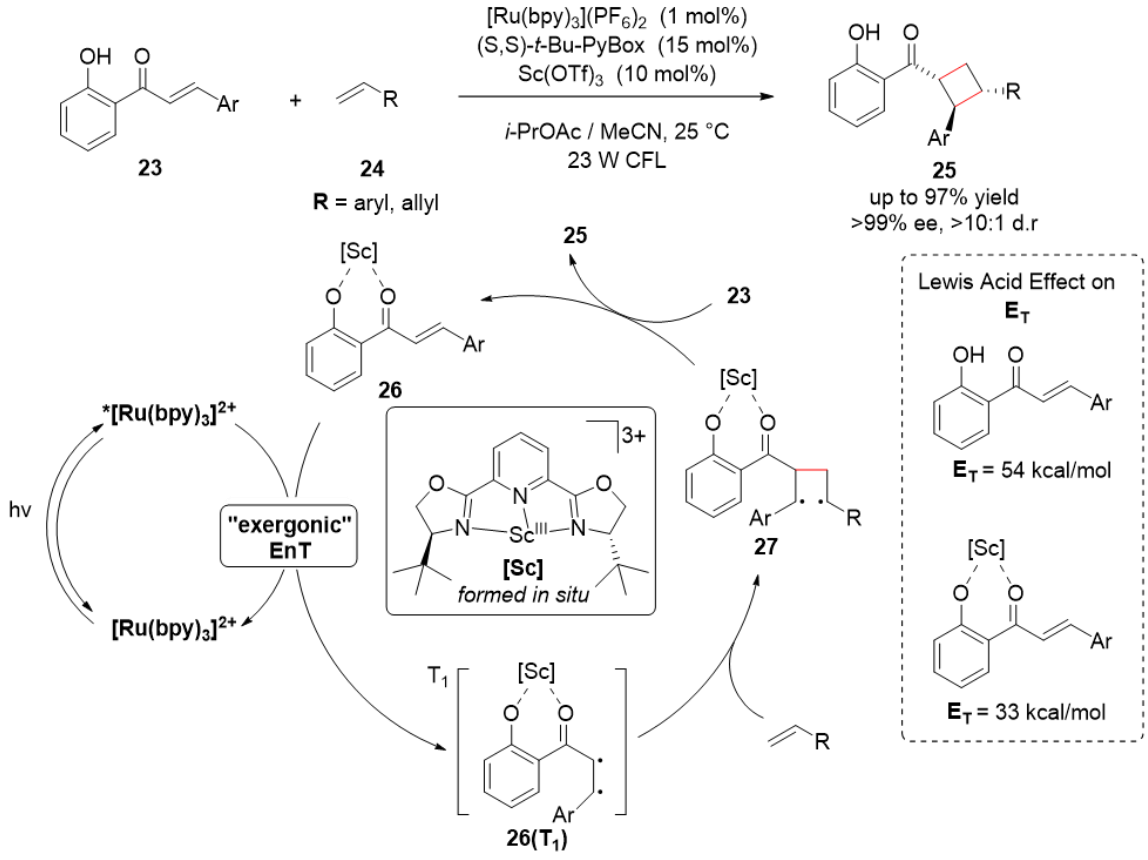

Scheme 1-10. EnT promoted enantioselective [2+2] photocycloaddition between 2'-hydroxychalcones and styrenes mediated by a chiral Lewis acid catalyst.

As a result, **26**, can undergo selective exergonic EnT with the photocatalyst $[Ru(bpy)_3](PF_6)_3$ (46.9 kcal/mol), thereby generating the chiral T_1 diradical intermediate **26(T_1)**. **26(T_1)** undergoes addition with **24** to form the benzylic-allylic 1,4-diradical **27**, which further cyclizes to afford chiral [2+2] vinyl cyclobutane products **25** with good yields and high enantioselectivity.

Meggers and coworkers developed a novel visible-light induced [2+2] photocycloaddition using a chiral rhodium complex **[Rh]** serving as both Lewis acid and photocatalyst to achieve high enantioselectivities (Scheme 1-11).[86] The authors' proposed EnT

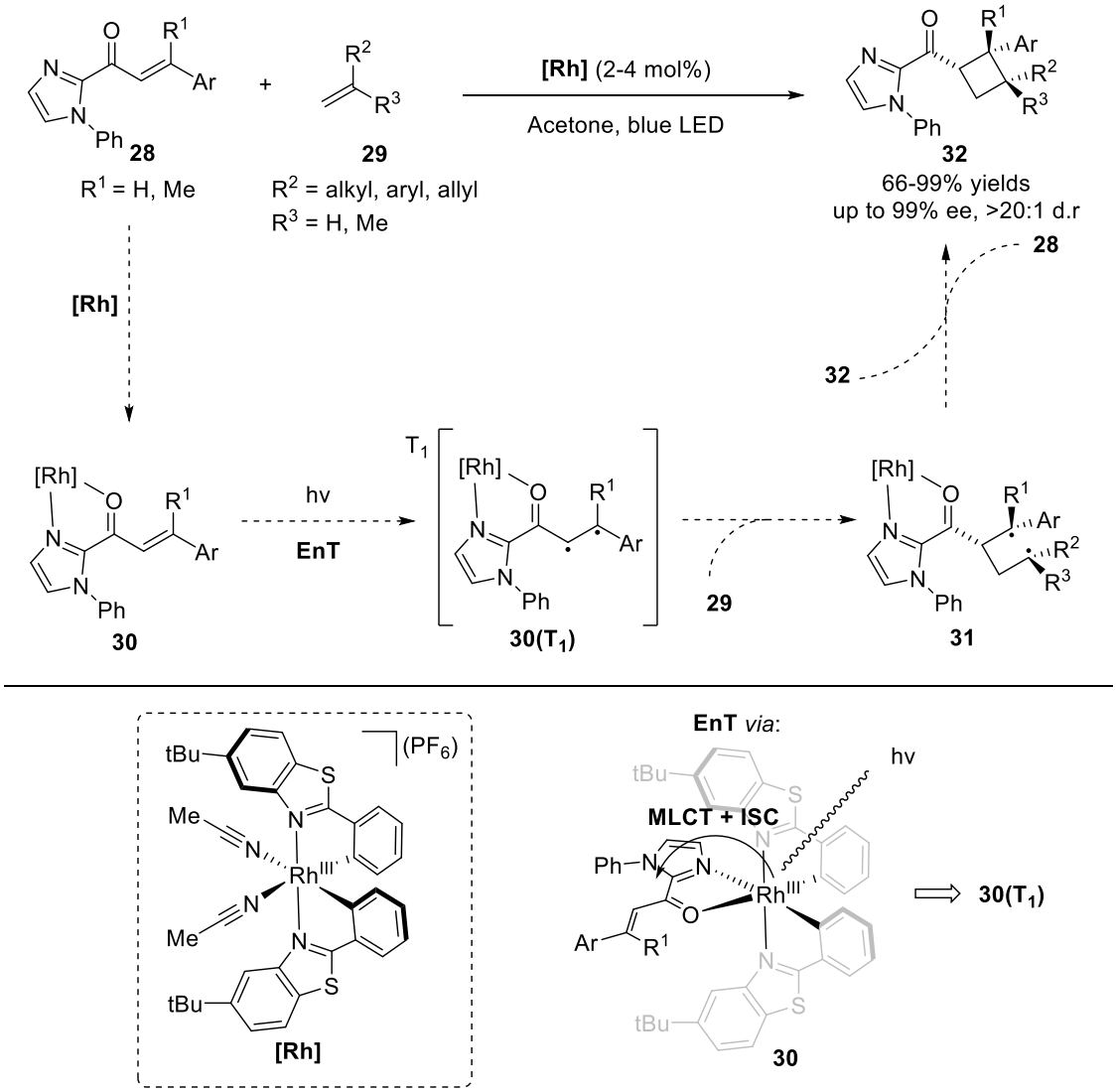

Scheme 1-11. [2+2] photocycloaddition via direct visible-light excitation of a chiral Rh Lewis acid-substrate complex.

proceeds in an intramolecular fashion via coordination of **28** with the chiral rhodium catalyst to form the chiral complex **30**, which upon photoexcitation (MLCT) followed by subsequent ISC gives rise to **30(T_1)**. This T_1 intermediate then undergoes [2+2] photocycloaddition with an α-substituted styrene **29** to generate the desired product **32**. Under control of the chiral environment, induced by the Rh catalyst, production of several cyclobutanes containing multiple stereogenic quaternary centers were obtained in a highly enantioselective manner.

In 2013, early investigations, by Bach an coworkers, reported a chiral oxazaborolidine complex capable of serving as a Lewis acid to induce the enantioselective intramolecular [2+2] photocycloaddition of enones by UV light.[87] Building on this preliminary study, Bach and coworkers successfully synthesized and applied a novel chiral thioxanthone (**PC-I**) in the visible-light EnT-mediated enantioselective intramolecular [2+2] photocycloaddition of various quinolone substrates **33** (Scheme 1-12).[88] In this approach a chiral hydrogen-bonded coordination complex **34** is formed between **PC-I** and **33**. Irradiation of this chiral coordination complex facilitates exergonic EnT from the thioxanthone (E_T = 74.1 kcal/mol) to the quinolone

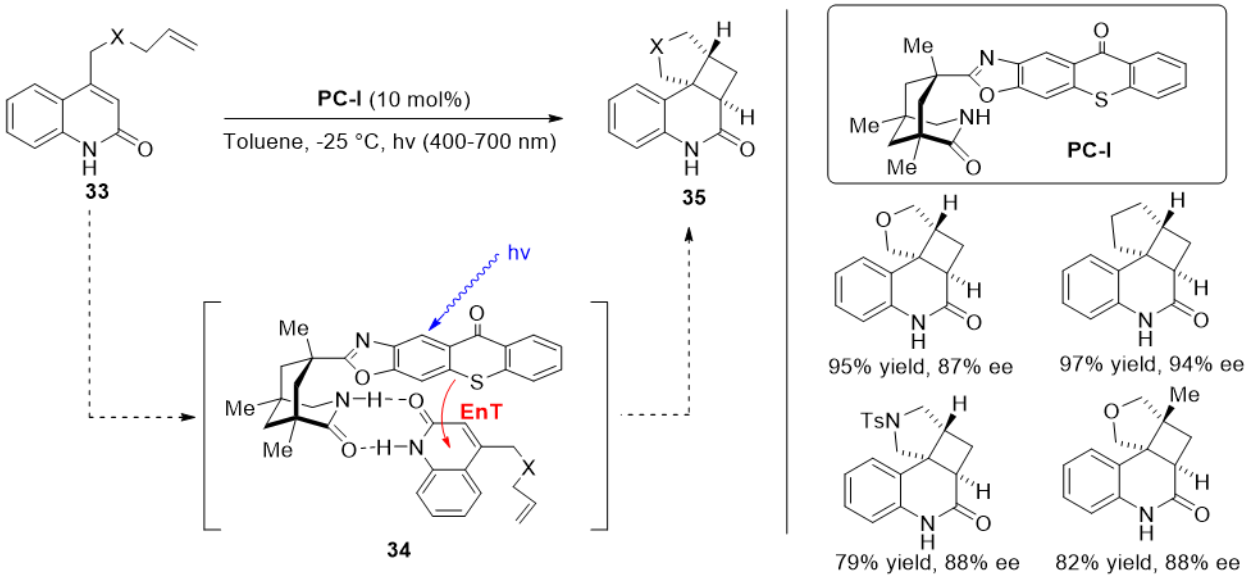

Scheme 1-12. Enantioselective intramolecular [2+2] photocycloaddition induced by a hydrogen-bonded chiral thioxanthone-substrate complex.

substrate (E_T = 66 kcal/mol). In turn, the resultant T_1 quinolone undergoes intramolecular [2+2] photocycloaddition on the opposite face, guided by the chiral environment of **34**, with a tethered alkene to generate the desired chiral cyclobutane product **35** in high enantioselectivity.

Subsequent investigations by the same group extended this approach to enantioselective intermolecular [2+2] photocycloaddition of quinolones with several substituted alkenes (Scheme 1-13).[89]

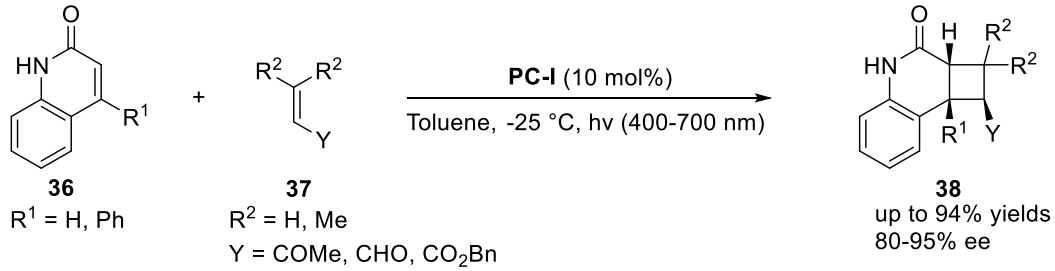

36
R^1 = H, Ph

37
R^2 = H, Me
Y = COMe, CHO, CO_2Bn

38
up to 94% yields
80-95% ee

Scheme 1-13. Extension of chiral thioxanthone photocatalyst to intermolecular [2+2] photocycloaddition.

Furthermore, Baik, Yoon and coworkers developed a similar strategy employing a chiral hydrogen-bonding iridium photocatalyst to promote analogous enantioselective [2+2] EnT reactions.[90] It is important to note that these reactions could also be carried out under direct sunlight while still maintaining high enantioselectivity.

1.5 Research Proposal

The previously outlined applications of visible-light-mediated EnT photocatalysis represent significant developments toward greener and more sustainable chemical processes, however, EnT photocatalysis predominantly relies on expensive and toxic transition-metal Ru- and Ir-polypyridyl photocatalysts.[26-30] To circumvent reliance on these precious metals many studies have been launched into developing more earth-abundant Cu, Cr, and Fe photocatalysts.[30,91,92] Conversely, the economical cost, ease of availability, and low toxicity of organic dyes offers an intriguing alternative to its transition metal counterparts for large-scale chemical production.[93] Common organic dyes such as Eosin Y, 9-mesityl-10-methylacridium (Mes-Acr^+), and others

have also been identified as productive photoredox catalysts due to their analogous photophysical and electrochemical properties to transition metal counterparts (Figure 1-8). Their photophysical properties and application to photoredox catalysis has been the subject of recent reviews.[94,95] Despite these advances, synthetic application of organic dyes is often limited by their challenging synthesis and subsequent derivatization.[96]

1.5.1 Structural and Photophysical Properties of 4CzIPN

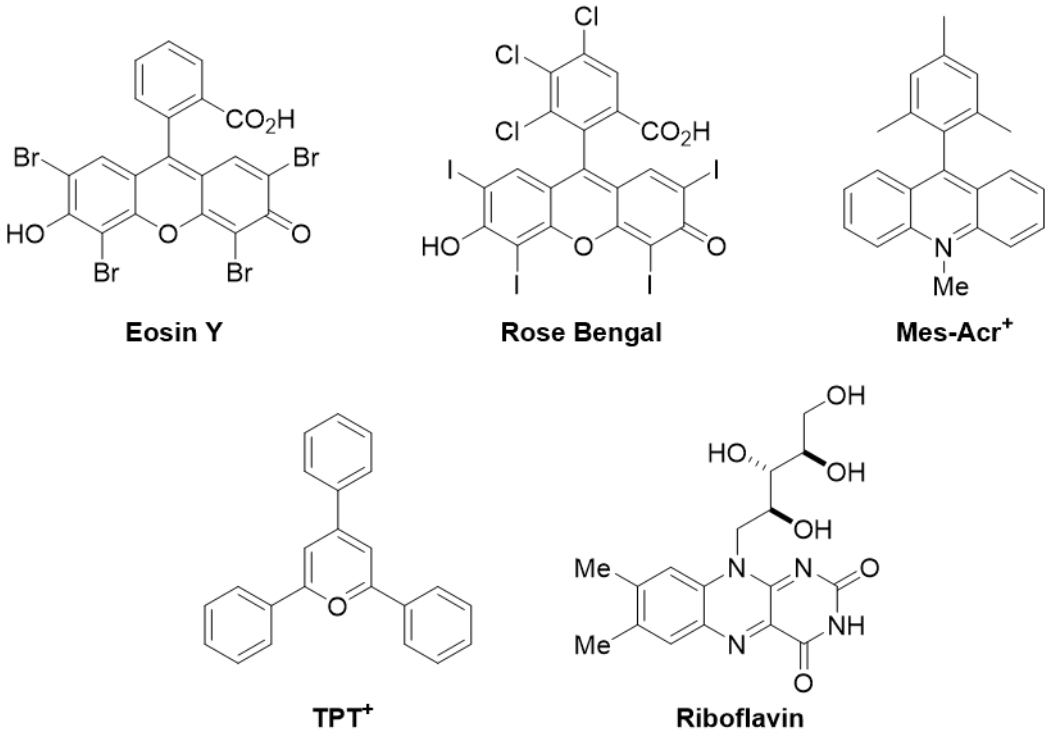

Figure 1-8. Chemical structures of common organic dyes used in photocatalysis.

To this end, recent developments of donor-acceptor (D-A) fluorophores such as carbozoyl dicyanobenzenes (CDCBs) offers a highly versatile low-cost framework capable of rapid derivatization.[97,98] The most notable and promising of these CDCBs for use in photocatalysis is 1,2,3,5-tetrakis(carbazole-9-yl)-4,6-dicyanobenzene (4CzIPN).[98] Computational modelling indicates that the HOMO and LUMO of 4CzIPN are localized on the electron-donor carbazolyl moiety (Cz) and electron-acceptor dicyanobenzene moiety,

respectively. Thereby, in a similar fashion to MLCT of Ru- and Ir-polypyridyl complexes, charge transfer (CT) occurs between the Cz and dicyanobeneze moieties upon photoexcitation with visible light to generate S_1, which then undergoes rapid ISC to generate the long-lived T_1 (5.1 μs) of 4CzIPN (Scheme 1-14a).[99,100]

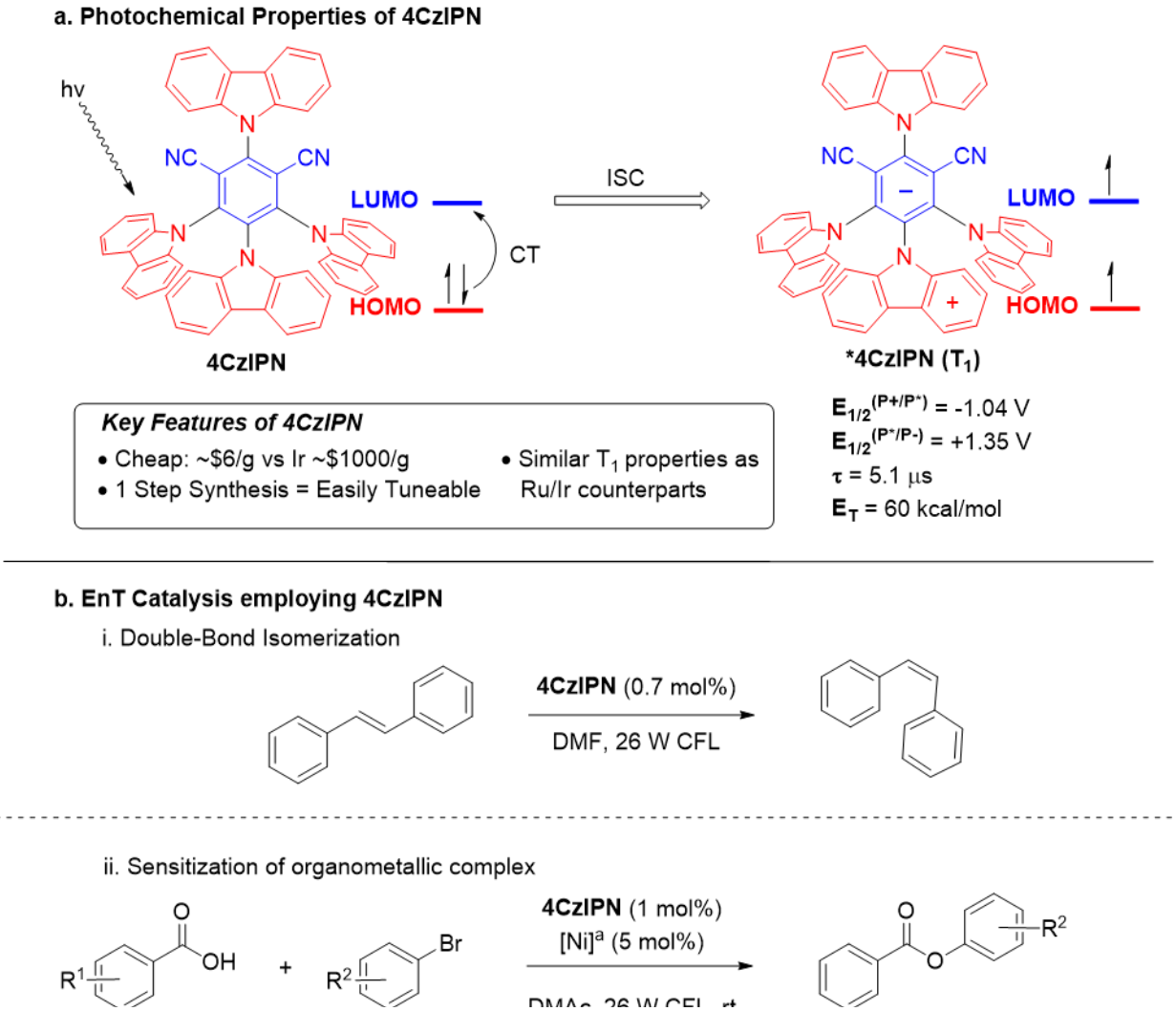

Scheme 1-14. (a) Photochemical properties of 4CzIPN. (b) Only examples of EnT processes employing 4CzIPN as photocatalyst. [a][Ni] = [$Ni(NO_3)_2 \cdot 6H_2O$ (5 mol%), dtbbpy (5 mol%)].[99]

The lifetime and redox potentials of *4CzIPN is analogous to Ru- and Ir-photocatalysts.[29] Specifically, E_T (60 kcal/mol) of 4CzIPN is strikingly similar to the commonly used photocatalyst [Ir(dF(CF_3)ppy)$_2$(dtbbpy)](PF_6) (60.8 kcal/mol).[101] The localized HOMO and LUMO of 4CzIPN enables specific fine-tuning of each orbital through facile modifications to the acceptor and donor moieties. This ultimately provides 4CzIPN and CDCBs alike with customizable photophysical and electrochemical properties to meet specific photocatalysis requirements.[100] As a result of these remarkable properties, 4CzIPN is becoming a desirable 'metal-free' alternative in many photoredox transformations, which has been the subject of recent reviews.[97] Application of 4CzIPN in EnT catalysis, however, has only been utilized in the isomerization of stilbenes and the sensitization of a Ni complex; both reported by Zhang in 2018 (Scheme 1-14b).[99]

1.5.2 The De Mayo Reaction

In 1962, Paul Jose De Mayo reported the UV light promoted reaction between β-diketones and olefins to form 1,5-diketones (Scheme 1-15a).[101] Deemed the De Mayo reaction, its introduction has enabled the assembly of complex macrocyclic scaffolds. Most notably, the De Mayo reaction has been used as a key step in the synthesis of the natural products (±)-ingenol and vindorosine (Scheme 1-15b).[102,103] In general, tautomerization of **39** to enol **41** is followed by excitation of **41** to its S_1 state by direct UV irradiation. After ISC to **(41)T$_1$**, addition with an alkene (**40**) generates a 1,4-biradical **42**, which cyclizes to form an unstable cyclobutanol intermediate **43**. Subsequent retro-aldol condensation of **43** forms the desired 1,5-diketone product **44**.

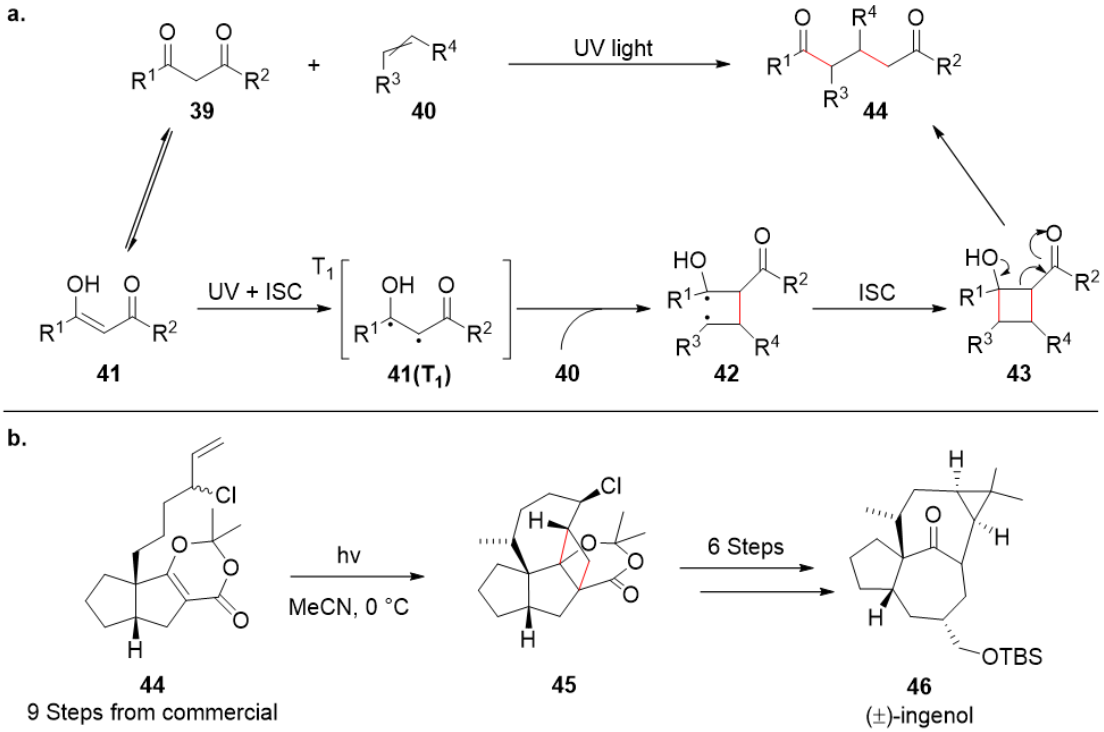

Scheme 1-15. (a) De Mayo reaction mechanism mediated by direct UV light sensitization. (b) Application of the De Mayo reaction in natural product synthesis.

Considering the recent developments of visible-light-mediated EnT, the De Mayo reaction represents a logical extension of the aforementioned methodology in Section 1.4. In 2018, König and coworkers made this connection and disclosed a visible-light EnT version of the De Mayo reaction (Scheme 1-16).[104] The authors demonstrated that the photocatalyst [Ir(dF(CF$_3$)ppy)$_2$(bpy)](PF$_6$) (E_T = 62 kcal/mol) could successfully undergo exergonic EnT with enolic 1,3-diketones **47** to enable [2+2] addition and subsequent retro-aldol condensation with substituted styrenes **48** to afford the desired 1,5-diketone product **49**. Moreover, they showed that this methodology was effective toward β-ketoesters, β-amido esters, and β-cyano ketones along with aryl- and alkyl-substituted ketones.

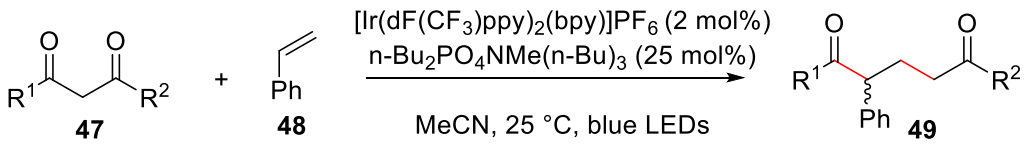

Scheme 1-16. Extension of EnT photocatalysis to the De Mayo reaction.

König detailed an elegant extension of modern photocatalysis to conventional methods, however, it exposed two key shortcomings. Firstly, the authors observed poor reactivity when screening the reaction with 4CzIPN. This was rationalized by the incompatible E_T values between 4CzIPN (60 kcal/mol) and the 1,3-diketones (~60 kcal/mol) to facilitate exergonic EnT. Secondly, several 1,5-diketones with multiple stereocenters were produced in good diastereoselective ratios, however, no enantioselectivity was induced or attempted.

1.5.3 Proposal

We propose that by adapting protocols outlined by Yoon (section 1.4.3) an asymmetric visible-light-mediated EnT version of the De Mayo reaction is feasible (Scheme 1-17).[84] We envision that coordination of enolic 1,3-diketone **50** to a chiral Lewis acid (**[LA]**) could (1) form a lower E_T coordination complex **51** to enable exergonic EnT from 4CzIPN, and (2) induce chirality within the cyclobutanol intermediate **53** to generate the α-arylated 1,5-diketone product **49** enatioselectively. Success on both fronts would ultimately further application of cost effective organic photocatalysts toward more challenging enantioselective bond formations.

The following chapters will discuss our progress made toward this proposal (Chapter 2) as well as highlight our published work toward designing a photoactive bridging ligand for use in intramolecular EnT processes (Chapter 3).

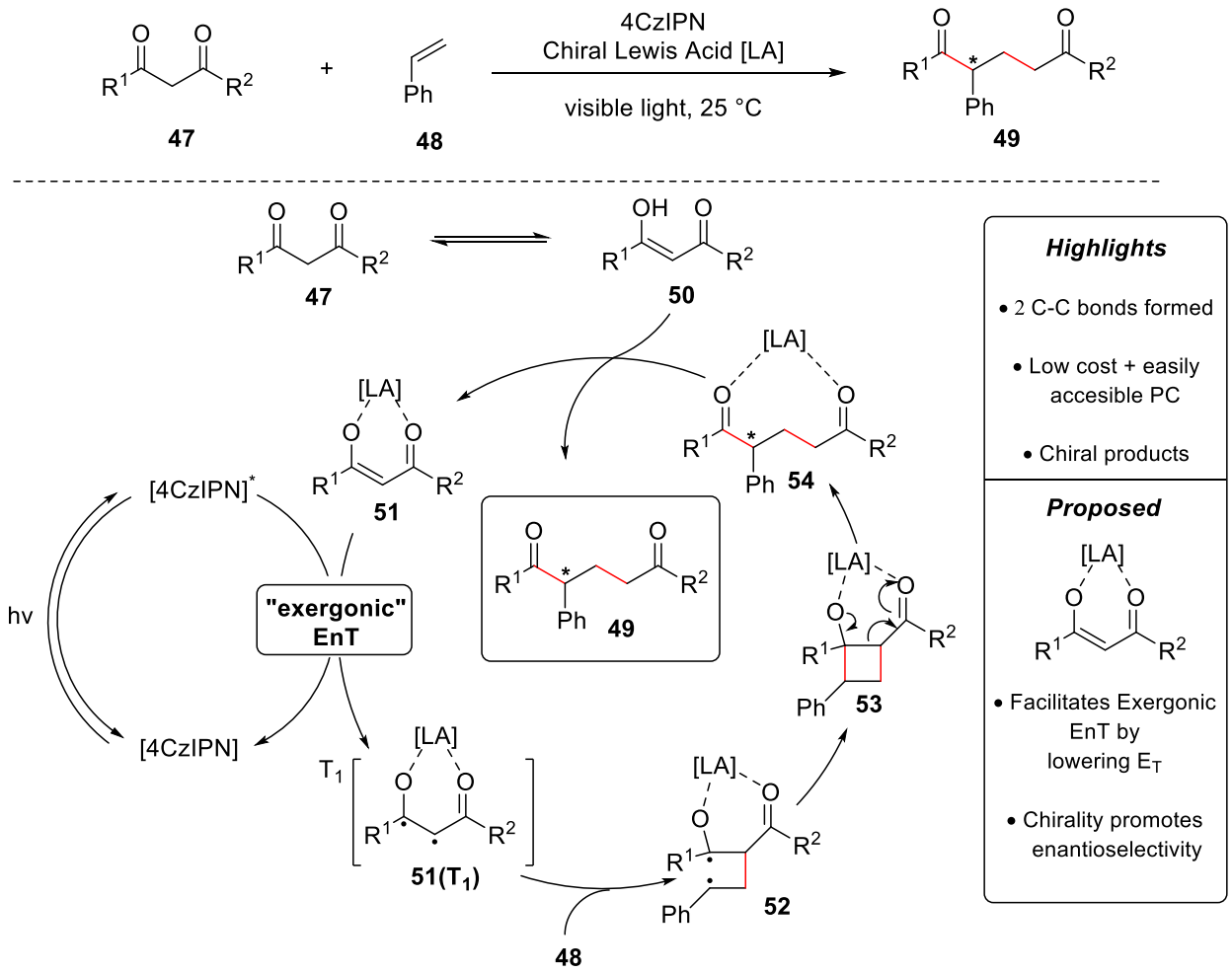

Scheme 1-17. Proposed asymmetric De Mayo reaction mediated by EnT from 4CzIPN to a chiral lewis acid-substrate complex.

Chapter 2: Efforts toward a Chiral Lewis Acid Co-catalyzed De Mayo reaction

2.1 Background

As stated in Section 1.5.2, Konig and coworkers reported a visible-light-mediated photocatalyzed De Mayo reaction, where the photosensitizer $[Ir(dF(CF_3)ppy)_2(bpy)](PF_6)$ (**[Ir]**) promotes a [2+2] cycloaddition between enolic β-diketones (**1**) and styrenes (**2**) to form α-substituted 1,5-diketones (**3**) (Scheme 2-1). The weak base tributylmethylammonium dibutyl phosphate was necessary to promote formation of the reactive **1(enol)** species.[104] The authors claim that the reaction proceeds by an EnT mechanism facilitated by the **[Ir]** photosensitizer.

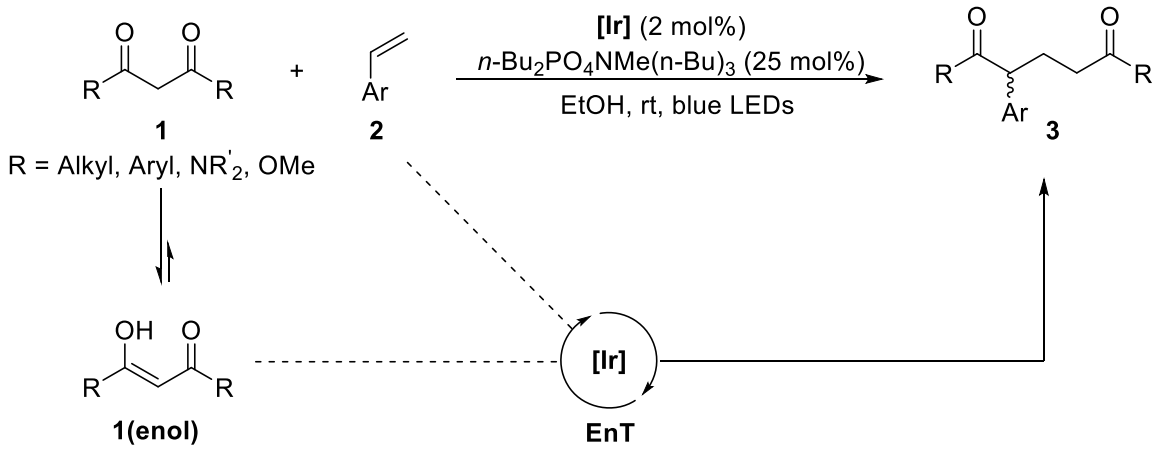

Scheme 2-1. Visible-Light-Mediated Photocatalyzed De Mayo reaction reported by Konig.

The E_T's of **1(enol)**, **2**, and **[Ir]** are ~59 kcal/mol,[105] ~60 kcal/mol,[50] and 62 kcal/mol,[106] respectively. These values indicate that exergonic EnT (E_T(substrate) – E_T(photosensitizer) < 0, Section 1.3.2) between **[Ir]** and both **1(enol)** and **2** is feasible. Evidence for this possible dual EnT pathway is supported by time resolved luminescence quenching experiments whereby **1(enol)** and **2** were observed to efficiently quench the emission of **[Ir]**.[104] Support for EnT mechanism is given by the lack of product when the authors deployed other common

photosensitizers with lower E_T values such as $Ru(bpy)_3^{2+}$ (E_T = 46.5 kcal/mol),[29] $Ir(ppy)_3$ (E_T = 55 kcal/mol),[107] and Mes-Acr^+ (E_T = 44.5 kcal/mol).[108]

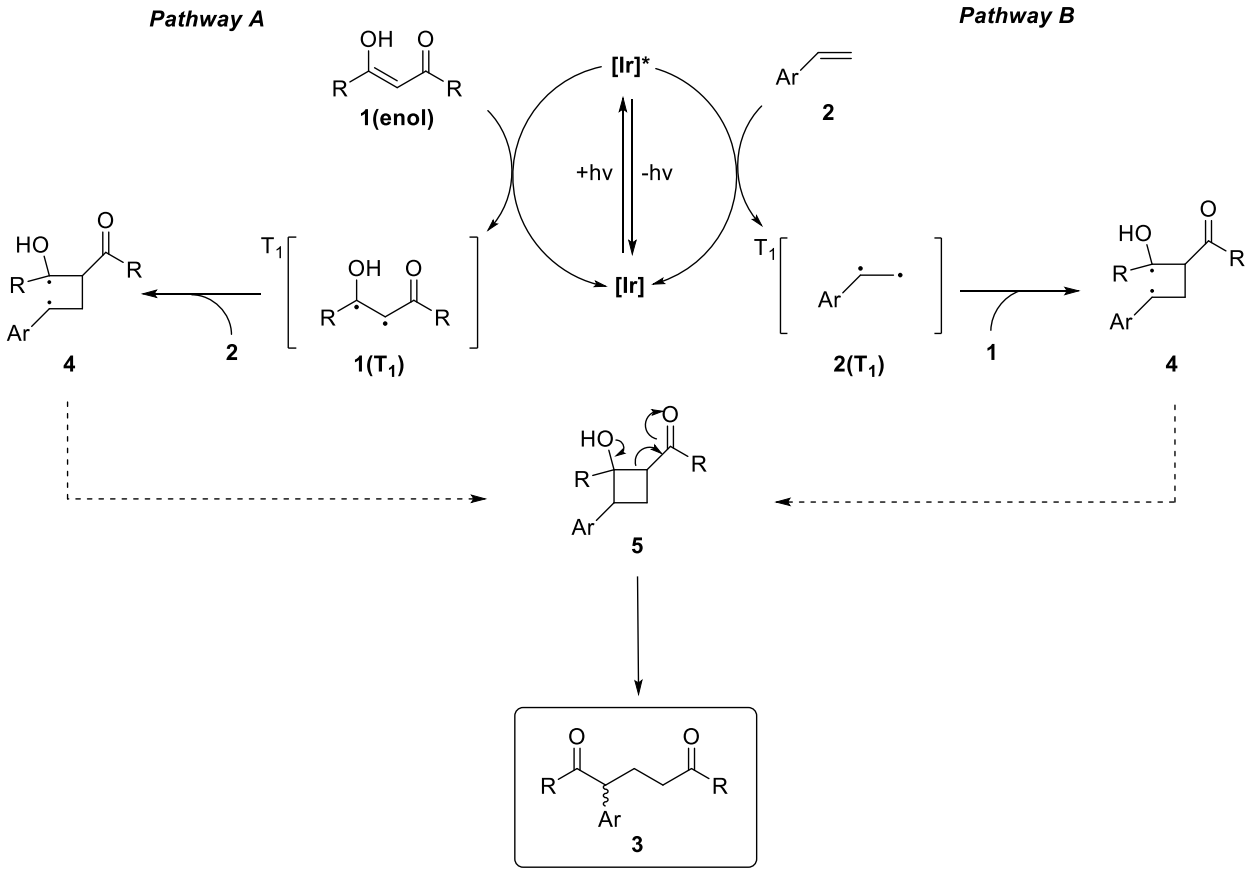

Scheme 2-2. Plausible mechanism for the visible-light-mediated De Mayo photocycloadditon.

A plausible mechanism for the reaction is shown in Scheme 2-2. After photoexcitation of **[Ir]**, exergonic EnT between **[Ir]*** and either **1(enol)** or **2** generates the triplet states **1(T_1)** or **2(T_1)**, respectively. Subsequent coupling of **1(T_1)** (pathway A) or **2(T_1)** (pathway B) with the corresponding ground state species generates the common 1,4-diradical intermediate **4**. Cyclization of **4** produces the unstable cyclobutanol intermediate **5**, that undergoes a retro aldol condensation to generate the α-substituted 1,5-diketone product **3**. The observed regioselectivity

likely results from the radical groups in **4** being in the most stable positions; α to the OH group and in the benzylic position.

Considering our research proposal outlined in Section 1.5, we reasoned an exergonic EnT mechanism between the organic photocatalyst 4CzIPN (E_T = 60 kcal/mol)[109] and the enol of β-diketone **1a(enol)** (E_T = 59 kcal/mol) would be favoured (see Section 1.3.2) over styrene **2a** (E_T = 60 kcal/mol). This is supported by the poor activity (< 44% conv.) observed when initially screening the reaction with 4CzIPN.[104] Based on previous reports by Yoon[84] and Bach[85] (Section 1.4.3), it was hypothesized that complexation of the carbonyl non-bonding electrons of **1a(enol)** with a Lewis acid would form the lowered E_T complex **6** (Scheme 2-3).[110,111] Formation of **6** would then facilitate the selective exergonic EnT with 4CzIPN to generate **6(T_1)**. Subsequent [2+2] addition between **6(T_1)** and **2a** then affords the desired 1,5-diketone **3a**. Moreover, it was reasoned that if **6** was generated in the presence of a chiral Lewis acid, than the reaction would form the cyclobutanol intermediate **7** enantioselectively to afford enantioenriched **3a**.

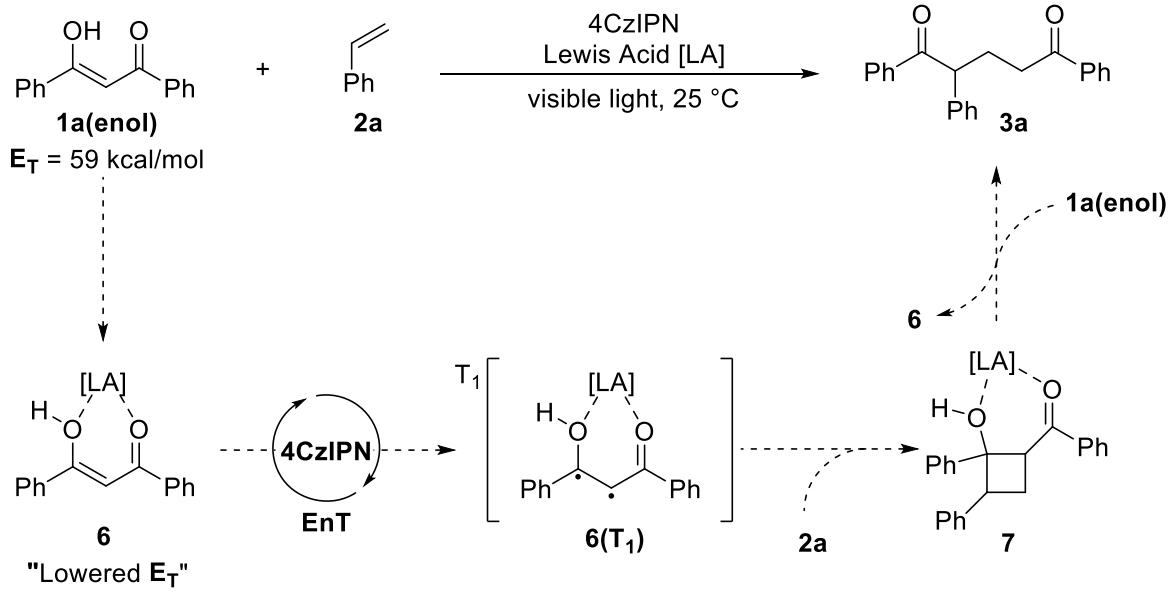

Scheme 2-3. Proposed Lewis acid catalyzed De Mayo reaction mediated by 4CzIPN.

2.2 Introduction of a Lewis Acid

$Sc(OTf)_3$ was selected to test our proposal due to its success in previously reported Lewis-acid catalyzed systems.[84,85] Solutions in acetonitrile containing **1a** and **2a** in the presence of 4 mol% 4CzIPN and either 10 mol% or 0 mol% $Sc(OTf)_3$ were irradiated with blue LEDs for 20 h at room temperature.

Table 2-1. Preliminary screening for a Lewis acid-catalyzed De Mayo reaction.

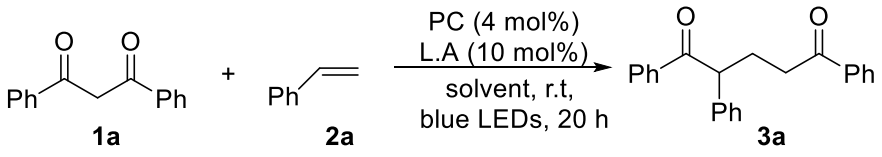

1a **2a** **3a**

Entry[a]	PC	LA	Solvent	Yield (%)
1	4CzIPN	-	MeCN	44[b]
2	4CzIPN	$Sc(OTf)_3$	MeCN	99[b]/74[c]
3	4CzIPN	$Sc(OTf)_3$	PhMe	86[c]
4	4CzIPN	$Sc(OTf)_3$	EtOH	51[c]
5	-	$Sc(OTf)_3$	PhMe	-
6[d]	4CzIPN	$Sc(OTf)_3$	PhMe	-
7	$Ru(bpy)_3^{2+}$	$Sc(OTf)_3$	PhMe	-

[a] Conditions: 0.1 mmol of **1a**, 0.5 mmol of **2a**, 2 mL of solvent.
[b] ^1H NMR yield. [c] Isolated yields after 20 h. [d] No Light.

To our delight, the presence of 10 mol% $Sc(OTf)_3$ afforded **3a** in 99% yield, higher than the 44% yield in the absence of $Sc(OTf)_3$ (Table 2-1; Entries 1 and 2). Building on these preliminary results we observed that the highest yields of **3a** were achieved in toluene while employing 4CzIPN (4 mol %) and $Sc(OTf)_3$ (10 mol%) (Entry 3). Control experiments showed that the presence of 4CzIPN and light are vital for product formation (Entries 5 and 6). Overall, these findings support formation of lower E_T complex **6** between $Sc(OTf)_3$ and **1a(enol)** to facilitate selective exergonic EnT with 4CzIPN. The E_T of **6** was not measured directly (Section

1.3.3), however, when the lower E_T photosensitizer $Ru(bpy)_3^{2+}$ (E_T = 46.5 kcal/mol) was used in the presence of $Sc(OTf)_3$ no **3a** was formed (Entry 6). Thus, we estimated the E_T of **6**, if formed, to be in the range of 46.5 – 59 kcal/mol. Coordination of **2a** with $Sc(OTf)_3$ is unlikely given the preferential hard-hard interaction between the carbonyl oxygen atoms of **1a** and Sc^{3+}.

2.3 Efforts toward Asymmetric De Mayo Reaction

Focus was then shifted our focus toward the enantioselective formation of **3a** by introduction of a chiral ligand (Scheme 2-4). It was envisioned that coordination of **1a(enol)** with a chiral scandium catalyst (**[Sc]**, generated *in-situ*) would lead to the formation of chiral complex **8**. Exergonic EnT of **8** with 4CzIPN would result in the formation of **8(T_1)**, which could then undergo [2+2] addition with **2a** to yield the cyclobutanol intermediate **9**. Subsequent retrol aldol condensation of **9** would afford the desired product **3a** as a single enantiomer.

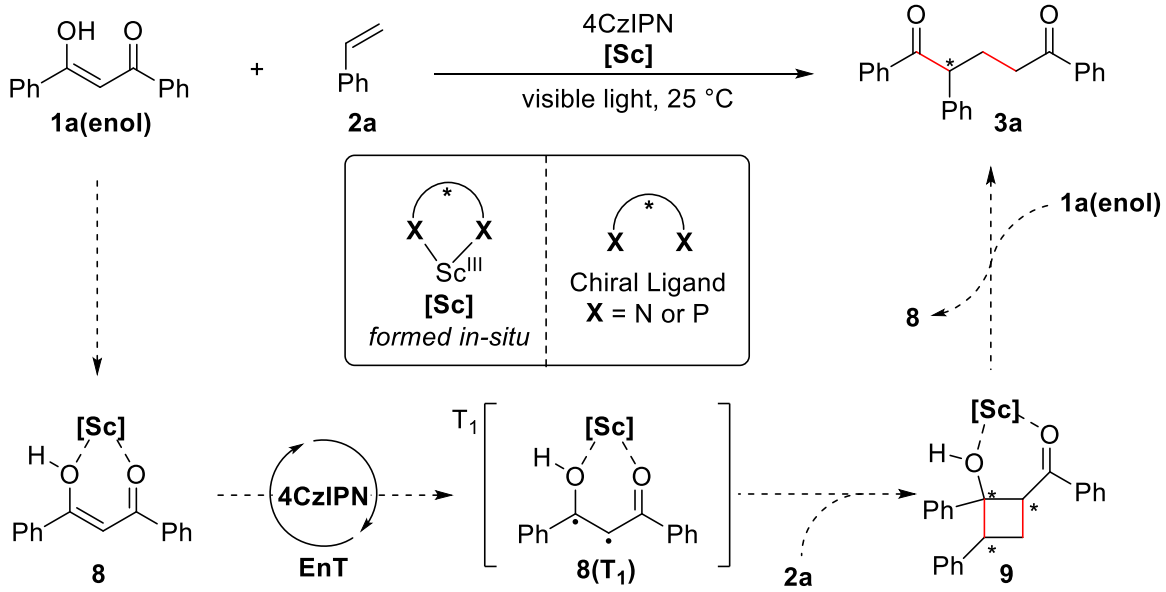

Scheme 2-4. Proposed chiral-scandium-catalyzed route for an asymmetric De Mayo reaction.

2.3.1 Chiral Ligand Screening

Several chiral ligands (**L***) were employed under our optimized conditions (Figure 2-1). To our dismay, no enantioselectivity was observed in **3a** with any of the chosen ligands. This result was surprising given that **L1** has been successfully deployed in closely related chiral scandium-catalyzed transformations.[84,112,113]

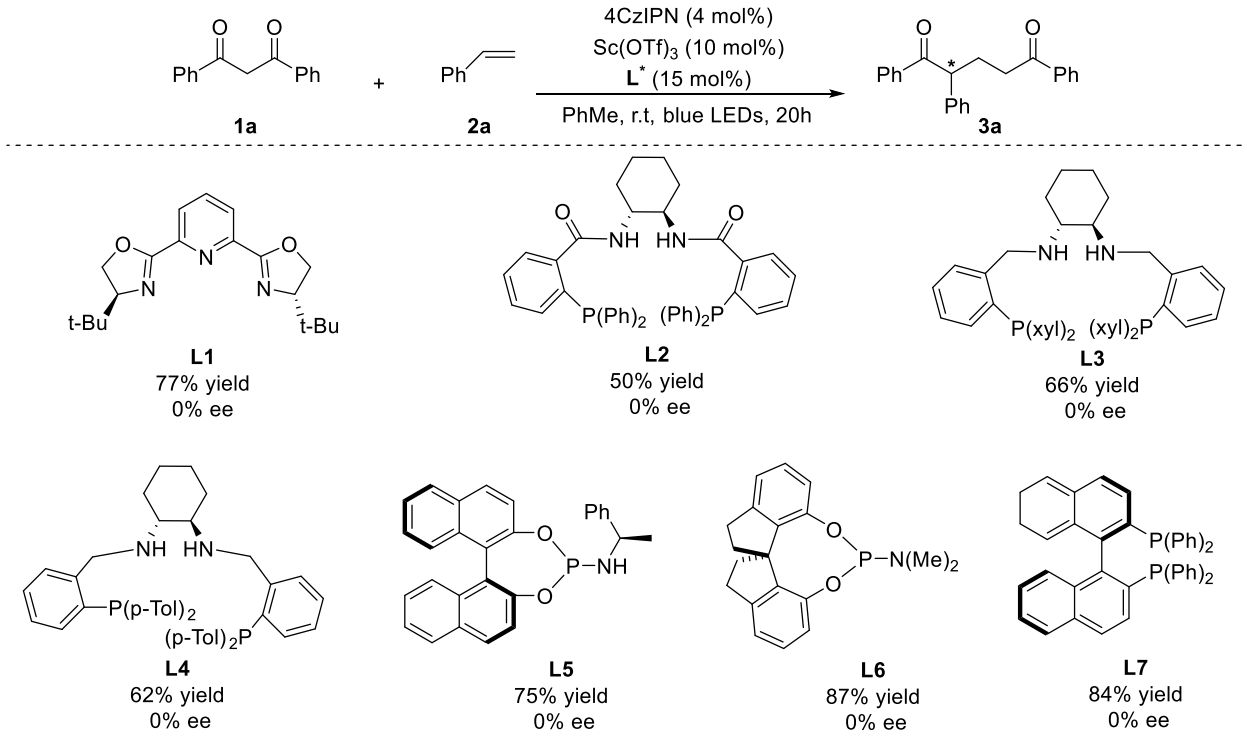

Figure 2-1. Chiral ligands screened during efforts to develop asymmetric De Mayo reaction.

2.3.2 Solvent & Temperature

Under the standard conditions listed in Figure 2-1 the solubility of $Sc(OTf)_3$ in toluene was low and a white precipitate often formed. We reasoned that the low solubility of $Sc(OTf)_3$ inhibited formation of the chiral scandium catalyst **[Sc]** necessary for enantioselectivity to occur. Thus, to improve solubility and promote formation of scandium complexes, several combinations of protic and aprotic polar solvents were explored (Table 2-2). Despite improving the solubility of $Sc(OTf)_3$ with polar solvents, no enantioselectivity was observed in **3a**. It is

possible that the more polar solvents were out competing **1a(enol)** for coordination with scandium center, which is consistent with the diminished yields (Entries 1 and 2). To address this concern, we tried 3:1 mixtures of non-polar/polar solvents, however, no enantiomeric excess was invoked in **3a** (Entries 3-6). Finally, assuming Curtin-Hammet control of this system we tried lower reaction temperatures were explored to exploit the energy-barrier difference ($\Delta\Delta G^{\ddagger}$) between the enantiomers of **3a**. Unfortunately, reactions performed in a freezer at -20 °C afforded **3a** in 0% ee (Entry 6 &7).

Table 2-2. Solvents and temperatures screened to invoke enantioselectivity in De Mayo reaction.

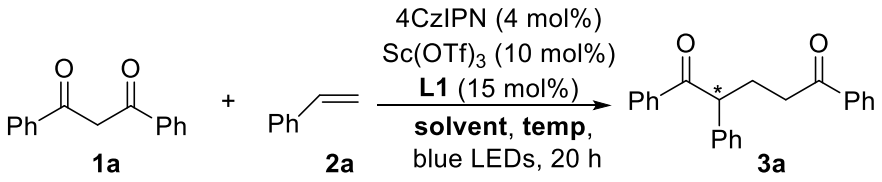

Entry[a]	Solvent	Temp (°C)	Yield (%)[b]	% ee
1	MeCN	r.t	27	0
2	EtOH	r.t	35	0
3	iPrOAc:MeCN[c]	r.t	63	0
4	THF:MeCN[c]	r.t	44	0
5	DCM:MeCN[c]	r.t	44	0
6	iPrOAc:MeCN[c]	-20	21	0
7	PhMe	-20	66	0

[a] Conditions: 0.1 mmol of **1a**, 0.5 mmol of **2a**, 2 mL of solvent.
[b] Isolated yields. [c] 3:1 Mixture of solvent/MeCN

2.4 Racemization of 1,5-diketone

After screening for multiple parameters (chiral ligands, solvent, temperature) with no success we considered that **3a**, upon formation, is racemizing in solution. Similar to **1a**, which predominately exists as **1a(enol)** in solution, tautomerization of **3a** would result in the loss of any

stereochemical information upon migration of the α-proton. Additionally, **[Sc]** could serve to catalyze enolization and thereby racemize any chiral **3a** upon formation (Scheme 2-5).

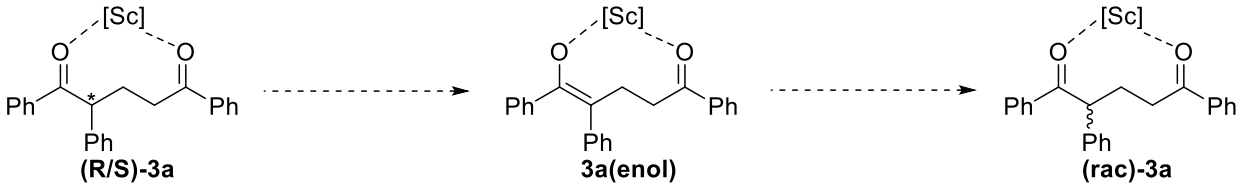

Scheme 2-5. Potential racemization of **3a** via enolization catalyzed by $Sc(OTf)_3$ during reaction progress.

To this end, we investigated styrenes that would produce stereocenters incapable of undergoing enolization under our prescribed conditions (Scheme 2-6). Addition of **1a** with α-methyl styrene (**2b**) afforded **3b** in modest yield, however, even the absence of an α-proton afforded no enantioselectivity. Dialin (**2c**) and **1a** afforded **3c** as a single diastereomer in good yield. Surprisingly, the addition of a second stereocenter in the β-position of **3c** did not lead to any enantioselectivity. These results suggested that the inability to induce enantioselectivity is not a result of enolization of the 1,5-diketone.

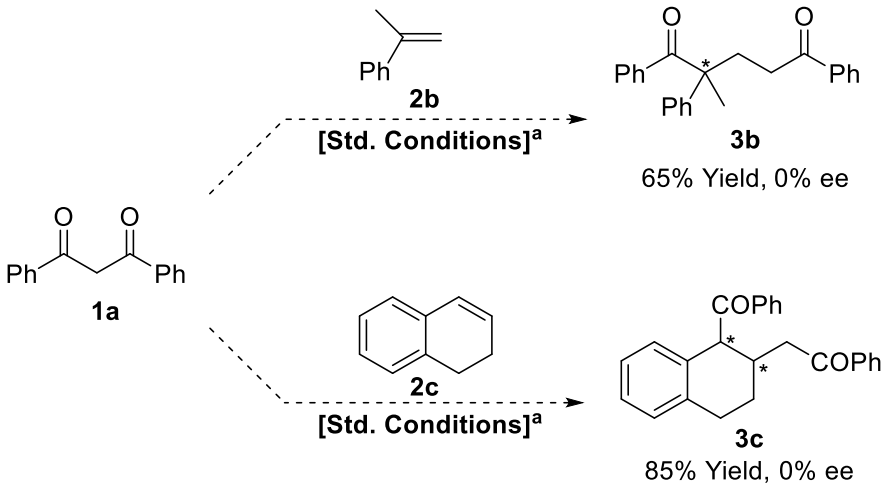

Scheme 2-6. Testing racemization hypothesis; [a]Standard Conditions: 0.1 mmol of **1a**, 0.5 mmol of styrene, $Sc(OTf)_3$ (10 mol%), **L1** (15 mol%), and 2 mL of PhMe.

2.5 Silyl Enol Ethers as Candidates for Photocatalyzed De Mayo

We then considered trapping cyclobutanol intermediate **5** (Scheme 2-2). We reasoned that the Lewis acid catalyzed [2+2] photocycloadditon between a silyl enol ether (**10**) and **2** would afford cyclobutane **11**; incapable of collapsing via retro-aldol condensation (Scheme 2-7 a). In addition to validating the proposed mechanism, the presence of a chiral Lewis acid during [2+2] addition could facilitate enantioselective formation of **11**. Moreover, cleavage of the silyl group and subsequent collapse of **11** would provide insight on the whether stereochemistry is retained or lost during formation of the α-substituted 1,5-diketone product (Scheme 2-7 b).

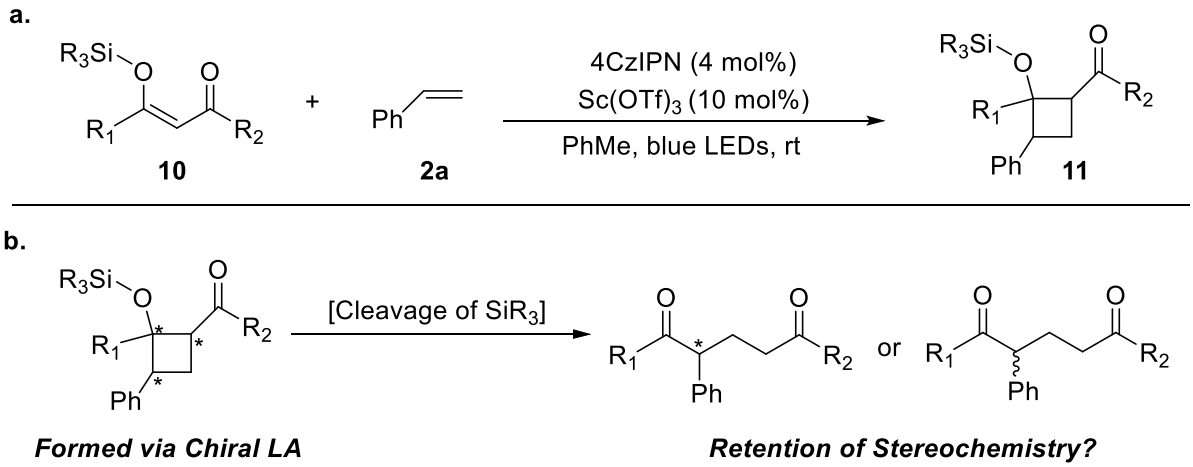

Scheme 2-7. (a) Proposal using silyl enol ethers to trap the cyclobutanol intermediate and invoke asymmetry; (b) Possible retention or destruction of stereochemistry during collapse of chiral cyclobutane.

2.5.1. Preparation of Protected 1,3 Keto-esters

To produce a stable silyl enol ether we attempted preparation of t-Bu$(CH_3)_2$Si (TBS) enolate of β-keto ester **1b**. Treatment of **1b** with NaH and TBSCl in THF at reflux for 12 h afforded **12** in a 1:1 ratio of separable Z/E stereoisomers. When the reaction solvent was changed to benzene **12** was obtained as single isomer, which based on characterization data reported for a similar substrate, is likely the Z isomer (Scheme 2-8).[114]

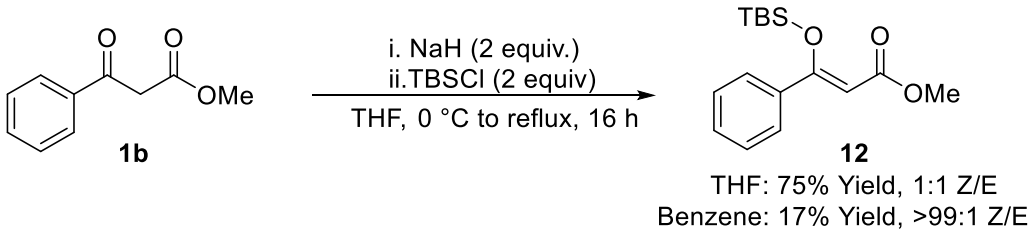

Scheme 2-8. Synthesis of silyl enol ether **12** from β-ketoester **1b**.

2.5.2 Photocatalyzed De Mayo with Silyl Enol Ethers

The [2+2] photocycloadditon between TBS-enolate **12** and **2a** was initially attempted under the standard conditions employed for 1,3-diketones (Table 2-3). **12-Z** was selected as the model substrate due to its favourable geometry toward coordination with an oxyphilic Lewis acid catalyst.

Table 2-3. Initial screening of silyl enol ether **12-Z** in photocatalyzed De Mayo Reaction.

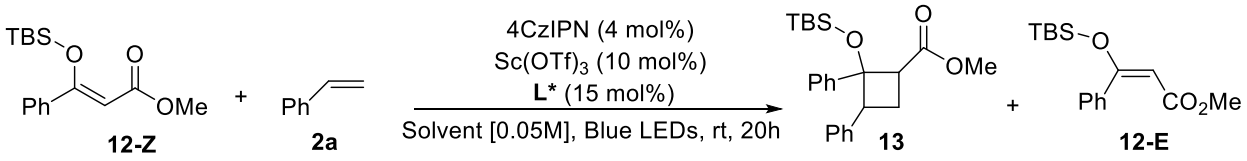

Entry[a]	L*	$Sc(OTf)_3$	Solvent	Conv. 12-Z (%)[b]	Major Pdt.
1	-	-	MeCN	52	**12-E**
2	-	Yes	MeCN	>99	**1b**
3	-	-	PhMe	83	**12-E**
4	-	Yes	DCM	>99	**1b**
5	-	Yes	PhMe	>99	**1b**
6	**L1**	Yes	PhMe	85	**12-E**

[a] Conditions: 0.1 mmol of **12-Z**, 0.5 mmol of **2a**, 2 mL of Solvent. [b] Crude ^{1}H NMR Yield.

Unfortunately, in all attempts no formation of the desired cyclobutane **13** was observed. Presence of $Sc(OTf)_3$ in the reaction mixture resulted in quantitative cleavage of the TBS group to generate **1b**. Interestingly, in the absence of a Lewis acid Z → E isomerization of **12** was

observed (entries 1 and 3), and thus provided evidence for photosensitization of **12-Z** to generate the T_1 necessary for [2+2] addition. Introduction of **L1** in the presence of $Sc(OTf)_3$ did not afford **13**, however, despite that the presence of a Lewis acid photoisomerization of **12-Z** proceeded efficiently (Entry 6). Presumably, coordination of **L1** to $Sc(OTf)_3$ prevented any interaction with **12-Z**.

Table 2-4. Exploring alternative reaction parameters for **12-Z** in De Mayo reaction.

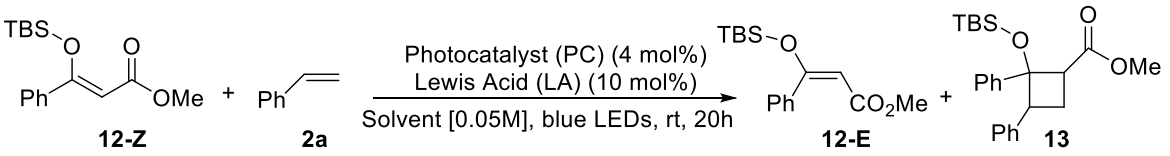

Entry[a]	PC	LA	Solvent	Conv. 12-Z (%)[b]	Major Pdt
1	$[Ru(bpy)_3](PF_6)_2$	-	MeCN	-	-
2	$[Ru(bpy)_3](PF_6)_2$	$Sc(OTf)_3$	MeCN	>99	**1b**
3	$[Ru(bpy)_3](PF_6)_2$	-	PhMe	-	-
4	$[Ru(bpy)_3](PF_6)_2$	$Sc(OTf)_3$	PhMe	>99	**1b**
5	**14**	-	MeCN	40	**12-E**
6	**14**	-	PhMe	83	**12-E**
7	**15**	-	MeCN	4	**12-E**
8	**15**	-	PhMe	6	**12-E**
9	4CzIPN	$Eu(OTf)_3$	PhMe	85	**12-E**
10[c]	-	-	PhMe	32	**12-E**

Varients of 4CzIPN:

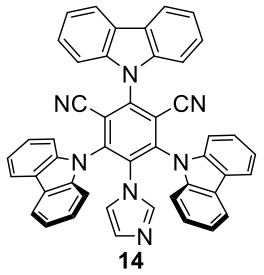

14

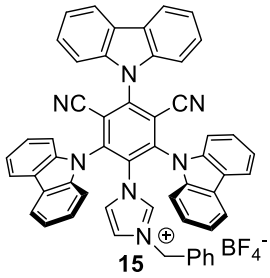

15

[a] Conditions: 0.1 mmol of **12-Z**, 0.5 mmol of **2a**, 2 mL of solvent. [b] Crude ^1H NMR Yield. [c] UV light source.

We then explored conditions employing other photosensitizers and Lewis acids to promote [2+2] photocycloaddition between **12-Z** and **2a** (Table 2-4). Again, formation of **13** was not observed. Unsurprisingly, the lower E_T species $Ru(bpy)_3^{2+}$ was unable to photosensitize **12-Z** (Entries 1 and 3). Attempts to lower the E_T of **12-Z** via coordination to $Sc(OTf)_3$, analogous to the approach employed by Yoon,[14] resulted in cleavage of the TBS group to yield **1b** (Entries 2 and 4). Analogues of 4CzIPN (**14** and **15**) were also evaluated. Interestingly, comparable

conversions were observed with **14**, while **15** was virtually inactive toward **12-Z**. Contrary to $Sc(OTf)_3$, relatively high conversion to **12-E** occurred in the presence of $Eu(OTf)_3$, however no addition with **2a** was detected (Entry 9). Direct excitation with UV light resulted in a 32% conversion to **12-E** (Entry 10).

2.5.3 Control Experiments

A series a control experiments were conducted to gain insight on the photoisomerization 'side reaction' of **12-Z** (Table 2-5). Isomerization of **12-Z** to **12-E** proceeded efficiently in the absence of **2a**, with higher conversions in toluene than acetonitrile (Entries 1 and 2). In contrast, when **12-E** was subjected to the same conditions no conversion to **12-Z** was observed (Entries 3 and 4).

Table 2-5. Control experiments to probe Z → E photoisomerization 'side reaction' of **12**.

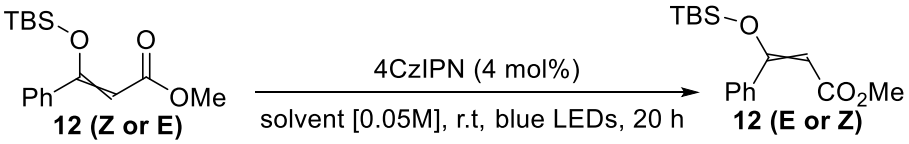

Entry[a]	Isomer	Solvent	Conv. (%)[b]
1	**12-Z**	MeCN	68
2	**12-Z**	PhMe	85
3	**12-E**	MeCN	-
4	**12-E**	PhMe	-

[a] Conditions: 0.1 mmol of **12**, 0.5 mmol of **2a**, 2 mL of solvent. [b] Crude ^{1}H NMR Yield to E or Z isomer.

These results indicated that 4CzIPN possesses an E_T < E_T (**12-E**), which enables selective photosensitization of **12-Z**, and results in the accumulation of **12-E** (Scheme 2-9). Photosensitization of **12-E** to **12(T_1)** is likely unfavoured due to nonbonding interactions and steric effects disrupting conjugation, thus resulting in an increased E_T. This explanation is

consistent with similarly reported systems, wherein the sterically hindered deconjugated isomer cannot undergo re-excitation to yield a statistical mixture of Z/E isomers.[51,115,116]

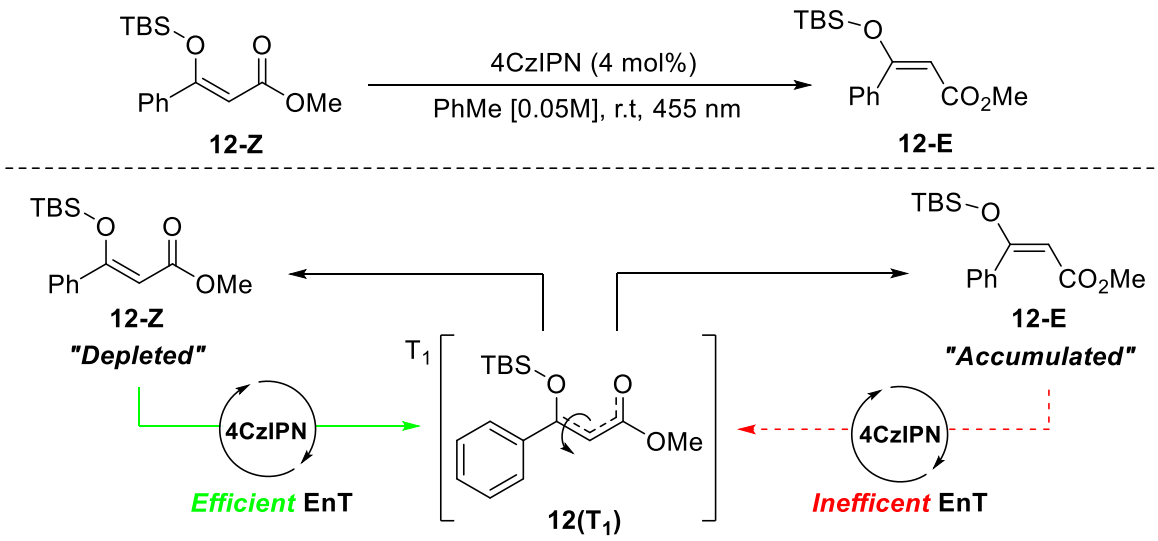

Scheme 2-9. Novel Z → E photoisomerization of silyl enol ether **12** facilitated by 4CzIPN.

Finally, **12-Z** was exposed to $Sc(OTf)_3$ in the absence of a photocatalyst and **2** (Scheme 2-10). As expected, when exposed to both light and dark conditions cleavage to **1b** occurred quantitatively. Presumably, an S_N2 type attack on Si to release TBS is facilitated either by trace water present in the $Sc(OTf)_3$.

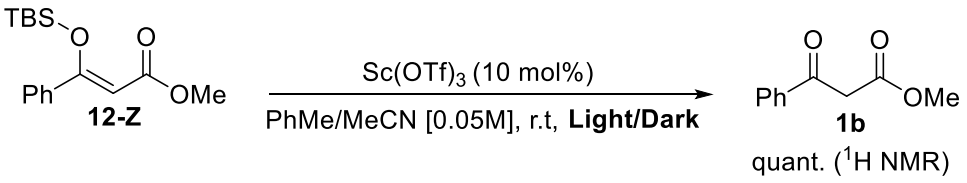

Scheme 2-10. Control reactions to investigate cleavage of TBS group in presence of $Sc(OTf)_3$.

2.6 Conclusion

In conclusion, we have made strides toward the development of a Lewis-acid catalyzed visible light driven De Mayo reaction. By employing $Sc(OTf)_3$ as a Lewis-acid, the low cost

organic photocatalyst 4CzIPN is able to efficiently facilitate [2+2] addition between enolic β-diketones and styrenes. These results demonstrated evidence for the formation of lower E_T complex **6** which undergoes exergonic EnT with 4CzIPN. Unfortunately, our efforts to extend these preliminary observations toward an enantioselective De Mayo reaction were unsuccessful. More experiments to better understand the relationship between $Sc(OTf)_3$ and **1a(enol)** are required. Finally, our extension of the De Mayo reaction to silyl enol ethers of β-ketoesters did not result in the desired 'trapped' cyclobutane, however, in the process a selective Z → E photoisomerization was discovered.

2.7 Experimental Procedures

2.7.1 General Methods and Materials

All operations were carried out under a N_2 atmosphere using standard Schlenk and glovebox techniques unless otherwise stated. Solvents were obtained from Sigma-Aldrich and were dried and distilled under a N_2 atmosphere using standard drying agents. Deuterated solvents were purchased from Cambridge Isotope Laboratories. Ligands used during screening were purchased through Strem. Photocatalysts 4CzIPN, **14**, and **15** were prepared according to previously reported literature procedures.[109,117] Unless otherwise stated, all other reagents were purchased from Sigma-Aldrich and were used as received. TLC monitoring was done using aluminum oxide coated alumina plates (MN TLC sheets ALUMGRAM® ALOX N/UV254), with visualization performed with UV light (254 or 366 nm). Flash chromatography was performed with Silicycle P60 (230-400 mesh) silica. Photocatalytic reactions were performed with 455 nm LED tape. The HPLC analysis was carried out with an Agilent (HP) 1100 series (G1322A degasser; G1312A binary pump; G1313A autosampler; G1316A TCC; G1314A VWD) with a Daciel CHIRALPAK® IB chiral column (250 x 4.6 nm) and eluting solvents Hexane (CHROMASOLV® for HPLC) and 2-propanol (HPLC grade). Enantiomeric excess (ee) values

were confirmed by comparing retention times to products prepared under racemic conditions. ^{1}H and $^{13}C\{^{1}H\}$ NMR spectra were taken using 400 MHz Varian Inova, 500 MHz Varian Inova, and 500 MHz Varian VNMRS spectrometers. ^{1}H and $^{13}C\{^{1}H\}$ NMR chemical shifts are reported in parts per million (δ) relative to TMS with the solvent as the internal reference. Coupling constants are reported in Hz and multiplicities are abbreviated as follows: s (singlet); d (doublet); t (triplet); sept (septet); br (broad); m (multiplet); dd (doublet of doublets); ddd (doublet of doublets of doublets); dt (douplet of triplets); td (triplet of doublets); and dtd (doublet of triplets of doublets). High resolution mass spectra were taken using either electron ionization in a Kratos Analytical MS-50G or electrospray in an Agilent 6220 oaTOF. Elemental analyses were collected with a Carlo Erba EA1108 Elemental Analyzer.

2.7.2 General Procedure A: Racemic Lewis-Acid Catalyzed De Mayo Reaction

To an oven-dried 5 mL vial equipped with a stir bar was added **1** (0.1 mmol) and 4CzIPN (0.004 mmol). The vial was placed under a N_2 atmosphere where $Sc(OTf)_3$ (0.01 mmol) was added. The vial was then sealed with a Teflon-lined cap and the contents were taken up in 2 mL of PhMe. After stirring the mixture for ~2-5 minutes to ensure solvation **2** (0.5 mmol) was added to the vial by syringe. The mixture was then irradiated with 455 nm LEDs for 20 h at room temperature. Upon completion (monitored by TLC), the crude mixture was absorbed on silica gel, solvent removed under reduced pressure, and the product purified by flash chromatography using eluent specified for each case. Compounds **3a**, **3b**, and **3c** have been previously reported in the literature.[1]

1,2,5-Triphenylpentane-1,5-dione (3a): Synthesized according to the General procedure A; 1,3-diphenylpropanedione (22.4 mg, 0.1 mmol), 4CzIPN (3.1 mg, 0.004 mmol), styrene (57 µL, 0.5 mmol), $Sc(OTf)_3$ (5 mg, 0.01 mmol). After purification by flash chromatography (9:1 PE/EtOAc) the product was obtained as a white solid (28 mg, 86%). Characterization data matched previously reported literature values.[1] ^{1}H NMR (500 MHz, $CDCl_3$) δ: 8.00 (d, *J* = 7.0 Hz, 2H), 7.92 (d, *J* = 7.0 Hz, 2H), 7.56 (m, 1H), 7.51-7.39 (m, 5H), 7.32 (m, 4H), 7.23 (m, 1H), 4.78 (t, *J* = 7.3 Hz, 1H), 3.07 -2.92 (m, 2H), 2.61 (dq, *J* = 14.5, 7.2 Hz, 1H), 2.35-2.22 (dq, *J* = 13.8, 7.2 Hz 1H); ^{13}C NMR (125 MHz, $CDCl_3$) δ 199.9, 199.6, 139.1, 136.8, 136.6, 133.0, 132.9, 129.0, 128.7, 128.5, 128.5, 128.3, 128.0, 127.2, 52.48, 36.01, 28.33; HRMS (ESI): $[M+Na]^+$ calcd for $C_{23}H_{20}NaO_2$: 351.1356, found: 351.1353.

2-Methyl-1,2,5-triphenylpentane-1,5-dione (3b): Synthesized according to the General procedure A; 1,3-diphenylpropanedione (22.4 mg, 0.1 mmol), 4CzIPN (3.1 mg, 0.004 mmol), α-methyl styrene (65 µL, 0.5 mmol), $Sc(OTf)_3$ (5 mg, 0.01 mmol). After purification by flash chromatography (9:1 PE/EtOAc) the product was obtained as a white solid (31.5 mg, 92%). Characterization data matched previously reported literature values.[1] ^{1}H NMR (500 MHz, $CDCl_3$) δ 7.83 (m, 2H), 7.52 (m, 3H), 7.40 (m, 7H), 7.32 (m, 1H), 7.25 (m, 2H), 2.85 (m, 2H), 2.50 (m, 2H), 1.68 (s, 3H); ^{13}C NMR (125 MHz, $CDCl_3$) δ 203.1, 199.9, 143.7, 136.7, 136.3, 132.9, 131.9, 129.6, 129.1, 128.5, 128.1, 128.0, 127.1, 126.2, 54.22, 34.81, 34.15, 24.39; HRMS (ESI): $[M+Na]^+$ calcd for $C_{24}H_{22}NaO_2$: 365.1512, found: 365.1509.

2-((1R,2S)-1-benzoyl-1,2,3,4-tetrahydronapthelene-2-yl)-1-phenylethanone (3c): Synthesized according to the general procedure; 1,3-diphenylpropanedione (22.4 mg, 0.1 mmol), 4CzIPN (3.1 mg, 0.004 mmol), 1,2-dihydronapthalene (66 µL,0.5 mmol), $Sc(OTf)_3$ (5 mg, 0.01 mmol).

After purification by flash chromatography (9:1 PE/EtOAc) the product was obtained as a white solid (31.6 mg, 89 %). Characterization data matched previously reported literature values.[1] ^{1}H NMR (500 MHz, $CDCl_3$) δ 8.01 (m, 2H), 7.77 (m, 2H), 7.50 (dqt, *J* = 7.6, 3.1, 1.3 Hz, 2H), 7.42 (m, 2H), 7.36 (m, 2H) 7.19 (m, 2H), 7.03 (app t, *J* = 7.3 Hz, 1H), 6.94 (d, *J* = 7.3 Hz, 1H), 5.30 (d, *J* = 4.9 Hz, 1H), 3.01 (m, 5H), 2.42 (m, 1H), 1.84 (m, 1H); ^{13}C NMR (125 MHz, $CDCl_3$) δ 202.6, 199.2, 138.7, 137.2, 136.9, 134.5, 133.1, 132.9, 129.6, 129.2, 128.7, 128.6, 128.4, 127.8, 126.7, 125.6, 47.19, 41.71, 33.31, 28.46, 25.14; HRMS (ESI): $[M+Na]^+$ calcd for $C_{25}H_{22}NaO_2$: 377.1512, found: 377.1509.

2.7.3 General Procedure B: Chiral Ligand Screening for Enantioselective De Mayo reaction

The following is a general procedure used for chiral ligand screening discussed in Section 2.3.1:

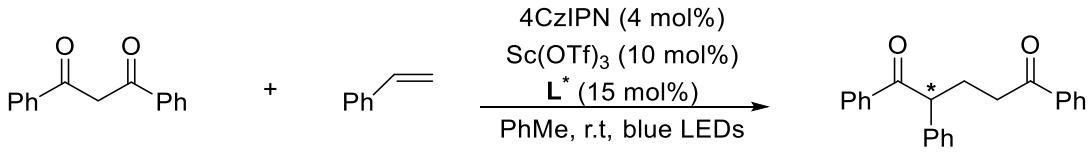

An example procedure follows. To an oven-dried 5 mL vial (vial A) equipped with a stir bar was added **1** (0.1 mmol) and 4CzIPN (0.004 mmol). Vial A was placed under a N_2 atmosphere, sealed with a Teflon-lined cap, and the contents dissolved in 1 mL of PhMe. Inside a N_2 filled dry box, a separate 5 mL vial (vial B) equipped with a stir bar was charged with $Sc(OTf)_3$ (0.01 mmol) and **L1** (0.015 mmol). Vial B was sealed with a Teflon-line cap, brought outside the dry box, charged with 1 mL of PhMe, and then stirred for 30 minutes at room temperature. The contents of Vial A were added to Vial B via double end needle followed by addition of **2** (0.5 mmol). The mixture was then irradiated with 455 nm LEDs for 20 h at room temperature. After the reaction was complete, the crude mixture was absorbed onto silica gel, solvent removed

under reduced pressure, and the product purified by flash chromatography (9:1 PE/EtOAc) to afford pure material for analysis.

1,2,5-Triphenylpentane-1,5-dione (3a): Synthesized according to the general procedure B; 1,3-diphenylpropanedione (22.4 mg, 0.1 mmol), 4CzIPN (3.1 mg, 0.004 mmol), styrene (57 μL, 0.5 mmol), $Sc(OTf)_3$ (5 mg, 0.01 mmol). After purification by flash chromatography (9:1 PE/EtOAc) the product was obtained as a white solid (28 mg, 86%); 0% ee (Daicel CHIRALPAK® IB, 95:5 Hexanes/i-PrOH. 1 mL/min, 250 nm; t_1 = 6.91 min, t_2 = 8.17 min). Characterization data matched values reported above.

2-Methyl-1,2,5-triphenylpentane-1,5-dione (3b): Synthesized according to the general procedure B; 1,3-diphenylpropanedione (22.4 mg, 0.1 mmol), 4CzIPN (3.1 mg, 0.004 mmol), α-methyl styrene (65 μL, 0.5 mmol), $Sc(OTf)_3$ (5 mg, 0.01 mmol), **L1** (5 mg, 0.015 mmol). After purification by flash chromatography (9:1 PE/EtOAc) the product was obtained as a white solid (22 mg, 65 %); 0% ee (Daicel CHIRALPAK® IB, 95:5 Hexanes/i-PrOH. 1 mL/min, 250 nm; t_1 = 6.43 min, t_2 = 6.60 min). Characterization data matched values reported above.

2-((1R,2S)-1-benzoyl-1,2,3,4-tetrahydronapthelene-2-yl)-1-phenylethanone (3c): Synthesized according to the general procedure B; 1,3-diphenylpropanedione (22.4 mg, 0.1 mmol), 4CzIPN (3.1 mg, 0.004 mmol), 1,2-dihydronapthalene (66 μL, 0.5 mmol), $Sc(OTf)_3$ (5 mg. 0.01 mmol), **L1** (5 mg, 0.015 mmol). After purification by flash chromatography (9:1 PE/EtOAc) the product was obtained as a white solid (30 mg, 85 %). 0% ee (Daicel CHIRALPAK® IB, 95:5 Hexanes/i-PrOH. 1 mL/min, 250 nm; t_1 = 8.34 min, t_2 = 8.88 min). Characterization data matched values reported above.

2.7.4 Preparation of Silyl Enol Ether 12

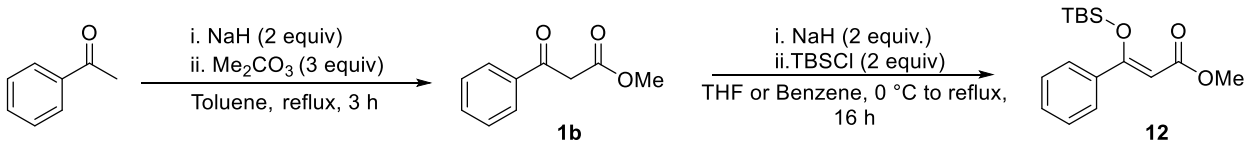

Methyl 3-oxo-3-phenylpropanoate (1b): To an oven dried 100 mL Schlenk flask equipped with a stir bar was added NaH (2 g, 60% w/w, 50 mmol). The flask was equipped with a claisen adapter, condenser, and then evacuated and refilled with N_2 for 3 cycles. Toluene (15 mL) followed by dimethyl carbonate (2.8 mL, 33.2 mmol) was added to the flask and the resulting suspension was heated to reflux under a N_2 atmosphere. A solution of acetophenone (1.94 mL 16.6 mmol) in toluene (8 mL) was added dropwise over 30 minutes. After an additional 3 hours of refluxing, the reaction mixture was cooled to 0 °C and quenched by slow addition of glacial acetic acid (5 mL). The resulting thick white precipitate was solvated by ice-cold water and the solution was extracted with EtOAc (3 x 20 mL). The combined organic layers were washed with brine (3 x 10 mL), dried over Na_2SO_4, and then concentrated under reduced pressure. Purification of the crude material by flash chromatography (9:1 PE/EtOAc) yielded 2.40 g (81%) of **1b** as a pale-yellow oil. Characterization data matched previously reported literature values.[1] The title product exists in solution ($CDCl_3$) as a 10:1 keto/enol mixture. Only signals corresponding to the keto species are reported here. ^{1}H NMR (500 MHz, $CDCl_3$) δ 7.94 (d, J = 7.2, 2H), 7.59 (m, 1H), 7.49 (app t, 7.6 Hz, 2H), 4.01 (s, 2H), 3.75 (s, 3H); ^{13}C NMR (125 MHz, $CDCl_3$) δ 192.3, 167.9, 135.9, 133.7, 128.8, 128.5, 52.45, 45.68; HRMS (ESI): $[M+Na]^+$ calcd for $C_{10}H_{10}NaO_3$: 201.0522 , found: 201.0523.

Methyl 3-(phenyl)-3-((tert-butyldimethylsilyl)oxy)acrylate (12): To a 50 mL Schlenk flask equipped with a stir bar was added NaH (453 mg, 60% w/w, 11.35 mmol). The flask was sealed and then evacuated and refilled with N_2 for 3 cycles. The NaH was rinsed with hexanes (3 x 5

mL) to remove the mineral oil. THF (3 mL) was added to the flask and the suspension was cooled to 0 °C. A solution **1b** (1 g, 5.68 mmol) in THF (2 mL) was added dropwise over 10 minutes followed by an additional 30 minutes of stirring at 0 °C. TBSCl (1.71 g, 11.35 mmol) was added in one portion and the mixture was then refluxed for 12 h. Upon cooling to 0 °C, 5 mL of saturated aq. NH_4Cl was added to mixture and then extracted with EtOAc (3 x 10 mL). The combined organic layers were washed with brine (3 x 10 mL), dried over Na_2SO_4, and then concentrated to give **12** as a 1:1 Z/E mixture. The crude mixture was purified and separated by flash chromatography (95:5 PE/EtOAc) to give **12-Z** (786 mg, 47%) as a colourless oil and **12-E** (457 mg, 28%) as a colourless oil, respectively. The reaction was also carried out in benzene following the same procedure; NaH (455 mg, 11.35 mmol), benzene (15 mL), **1b** (1 g, 5.68 mmol), TBSCl (1.72 g, 11.35 mmol). After work up **12-Z** (275 mg, 17%) was obtained as a colourless oil. **12-Z**: ^{1}H NMR ($CDCl_3$) δ 7.56 (m, 2H), 7.39 (m, 3H), 5.65 (s, 1H), 3.75 (s, 3H), 0.98 (s, 9H), 0.07 (s, 6H); ^{13}C NMR ($CDCl_3$) 166.0, 164.2, 138.4, 129.9, 128.2, 126.8, 100.7, 50.80, 25.71, 18.57, -4.169; HRMS (ESI): $[M+H]^+$ calcd for $C_{16}H_{25}O_3Si$: 293.1567, found 293.1570. **12-E**: ^{1}H NMR ($CDCl_3$) δ 7.49 (m, 2H), 7.40 (m, 3H), 5.48 (s, 1H), 3.61 (s, 3H), 0.97 (s, 9H), 0.17 (s, 6H); ^{13}C NMR ($CDCl_3$) δ 167.8, 167.1, 136.5, 129.5, 128.7, 127.5, 100.5, 50.83, 25.52, 18.22, -4.532; HRMS (ESI): $[M+H]^+$ calcd for $C_{16}H_{25}O_3Si$: 293.1567, found 293.1567.

2.7.5 General Procedure for Screening Silyl Enol Ether

The following is a general procedure used for screening TBS-enolates activity toward the De Mayo reaction discussed in Section 2.5:

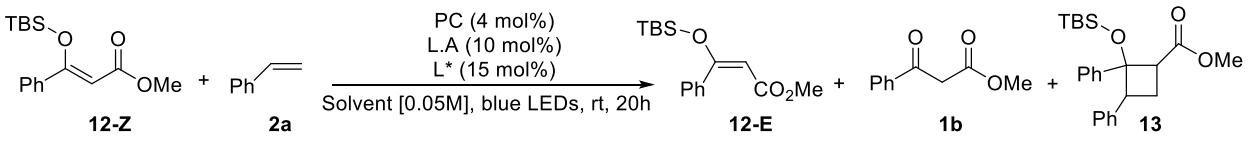

To an oven dried 5 mL vial equipped with a magnetic stir bar was added a photocatalyst (PC) (0.004 mmol). The vial was then placed under a N_2 atmosphere where a Lewis Acid (L.A) was added (0.01 mmol) followed by a chiral ligand (L*) (0.015 mmol). The vial was sealed with Teflon-lined cap and the contents were taken up in 2 mL of solvent. After stirring the mixture for ~2-5 minutes to ensure solvation **12-Z** (0.1 mmol) and **2a** (0.5 mmol) were added sequentially by syringe. The mixture was then irradiated with a light source (455 or 355 nm) for 20 h at room temperature. At 20 h, the reaction mixture was concentrated under vacuum and the conversion of the crude material was obtained by ^{1}H NMR (in $CDCl_3$).

2.7.6 Control Experiments with Silyl Enol Ether *12-Z*

Control Experiments A – Z/E Isomerization:

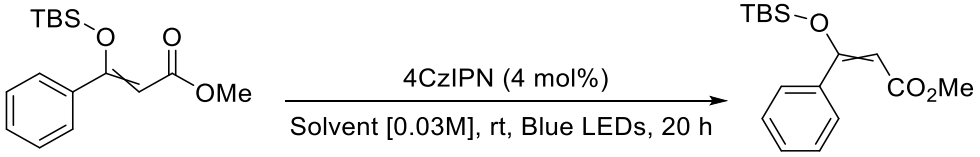

To a 5 mL vial equipped with a stir bar was added either **12-Z** or **12-E** (0.1 mmol) and 4CzIPN (0.004 mol). The vial was placed under a N_2 atmosphere and then sealed with a Teflon-lined cap. To the contents was added 2 mL of solvent (PhMe or MeCN) by syringe. The mixture was then irradiated with 455 nm LEDs for 20 h at room temperature. At 20 h, the reaction mixture was concentrated under vacuum and the conversion of the crude material was obtained by ^{1}H NMR (in $CDCl_3$). The following H NMR spectra depict photoisomerization conversion of both E and Z isomers after 20 h. Note: no isomerization occurred with **12-E** (Figure 2-3); any **12-Z** in the spectra is a result of imperfect purification.

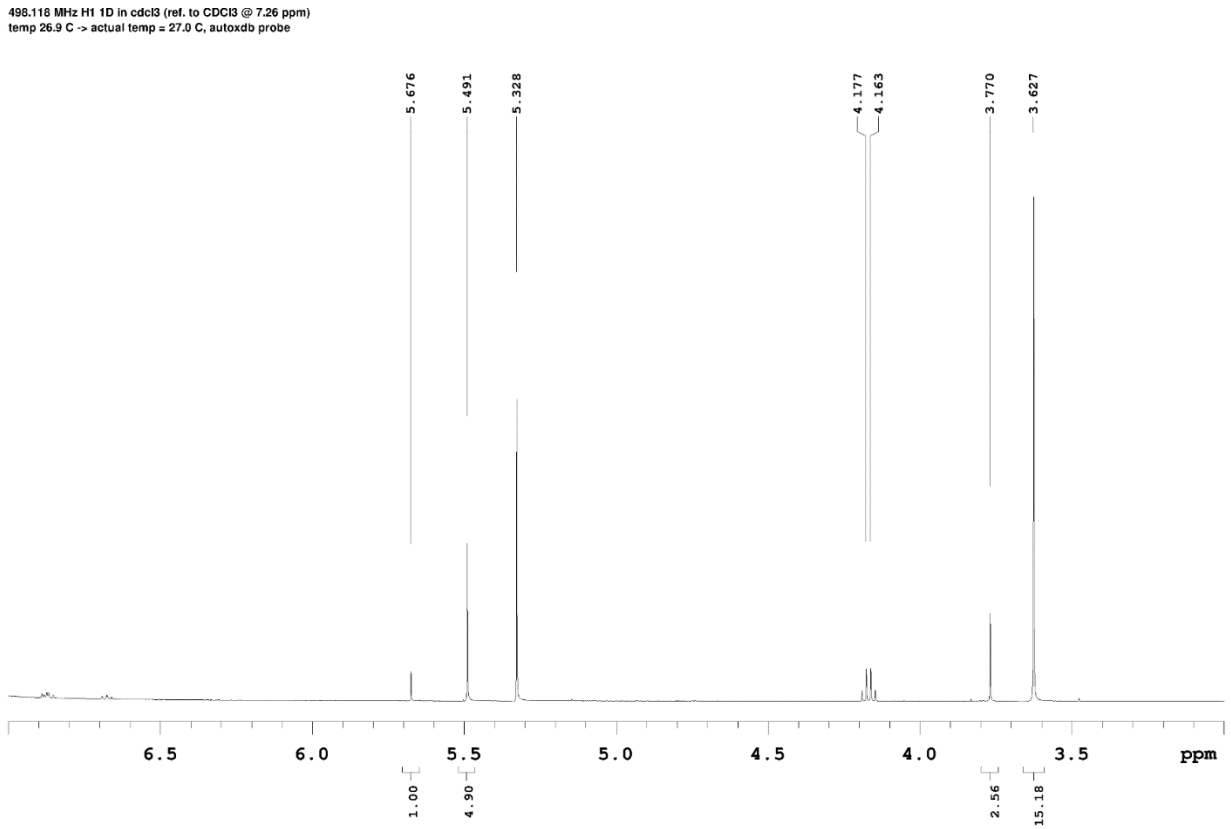

Figure 2-2. Isomerization of **12-Z** to **12-E** in toluene; ^{1}H NMR spectra shows an 83% conv of Z to E after 20 h.

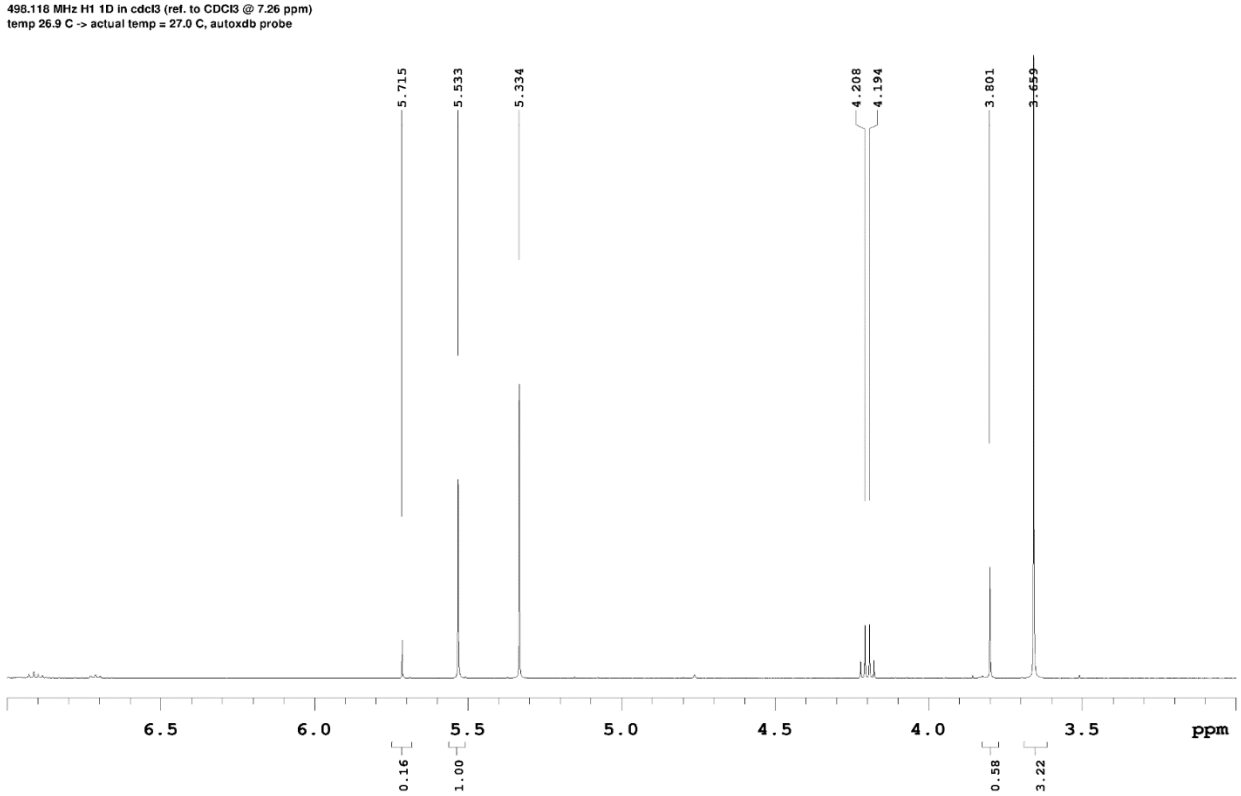

Figure 2-3. Isomerization of **12-E** to **12-Z** in toluene.

Control Experiments B – TBS Cleavage with $Sc(OTf)_3$:

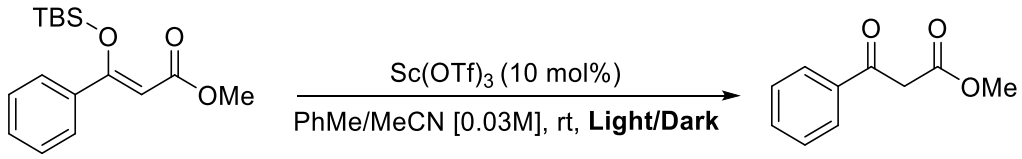

In a N_2 filled dry box, a 5 mL vial equipped with a stir bar was added $Sc(OTf)_3$ (mg, 0.01 mmol). The vial was sealed with a Teflon-lined cap, brought outside the dry box, and charged with 2 mL of solvent (PhMe or MeCN). To the vial was added **12-Z** (0.1 mmol) by syringe, and the mixture was then either irradiated under 455 nm LEDs or stirred in the dark for 20 h At 20 h, the reaction mixture was concentrated under vacuum and the conversion of the crude material was obtained by ^1H NMR (in $CDCl_3$). As stated in Section 2.5, in all cases presence of $Sc(OTf)_3$ in the reaction mixture resulted in cleavage of TBS to afford **1b** quantitatively.

2.7.7 Selected ^1H NMR spectra

The following spectra are shown to support the experiments performed in Section 2.5.3.

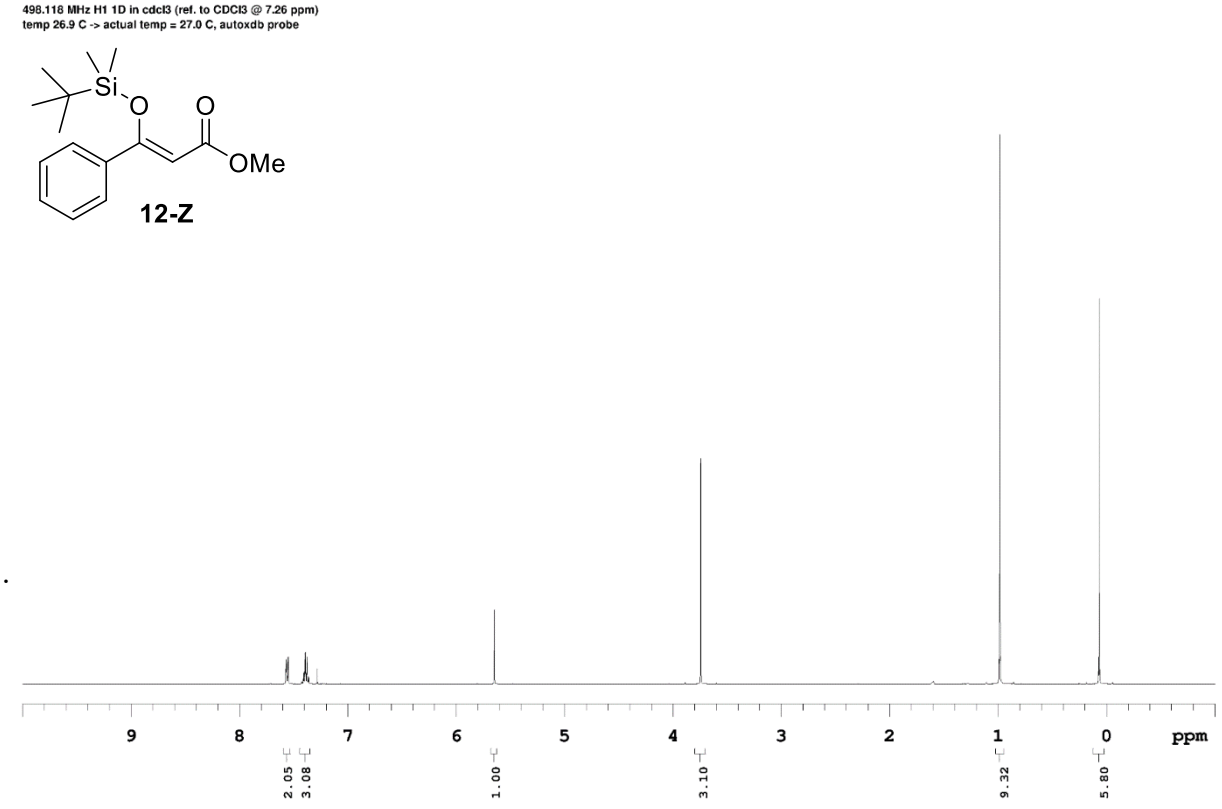

Figure 2-4. ^1H NMR spectrum of **12-Z**.

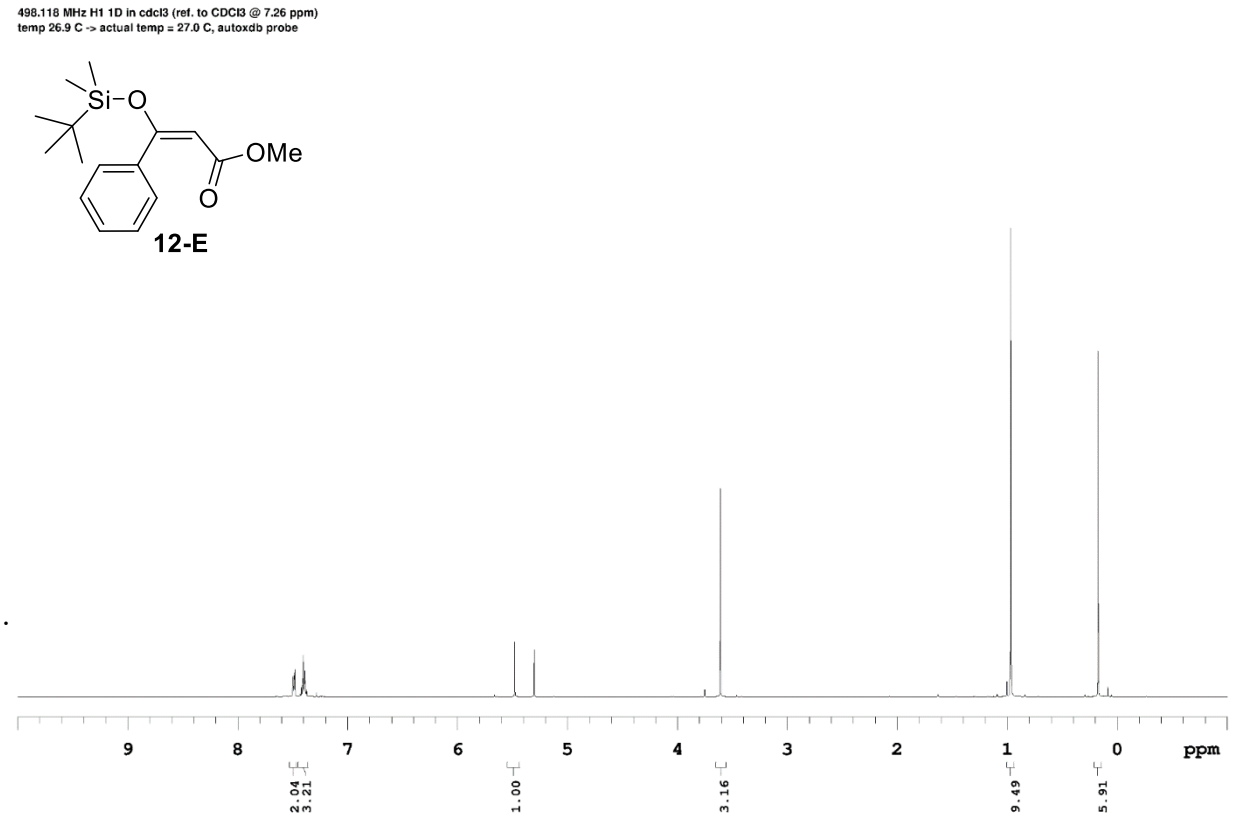

Figure 2-5. ^{1}H NMR spectrum of **12-E**.

Chapter 3: Investigation into the Properties of a Ruthenium(Polypyridyl)-NHC Compound

3.1 Background

Another approach utilizing energy transfer pathways in organic transformations is the merger of photocatalysis with transition metal catalysis.[118,29] In general, this 'merger' is achieved either by a bridging atom or ligand that links the photocatalyst and active metal center together.

An example of such approach was demonstrated by Osawa and coworkers. In their report they prepared the $Ru(bpy)_3^{2+}$ analogue **Pru** containing a diphenylphosphine group on the C3 of the 1,10-phenanthroline (phen) ligand.[119] The authors were then able to synthesize the bimetallic species **1**, whereby the phosphine group of **Pru** acts as a bridge between the photoactive ruthenium complex and the non-photoactive transition metal complex. Interestingly, **1** was found to efficiently catalyze the E → Z isomerization of 4-cyanostilbene (**2**). The authors postulate that upon coordination of 4-cyanostilbene with **1** EnT proceeds intramolecularly via the bridging ruthenium complex to facilitate the isomerization of **2-E** to **2-Z** (Scheme 3-1).

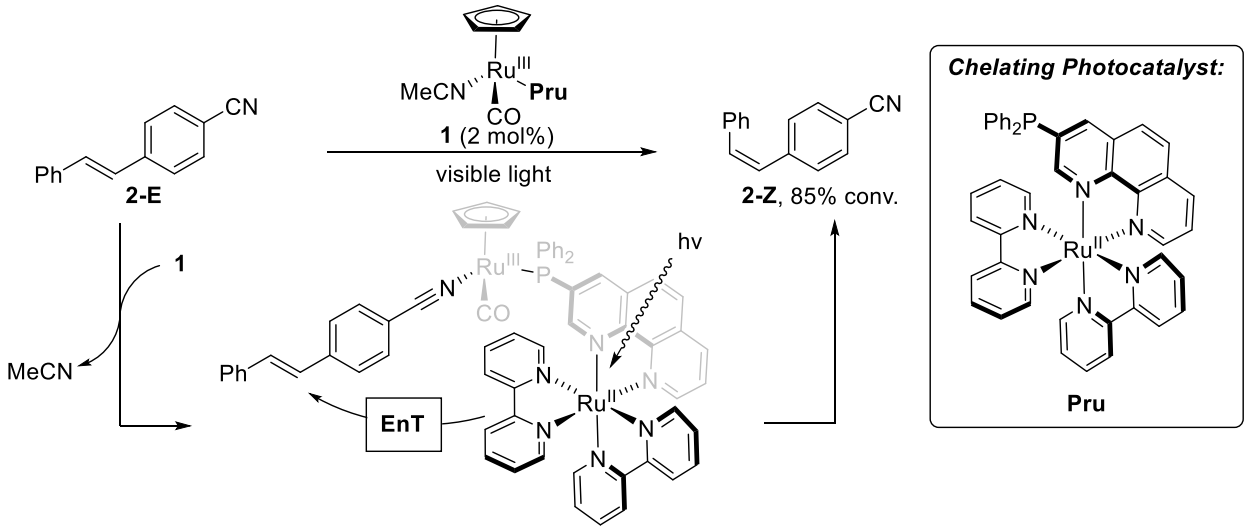

Scheme 3-1. E → Z isomerization of 4-cyanostillbene via intramolecular EnT from a bridged $Ru(bpy)_3^{2+}$ type ligand.

Similarly, Inagaki and coworkers prepared the binuclear Ru-Pd complex **3**, in which a 2,2'-bipyrimidine served as a bridging ligand to coordinate both a photoactive ruthenium centre and a catalytically active palladium centre.[120-122] Surprisingly, the presence of a second metal centre did not drastically impact the photophysical properties of the ruthenium complex, and **3** was employed as an efficient catalyst for the visible-light driven dimerization of α-methylstyrene (**4**). During the catalytic cycle (Scheme **3-2**), the authors proposed that EnT between the ruthenium and palladium centres of intermediate **9** promotes migratory insertion of second equivalent of **4** to give **10**.[123] Subsequent β-hydride elimination affords the product **5** and closes the catalytic cycle.

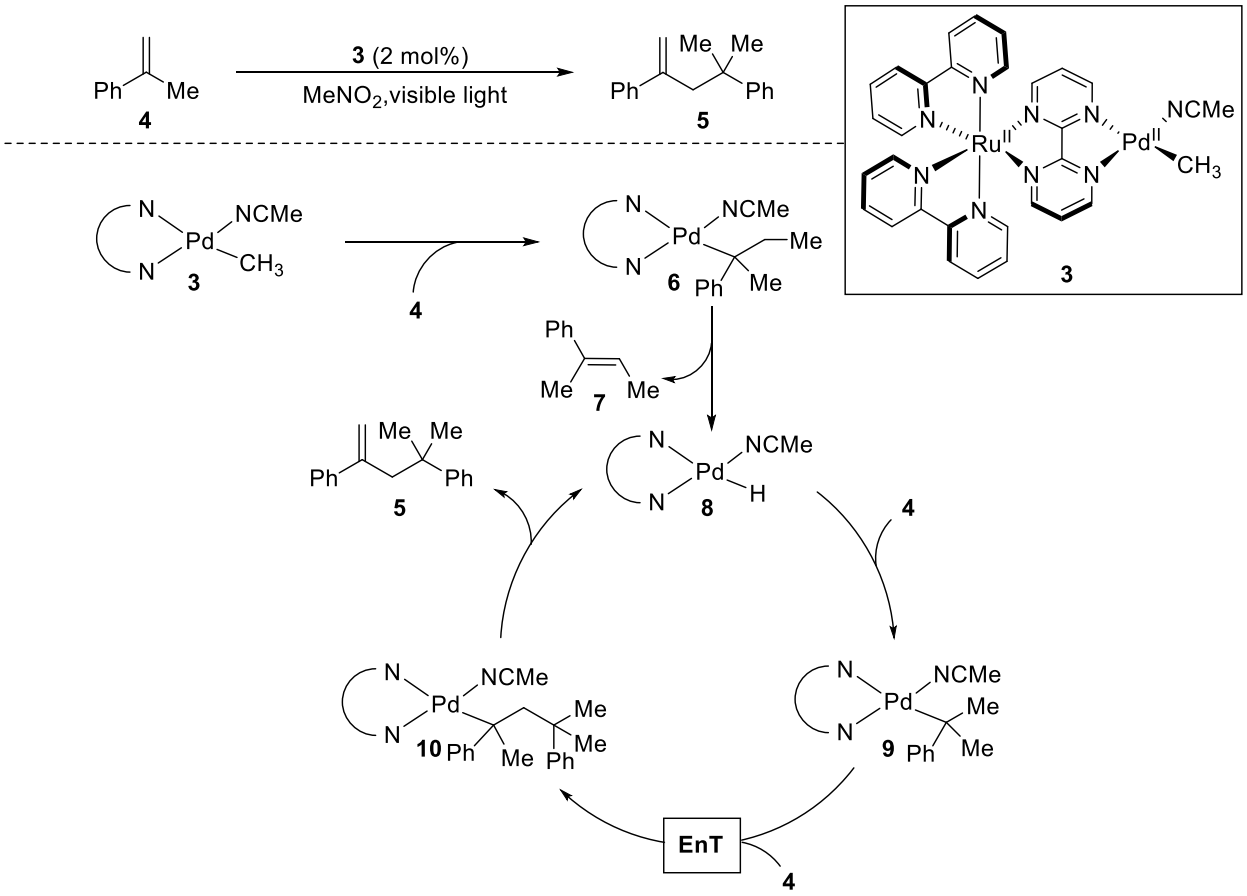

Scheme 3-2. Visible-light driven dimerization of α-methylstyrene by a binuclear Pd/Ru complex.

Building on these examples an interesting combination that has been extensively investigated by Rau and coworkers is to incorporate a N-heterocyclic carbene (NHC) ligand at the periphery of a phen ligand in a Ru-polypyridyl dye.[124] In a similar fashion to Inagaki, the NHC group can be used to bond to homogeneous catalysts for a variety of reactions. Rau and coworkers reported that attempts to prepare the free NHC of compounds related to **11** were unsuccessful, and alternatives such as silver adducts were employed instead (Figure 3-1a).

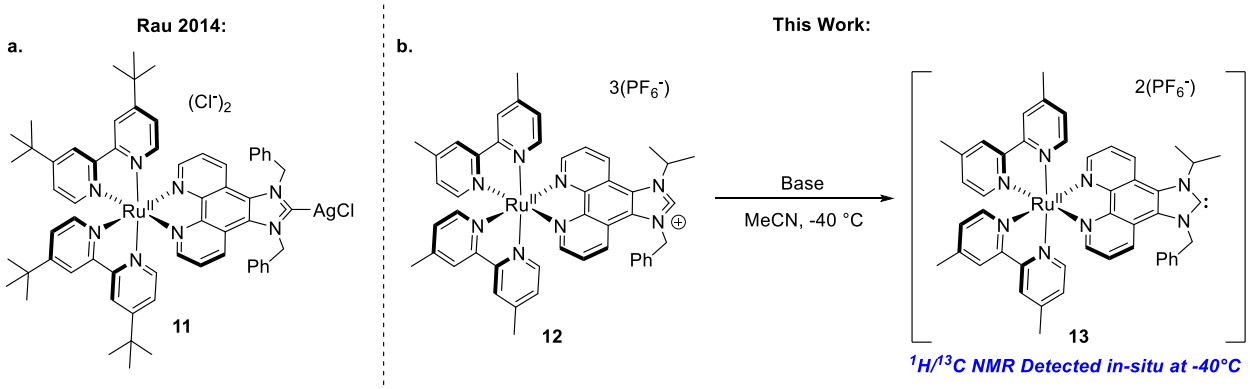

Figure 3-1. (a) Silver-NHC adduct prepared by Rau and coworkers in 2014. (b) Our work to detect free carbene of Ru-polypyridyl-NHC species, $[Ru(dmbpy)_2(bpip)_2](PF_6)_3$ (**12**).

In this chapter we report the preparation of precursor **12** (Figure 3-1b) and detail low temperature NMR studies along with ^{13}C isotope labelling to investigate its deprotonation as an attempt to prepare the free NHC complex **13**.

3.2 Results & Discussion

We chose the isopropyl analogue **12** assuming that the isopropyl group would sterically protect the corresponding free NHC, but not hinder coordination to metal centres. The isopropyl group has been extensively utilized, for example, in the NHC chemistry developed by the Crudden group.[125] Scheme 3-3a shows the synthesis we employed to prepare **12**. The synthetic route is a modification of previously reported methods, whereby the starting material 1,10-phenanthroline-5,6-diamine is used instead of the commonly used 1,10-phenanthroline-5,6-

dione.[124] The condensation between 1,10-phenanthroline-5,6-diamine and triethyl orthoformate proceeded in 87 % yield to generate the imidazole **14**. Alkylation with 2-iodopropane with Cs_2CO_3 as base gave the isopropyl derivative **15** in 96 % yield. The alkylation reaction between **15** and benzyl bromide proceeded in DMF at 120 °C to give the target unsymmetric imidazolium **16** in 70 % recrystallized yield. The reaction sequence was modified to employ one equivalent of ^{13}C-labelled triethyl orthoformate under reflux in the first step, rather than a large excess of formate at room temperature (Scheme 3-3b). Reaction between **16** or **16(^{13}C)** and $[Ru(dmbpy)_2Cl_2]$ proceeded in refluxing ethanol-water over 18 h, followed by anion exchange with $[NH_4]PF_6$ to give **12** and **12(^{13}C)** as the PF_6 salt in 80 % yield.

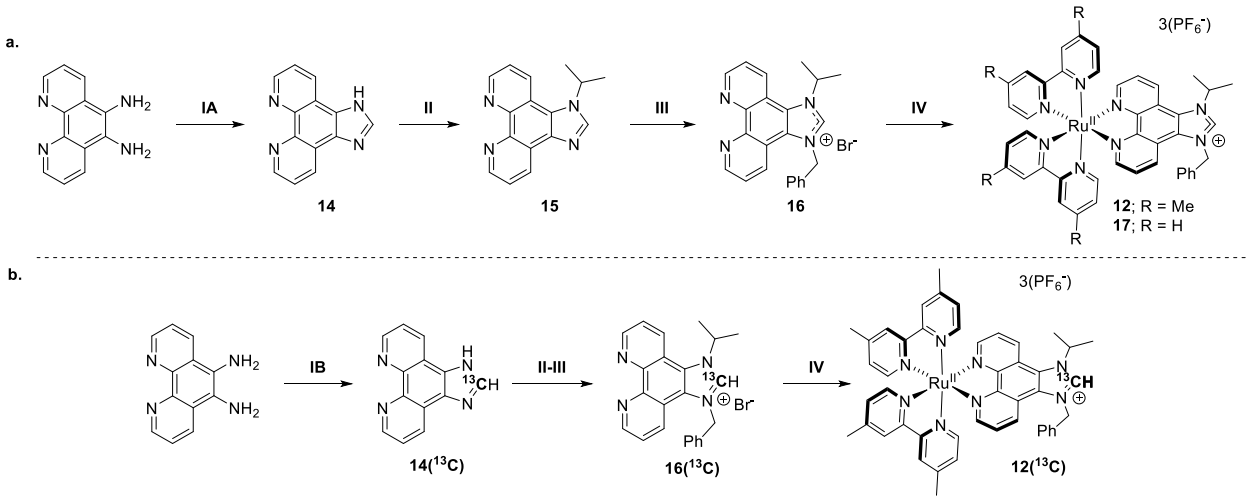

Scheme 3-3. (a) IA: $HC(OEt)_3$, Sulfamic Acid, MeOH, r.t; II: 2-Iodopropane, Cs_2CO_3, MeCN, 85 °C; III: BnBr, DMF, 120 C; IV: i. $[Ru(Cl)_2(dmbpy)_2]$/$[Ru(Cl)_2(bpy)_2]$, EtOH/H_2O (3:1), reflux ii. NH_4PF_6, H_2O, rt. (b) IB: $H^{13}C(OEt)_3$, Sulfamic acid, MeOH, reflux.

Figure 3-2(a) and (b) shows the aromatic region of the ^{1}H NMR spectrum of **12(C^{13})** before and after deprotonation by ~1 equivalent KO^{t}Bu in MeCN-d_3 at -40 °C, respectively. The signal assigned to the NHC hydrogen (doublet at 9.5 ppm) disappears upon addition of the base, and the signals assigned to the -C*H*(Me)$_2$ and -C*H*$_2$Ph groups in the imidazolium group broaden significantly. Figure 3-2c and d also shows the corresponding ^{13}C{^{1}H} NMR spectra. The

$^{13}C\{^{1}H\}$ NMR spectra for **12(C^{13})** contains a very tall peak assigned to the label at C2 of the imidazolium group.

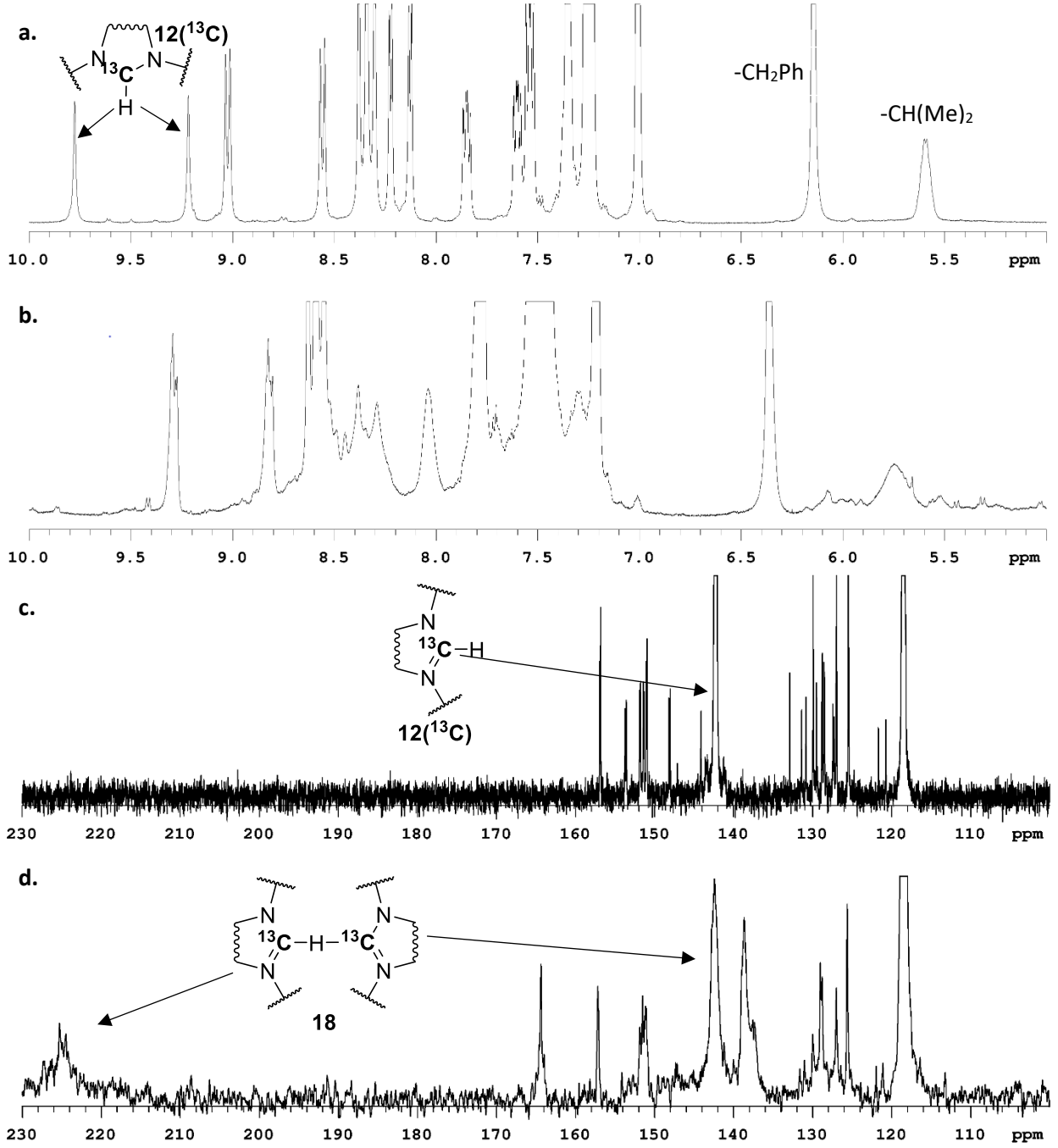

Figure 3-2. Deprotonation of **12(**^{13}**C)** with KO^{t}Bu at -40 °C in MeCN. (a) ^{1}H NMR of **12(**^{13}**C)** at -40 °C in MeCN; (b) ^{1}H NMR at -40 °C after 5 min of addition of KO^{t}Bu to **12(**^{13}**C)**, spectra depicts loss of C2 proton; (c) $^{13}C\{^{1}H\}$ NMR of **12(**^{13}**C)** at -40 °C in MeCN; (d) $^{13}C\{^{1}H\}$ NMR at -40 °C after additon KO^{t}Bu, spectra depicts plausible formation of H-bridging species **18**.

Surprisingly, there are no corresponding tall peaks in the spectrum after the reaction with base. There is a broad peak at ~225 ppm that may correspond to the NNC[126] of **13** and another broad peak at ~142 ppm that is in a similar chemical shift to the unreacted starting material. A spin saturation transfer experiment showed that the peaks at ~225 and ~142 ppm are in rapid exchange (Figure 3.7, Section 3.4.4). We propose that the free NHC and the imidazolium starting material, **12(**^{13}**C)** are in rapid equilibrium with the hydrogen bridging species **18** under these conditions (Figure 3-2d). Similar H bridging compounds are known for other NHC species in the literature.[127]

To investigate the deprotonation further, we employed the stronger base $KN(SiMe_3)_2$. Figure 3-3a and b shows the aromatic region of the ^{1}H NMR spectrum of **12(**^{13}**C)** before and after deprotonation by ~1 equivalent of $KN(SiMe_3)_2$ in MeCN-d_3 at -40 °C, respectively. As with KO^{t}Bu, the signals assigned to the NHC hydrogen (doublet at 9.5 ppm) disappears upon addition of the base, and the signals assigned to the -C*H*$(Me)_2$ and -CH_2Ph groups in the imidazolium group broaden significantly. The ^{13}C{^{1}H} spectra (Figure 3c and d) are also similar to the results obtained with KO^{t}Bu. Addition of ~0.3 equivalents more $KN(SiMe_3)_2$ resulted in complete loss of the signal at ~142 ppm, and a significant sharpening of the signal at ~225 ppm (Figure 3-3d). An ^{1}H-^{13}C gHMBC experiment verified that the ^{13}C resonances at ~225 ppm correlates to the ^{1}H NMR signal at ~6.18 ppm, assigned to the benzylic, -CH_2Ph, protons (Figure 3.8, Section 3.4.4). We therefore conclude that addition of excess base removed the unreacted imidazolium and generated a small amount of the free NHC, **13**. There appeared to be new peaks in the ^{13}C{^{1}H} spectra at ~164 and 138 ppm. We propose that these peaks arise from decomposition of **13**, and

may be the corresponding olefins resulting from dimerization of the NHC. More research is required to conclusively identify the decomposition products.

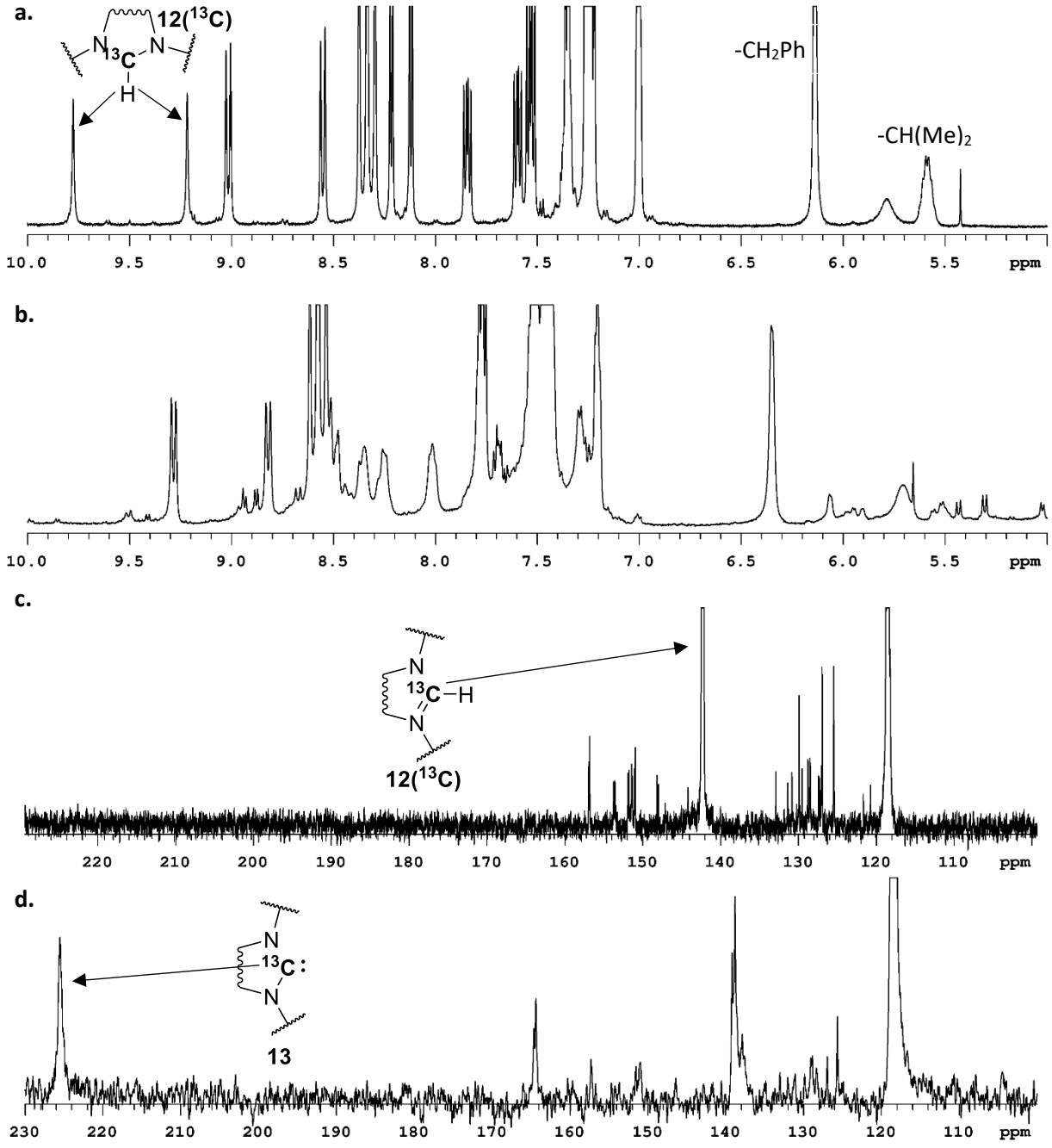

Figure 3-3. Deprotonation of **12(13C)** with $KN(SiMe_3)_2$ at -40 °C in MeCN. (a) ^1H NMR of **12(13C)** at -40 °C in MeCN; (b) ^1H NMR at -40 °C after 5 min of addition of $KN(SiMe_3)_2$ to **12(13C)**, spectra depicts loss of C2 proton; (c) $^{13}C\{^1H\}$ NMR of **12(13C)** at -40 °C in MeCN; (d) $^{13}C\{^1H\}$ NMR at -40 °C after addition of 1.3 equiv of $KN(SiMe_3)_2$, spectra depicts formation of free carbene **13** at 225 ppm.

3.3 Conclusion

Deprotonation of the imidazolium precursors to these photoactive NHC compounds is complicated by reaction between the NHC product and starting material. The free NHC, **13**, can be prepared with excess base, but it appears to be unstable at -40 °C. The exact identities of the decomposition products require further investigation. Ligand modification, or generation of the free NHC in the presence of a coordinating species are suggested strategies to utilize these coordinating dyes.

3.4 Experimental Procedures

3.4.1 General

All operations were carried out under a N_2 atmosphere using Standard Schlenk and glovebox techniques unless otherwise stated. Solvents were dried and distilled under a N_2 atmosphere using standard drying agents. Solvents were obtained from Sigma-Aldrich. Deuterated solvents were purchased from Cambridge Isotope Laboratories. All common commercial chemicals were purchased from Sigma-Aldrich. 1,10-Phenathroline-5,6-diamine was purchased from Shanghai UCHEM Inc. ^{13}C labelled triethyl orthoformate was purchased from Cambridge Isotope Laboratories and used as received. Benzyl bromide, if discoloured, was distilled under vacuum prior to use. $[Ru(dmbpy)_2Cl_2]$ was prepared according to a previously reported literature procedure.[128] All other commercial reagents were used as received unless otherwise stated. ^1H and $^{13}C\{^1H\}$ NMR spectra were taken using 400 MHz Varian Inova, 500 MHz Varian Inova, and 500 MHz Varian VNMRS spectrometers. ^1H and $^{13}C\{^1H\}$ NMR chemical shifts are reported in parts per million (δ) relative to TMS with the solvent as the internal reference. Coupling constants are reported in Hz and multiplicities are abbreviated as follows: s (singlet); d (doublet); t (triplet); sept (septet); br (broad); m (multiplet); dd (doublet of doublets); ddd (doublet of doublets of doublets); dt (douplet of triplets); td (triplet of doublets);

and dtd (doublet of triplets of doublets). High resolution mass spectra were taken using either electron ionization in a Kratos Analytical MS-50G or electrospray in an Agilent 6220 oaTOF. Elemental analyses were collected with a Carlo Erba EA1108 Elemental Analyzer.

Low temperature NMR studies were carried out in silanized (TMSCl) NMR tubes fitted with rubber septa under an atmosphere of N_2 unless stated otherwise. Acetonitrile-d_3 and THF-d_8 were freshly distilled over appropriate drying agents and used immediately for each experiment unless stated otherwise. KO^{t}Bu was sublimed at 120 °C under reduced pressure prior to use. ^{1}H and ^{13}C{^{1}H}NMR spectra were collected using a 400 MHz Varian Inova spectrometer. NMR peak assignments were made using ^{1}H-^{1}H gCOSY, ^{1}H-^{13}C gHSQC, and ^{1}H-^{13}C gHMBC 2D NMR experiments.

3.4.1 Preparation of 12 and 12(^{13}C)

1*H*-imidazo[4,5-*f*][1,10]phenanthroline (14) Inside a glovebox, 1.5 g of 1,10-phenanthroline-5,6-diamine (7.13 mmol, 1 equiv) was added to a 500 mL Schlenk flask. The flask was sealed, brought outside the glove box where 250 mL of dry MeOH and 24 mL of triethyl orthoformate (142 mmol, 20 equiv) was added to the flask via syringe. Under positive N_2 pressure 138.9 mg of sulfamic acid (1.4 mmol, 0.2 equiv.) was added to the mixture. Upon addition of the acid the mixture immediately turned a dark brown. After 18 hours of stirring at room temperature a pale-yellow precipitate was formed. In air, the precipitate was filtered, washed with cold MeOH and Et_2O and then dried under high vacuum for 1 h to yield the desired product as an off-white solid (1.34 g, 87%). Characterization data was consistent with previously reported literature values.[20]

1-isopropyl-1*H*-imidazo[4,5-*f*][1,10]phenanthroline (15) To a 250 mL round-bottom flask under dinitrogen atmosphere, 950 mg of **14** (4.3 mmol, 1 equiv) and 4.2 g of Cs_2CO_3 (13 mmol, 3 equiv) were suspended in 120 mL of dry MeCN. The suspension was stirred at room

temperature for 30 min then 2.25 mL of 2-propyliodide (21.5 mmol, 5 equiv) was added dropwise via syringe over 1 min. After stirring for 24 h at 85 °C the reaction mixture was concentrated under vacuum. The resulting residue was dissolved in DCM and filtered through a celite plug in air. The filtrate was concentrated under vacuum and the crude product was further purified by flash chromatography (9:1 DCM/MeOH) to afford the desired product as a dark brown solid (1.1 g, 96%).**^{1}H NMR** (599.928 MHz, CD_3OD): δ 1.71 (d, *J* = 6.6 Hz, 6H), 5.17 (sept, *J* = 6.6 Hz, 1H), 7.67 (dd, *J* = 8.4, 4.3 Hz, 1H), 7.70 (dd, *J* = 8.1, 4.3 Hz, 1H), 8.35 (s, 1H), 8.62 (dd, *J* = 8.5, 1.3 Hz, 1H), 8.76 (dd, *J* = 8.1, 1.7 Hz, 1H), 8.90 (dd, *J* = 4.3, 1.4 Hz, 1H), 8.92 (dd, *J* = 4.3, 1.7 Hz, 1H); **^{13}C{^{1}H} NMR** (150.869 MHz, CD_3OD) δ 21.9, 49.8, 119.7, 122.9, 123.4, 123.4, 123.5, 129.1, 129.8, 135.7, 139.5, 143.0, 143.4, 146.9, 147.8; **HRMS (ESI) m/z**: Calcd for $C_{16}H_{15}N_4$ $[M+H]^+$: 263.1291. Found: 263.1288.

1-benzyl-3-isopropyl-1*H*-imidazo[4,5-*f*][1,10]phenanthrolinium bromide (16) Adapted from a previously reported literature procedure.[6] To a 25 mL Schlenk flask under a N_2 atmosphere, 350 mg of **15** (1.3 mmol, 1 equiv) was suspended in 2 mL of benzyl bromide (17 mmol, 13 equiv). The solution was heated to 120 °C for 2h, during which the formation of a yellow precipitate appeared. Anhydrous DMF (3.5 mL) was added to the solution and further heated at 120 °C for 2 h resulting in the formation of a light-yellow precipitate. After cooling the suspension, the precipitate was filtered and then washed with an excess of Et_2O. The crude product was recrystalized from $PhCH_3$/MeOH to afford the desired product as an off-white solid (404 mg, 70%). **^{1}H NMR** (499.789 MHz, CD_3OD) δ 1.96 (d, *J* = 6.5 Hz, 6H), 5.81 (sept, *J* = 6.5 Hz, 1H), 6.35 (s, 2H), 7.33-7.42 (m, 5H), 7.75 (dd, *J* = 8.5, 4.4 Hz, 1H), 8.03 (dd, *J* = 8.6, 4.4 Hz, 1H), 8.74 (dd, *J* = 8.5, 1.2 Hz, 1H), 9.09 (dd, *J* = 4.3, 1.1 Hz, 1H), 9.16 (d, *J* = 8.6 Hz, 1H), 9.19 (dd, *J* = 4.3, 1.0 Hz, 1H), 10.09 (s, 1H); **^{13}C{^{1}H} NMR** (125.686 MHz, CD_3OD) δ 23.0,

54.8, 55.4, 119.1, 119.9, 125.4, 126.0, 127.1, 127.2, 127.5, 130.0, 130.7, 132.8, 134.5, 142.1, 145.7, 145.9, 151.3, 151.5; **HRMS (ESI)** ***m/z***: Calcd for $C_{23}H_{21}N_4$ [M]+: 353.1761. Found: 353.1760.

[Ru(dmbpy)$_2$(bpip)](PF$_6$)$_3$ (12) To a 100 mL Schlenk flask 50 mg of [Ru(dmbpy)$_2$(Cl)$_2$] (0.35 mmol, 1 equiv) and 52 mg of **16** (0.46 mmol, 1.3 equiv) were suspended in 10 mL of EtOH/H_2O (3:1 v/v) and refluxed under N_2 atmosphere for 24 h. The solvent was removed under vacuum and the residual solid was dissolved in a minimal amount of distilled water. The solution was heated to 50 °C and then an aqueous solution of NH_4PF_6 (596 mg, 3.5 mmol, 10 equiv) was added dropwise resulting in the appearance of a bright orange precipitate. The mixture was stirred for 30 min at 50 °C. The precipitate was filtered and washed with distilled H_2O (5 mL x3) and Et_2O (5 mL x3) to afford the desired product as a pale orange solid (80 mg, 68%). **^{1}H NMR** (499.789 MHz, CD_3CN): δ 1.88 (d, *J* = 6.5 Hz, 3H), 1.92 (d, *J* = 6.5 Hz, 3H), 2.48 (s, 3H), 2.49 (s, 3H), 2.57 (s, 3H), 2.59 (s, 3H), 5.69 (sept, *J* = 6.5 Hz, 1H), 6.20 (s, 2H), 7.06-7.08 (m, 2H), 7.29-7.35 (m, 4H), 7.41-7.46 (m, 5H), 7.60 (dd, *J* = 10.2, 5.7 Hz, 2H), 7.70 (dd, *J* = 8.3, 5.3 Hz, 1H), 7.93 (dd, *J* = 8.6, 5.4 Hz, 1H), 8.21 (d, *J* = 5.1 Hz, 1H), 8.30 (d, *J* = 5.1 Hz, 1H), 8.35 (s, 1H), 8.37 (s, 1H), 8.38 (s, 1H), 8.41 (s, 1H), 8.69 (d, *J* = 8.3 Hz, 1H), 9.07 (d, *J* = 8.3 Hz, 1H), 9.46 (s, 1H); **^{13}C{^{1}H} NMR** (125.686 MHz, CD_3CN): δ 20.2, 20.3, 20.3, 21.5, 53.7, 54.5, 120.4, 121.2, 124.9, 126.5, 126.7, 126.7, 126.9, 126.9, 128.0, 128.0, 128.3, 128.4, 129.1, 129.4, 130.4, 130.8, 132.1, 141.4, 147.7, 147.8, 150.5, 150.6, 150.7, 151.1, 152.9, 153.0, 156.4, 156.5; **HRMS (ESI)** ***m/z***: Calcd for $C_{47}H_{45}F_{12}N_8P_2{}^{102}Ru$ $[M]^+$: 1113.2089. Found: 1113.2094.

[Ru(bpy)$_2$(bpip)](PF$_6$)$_3$ (**17**) was prepared by following the procedure outlined for **12**; [Ru(bpy)$_2$(Cl)$_2$] (171 mg, 0.35 mmol, 1 equiv), **16** (200 mg, 0.46 mmol, 1.3 equiv), and NH_4PF_6 (596 mg, 3.5 mmol, 10 equiv). **17** was obtained as a bright orange solid (340 mg, 80 %). **^{1}H**

NMR (499.789 MHz, CD_3CN): δ 1.88 (d, *J* = 6.5 Hz, 3H), 1.92 (d, *J* = 6.5 Hz, 3H), 5.67 (sept. *J* = 6.68 Hz, 1H), 6.21 (s, 2H), 7.24-7.28 (m, 2H), 7.35-7.37 (m, 2H), 7.42-7.49 (m, 5H), 7.50-7.54 (m, 3H), 7.72 (dd, *J* = 8.5, 5.7 Hz, 1H), 7.80 (d, *J* = 5.7 Hz, 1H), 7.82 (d, *J* = 5.7 Hz, 1H), 7.95 (dd, *J* = 8.2, 5.3 Hz, 1H), 8.01-8.06 (m, 2H), 8.13 (dtd, *J* = 11.7, 7.9, 1.4 Hz, 2H), 8.21 (dd, *J* = 5.4, 1.0 Hz, 1H), 8.30 (dd, *J* = 5.3, 1.0 Hz, 1H), 8.50-8.58 (m, 4H), 8.72 (dd, *J* = 8.6, 1.0 Hz, 1H), 9.11 (d, *J* = 8.6 Hz, 1H), 9.47 (s, 1H); **^{13}C{^{1}H} NMR** (125.685 MHz, CD_3CN) δ 21.4, 21.5, 53.7, 54.5, 120.5, 121.3, 124.3, 124.4, 126.6, 126.7, 126.8, 126.9, 127.0, 127.4, 127.5, 127.6, 127.7, 129.1, 129.4, 130.8, 131.3, 132.0, 138.0, 138.0, 138.1, 138.1, 141.5, 147.4, 147.6, 151.8, 151.8, 151.9, 151.9, 153.1, 153.2. 156.9, 156.9; **HRMS (ESI) *m/z***: Calcd for $C_{43}H_{37}F_{12}N_8P_2{}^{102}Ru$ $[M]^+$: 1057.1463. Found: 1057.1461.; Calcd for $C_{43}H_{37}F_6N_8P^{102}Ru$ $[M]^{2+}$: 456.0908. Found: 456.0914.

1*H*-imidazo[4,5-*f*][1,10]phenanthroline-2-^{13}C (14(^{13}C)) Inside a glovebox, 587 mg of 1,10-phenanthroline-5,6-diamine (2.8 mmol, 1 equiv) was weighed into a 50 mL Schlenk flask. The flask was sealed, brought outside the glove box where 15 mL of dry methanol and 5 mL of 0.335 M (^{13}C)-triethyl orthoformate (3.4 mmol, 1.2 equiv) suspended in methanol was added to the flask via syringe. Under a cone of dinitrogen 54 mg of sulfamic acid (0.56 mmol, 0.2 equiv) was added to the mixture. Upon addition of sulfamic acid the mixture immediately turned dark brown. The mixture was refluxed under N_2 for 3 h. Reaction progress was monitored by ^{1}H NMR and upon completion an off-white precipitate was formed. In air, the precipitate was filtered, washed with cold methanol and diethyl ether and then dried under vacuum for 1 h to yield the desired product as an off-white solid (237 mg, 77%). **^{1}H NMR** (498.120 MHz, DMSO-d_6) δ ; 7.80 (dd, *J* = 4.03, 8.14 Hz, 2H), 8.44 (d, J^{H-C} = 208 Hz, 1H), 8.81 (br, 2H), 9.01 (dd, *J* = 4.03, 1.51 Hz, 2H); **^{13}C{^{1}H} NMR** (125.686 MHz, DMSO-d_6) δ 122.5, 139.1, 139.3, 139.5,

142.6, 146.9, 153.4; **HRMS (ESI) *m/z***: Calcd for $C_{12}{}^{13}CH_8N_4Na$ $[M+Na]^+$: 244.0675. Found: 244.0671.

1-isopropyl-1*H*-imidazo[4,5-*f*][1,10]phenanthroline-2-^{13}C (15(^{13}C)) was prepared following the procedure outlined for **15**; **14(^{13}C)** (250 mg, 1.14 mmol, 1 equiv), Cs_2CO_3 (1.1 g, 3.42 mmol, 3 equiv), 2-propyliodide (0.6 mL, 5.7 mmol, 5 equiv), MeCN (25 mL). **15(^{13}C)** was isolated obtained as a dark brown solid (263 mg, 88%). **^{1}H NMR** (498.120 MHz, CD_3OD): δ 1.77 (d, *J* = 6.6 Hz, 6H), 5.33 (sept, *J* = 6.6 Hz, 1H), 7.78 (ddd, *J* = 14.9, 8.3, 4.2 Hz, 2H), 8.45 (d, J^{H-C} = 208 Hz, 1H), 8.81 (dt, *J* = 8.3, 1.5 Hz, 1H), 8.87 (dt, *J* = 8.1, 1.6 Hz, 1H), 8.99 (td, *J* = 4.6, 1.7 Hz, 2H); **^{13}C{^{1}H} NMR** (150.869 MHz, MeOD): δ 21.9, 49.9, 123.1, 123.6, 129.4, 130.0, 139.7, 140.2, 142.0, 142.1, 147.0, 147.9, 154.1; **HRMS (ESI) *m/z***: Calcd for $C_{15}{}^{13}CH_{15}N_4$ $[M+H]^+$: 264.1325. Found: 264.1320.

1-benzyl-3-isopropyl-1*H*-imidazo[4,5-*f*][1,10]phenanthrolinium-2-^{13}C bromide (16(^{13}C)) was prepared by following the procedure outlined for **16**; **15(^{13}C)** (200 mg, 0.76 mmol, 1 equiv), benzyl bromide (1.2 mL, 10 mmol, 13 equiv), DMF (2 mL). **16(^{13}C)** was obtained as pale-yellow solid (208 mg, 64%). ^{1}H NMR (399.980 MHz, CD_3OD) δ 1.98 (d, J = 6.6 Hz, 6H), 5.89 (sept, *J* = 6.2 Hz, 1H), 6.43 (d, *J* = 5.5 Hz, 2H), 7.41 (m, 5H), 8.19 (dd, *J* = 8.4, 5.1 Hz, 1H), 8.47 (dd, *J* = 8.4, 5.1 Hz, 1H), 9.16 (dd, *J* = 8.6, 1.3 Hz, 1H), 9.32 (dd, *J* = 4.9, 1.2 Hz, 1H), 9.43 (dd, *J* = 5.0, 1.2 Hz, 1H), 9.65 (dd, *J* = 8.8, 1.2 Hz, 1H), 10.2 (d, J^{H-C} = 223 Hz, 1H); **^{13}C{^{1}H} NMR** (125.686 MHz, CD_3OD) δ 21.4, 53.5, 54.4, 119.2, 119.3, 120.1, 120.1, 125.8, 125.9, 126.0, 126.2, 126.6, 128.7, 129.3, 132.4, 135.6, 136.2, 138.5, 138.6, 141.6, 146.1, 147.4, 147.8; **HRMS (ESI) *m/z***: Calcd for $C_{22}{}^{13}CH_{21}N_4$ $[M]^+$: 354.1794. Found: 354.1794.

[Ru(dmbpy)$_2$(bpip-^{13}C)](PF$_6$)$_3$ (12(^{13}C)) was prepared by following the procedure outlined for **12**; $[Ru(dmbpy)_2(Cl)_2]$ (63 mg, 0.12 mmol, 1 equiv), **16(^{13}C)** (50 mg, 0.11 mmol, 0.98 equiv),

and NH_4PF_6 (207 mg, 1.2 mmol, 10 equiv). **12(13C)** was obtained as a pale orange solid (mg, %). **1H NMR** (498.120 MHz, CD_3CN) δ 1.86 (d, *J* = 6.3 Hz, 3H), 1.89 (d, *J* = 6.3 Hz, 3H), 2.47 (s, 3H), 2.48 (s, 3H), 2.55 (s, 3H), 2.57 (s, 3H), 5.64 (sept, *J* = 6.3 Hz, 1H), 6.18 (d, *J* = 5.0 Hz, 2H), 7.04 (m, 2H), 7.34-7.26 (m, 5H), 7.42 (m, 3H), 7.58 (dd, *J* = 10.4, 6.1 Hz, 2H), 7.68 (dd, *J* = 8.2, 5.3 Hz, 1H), 7.91 (dd, *J* = 8.4, 5.3, 1H), 8.18 (dd, *J* = 5.2, 1.1 Hz, 1H), 8.27 (dd, *J* = 5.4, 1.0 Hz, 1H), 8.36 (m, 4H), 8.67 (dd, *J* = 8.6, 1.1 Hz, 1H), 9.05 (dd, *J* = 8.8, 1.0 Hz, 1H), 9.44 (d, J^{H-C} = 223 Hz, 1H); **13C{1H} NMR** (100 MHz, Solv): δ 20.2, 20.3, 20.3, 21.5, 53.7, 54.5, 120.4, 121.2, 124.9, 126.5, 126.7, 126.9, 126.9, 128.0, 1228.0, 128.3, 128.3, 129.1, 129.4, 130.4, 130.8, 132.0, 138.8, 139.7, 140.6, 141.4, 142.0, 142.3, 143.2, 143.4, 146.4, 147.7, 147.8, 150.5, 150.6, 150.7, 150.7, 151.0, 151.1, 152.9, 153.0, 156.4, 156.5; **HRMS (ESI)** ***m/z***: Calcd for $C_{46}{}^{13}CH_{45}F_{12}N_8P_2{}^{102}Ru$ $[M]^+$: 1114.2122. Found: 1114.2108.

3.4.3 Low temperature NMR Studies

General Method

Inside a nitrogen filled glovebox, to separate NMR tubes was added **12(13C)** (0.015 mmol, 1 equiv, Tube A) and KHMDS/KO^{t}Bu (0.015 mmol, 1 equiv, Tube B). The tubes were sealed with a septum and removed from the glovebox. Approximately 0.4 mL of dry MeCN-d_3 was added to Tube A and 0.1 mL of THF-d_8 added to Tube B. ^1H, ^{13}C, and HSQC NMR spectra of **12(13C)** were recorded at -40 °C (See Figure 3-4, 3-5, 3-6). Both Tubes A and B were submerged in a -40 °C cooling bath for 5 min. After sufficient cooling, contents of Tube B were canula transferred dropwise over ~1 min into Tube A, followed by an additional 0.1 mL of THF-d_8 to quantitatively transfer the base. Immediately upon addition, Tube A was shaken for 1 s and then returned to the cooling bath to mix the contents while maintain the temperature of the solution at -40 °C. NMR spectra were recorded at -40 °C approximately 5 min after addition of base solution.

*Method A: Deprotonation of **12(^{13}C)** with KO^{t}Bu*

Followed the general procedure; **12(^{13}C)** (20 mg, 0.015 mmol, 1 equiv) and KO^{t}Bu (1.8 mg, 0.015 mmol, 1 equiv). NMR spectra recorded at -40 °C after ~5 min indicated **12(^{13}C)** had reacted with KO^{t}Bu. Saturation transfer experiments performed at -40 °C supported the formation of the bridging species **18** (See Figure 3-7).

*Method B: Deprotonation of **12(^{13}C)** with KHMDS*

Followed the general procedure; **12(^{13}C)** (10 mg, 0.008 mmol, 1 equiv), KHMDS (1.6 mg, 0.008 mmol, 1 equiv). NMR spectra recorded at -40 °C after ~5 min showed that **12(^{13}C)** had reacted with KHMDS. Saturation transfer experiments performed at -40 °C indicated formation of bridging species **18**. Additional KHMDS (0.47 mg, 0.0024 mmol, 0.3 equiv) was added via general procedure (0.1 mL of THF-d_8 to transfer). ^{1}H, ^{13}C and ^{1}H-^{13}C gHMBC NMR spectra at -40 °C showed that **12(^{13}C)** had successfully reacted with KHMDS to form **13** (Figures 3-8).

3.4.4 Selected NMR Spectra

The following ^{1}H and ^{13}C NMR are shown to corroborate the low temperature NMR experiments discussed in section 3.2.

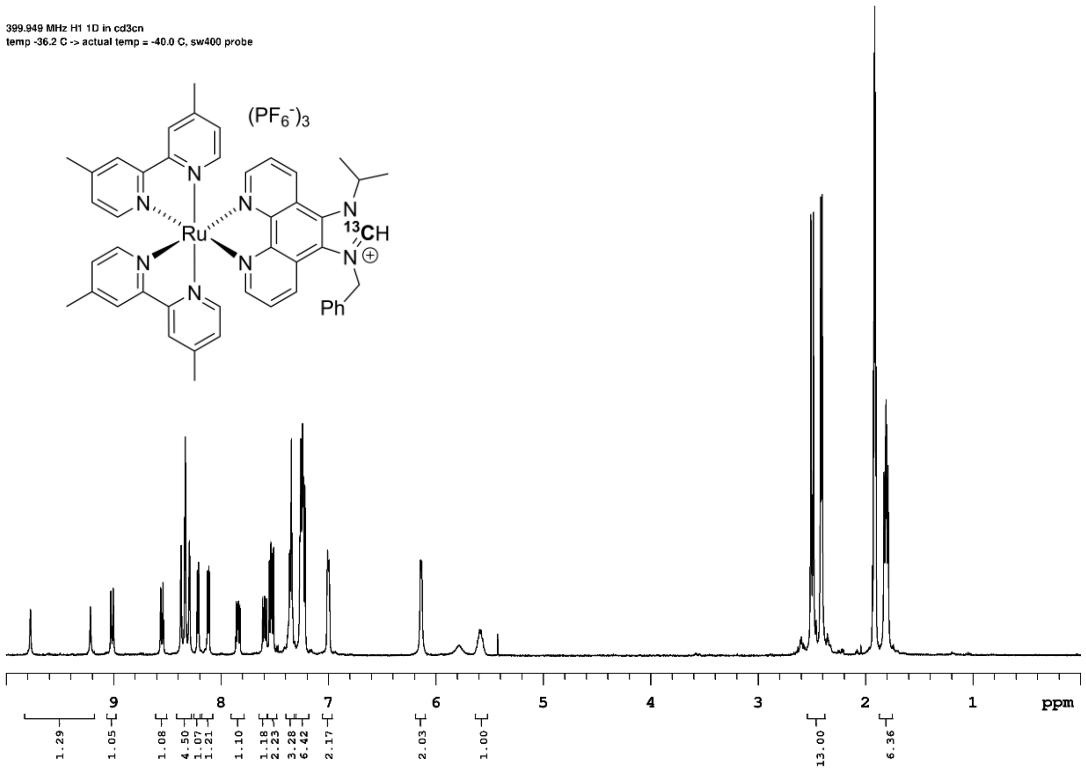

Figure 3-4. ^{1}H NMR spectrum of **12(**^{13}**C)** at -40 °C.

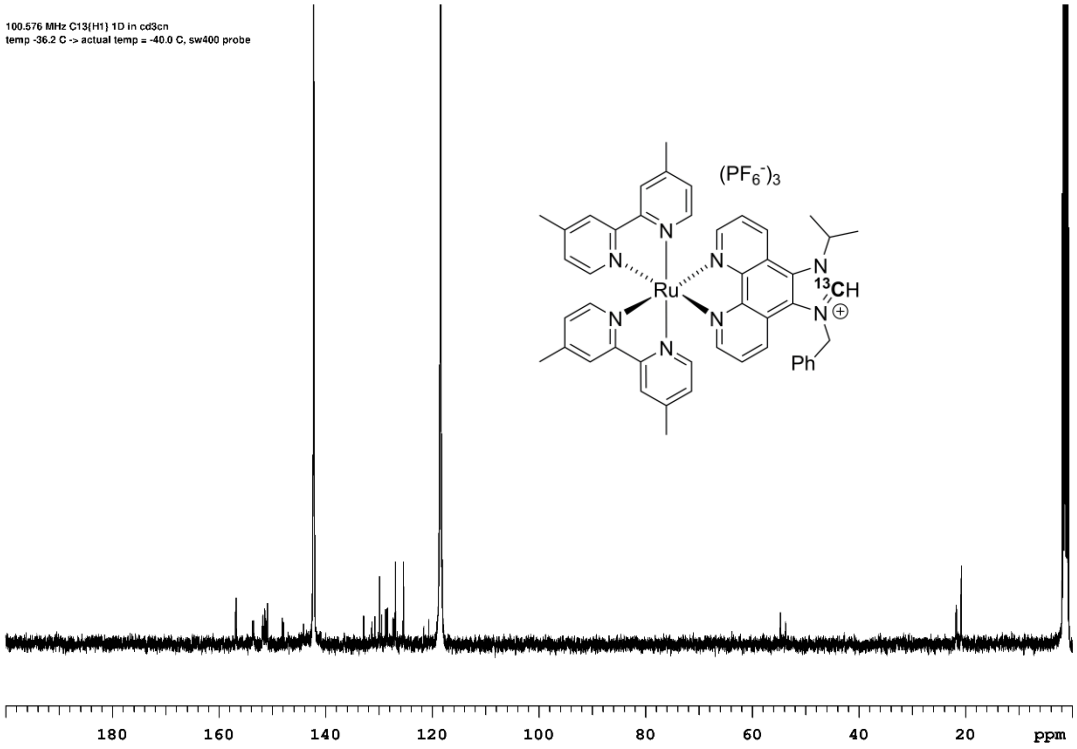

Figure 3-5. ^{13}C NMR spectrum of **12(**^{13}**C)** at -40 °C.

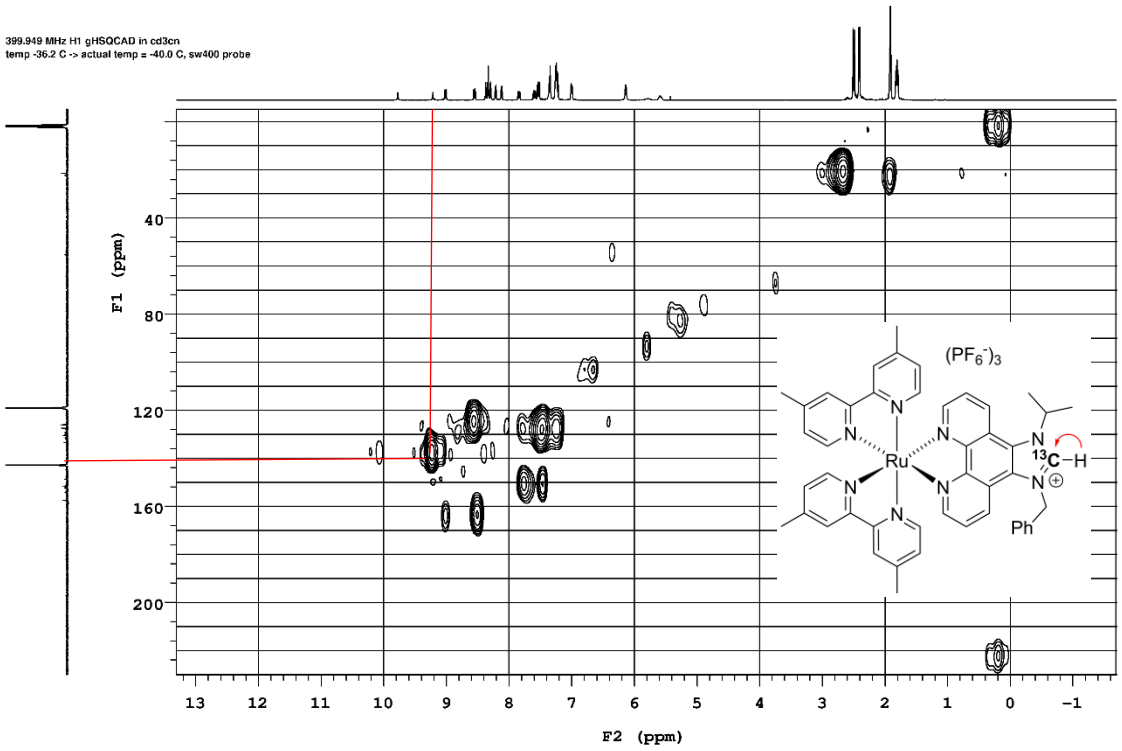

Figure 3-6. ^{1}H-^{13}C gHSQC of **12(^{13}C)** at -40 °C.

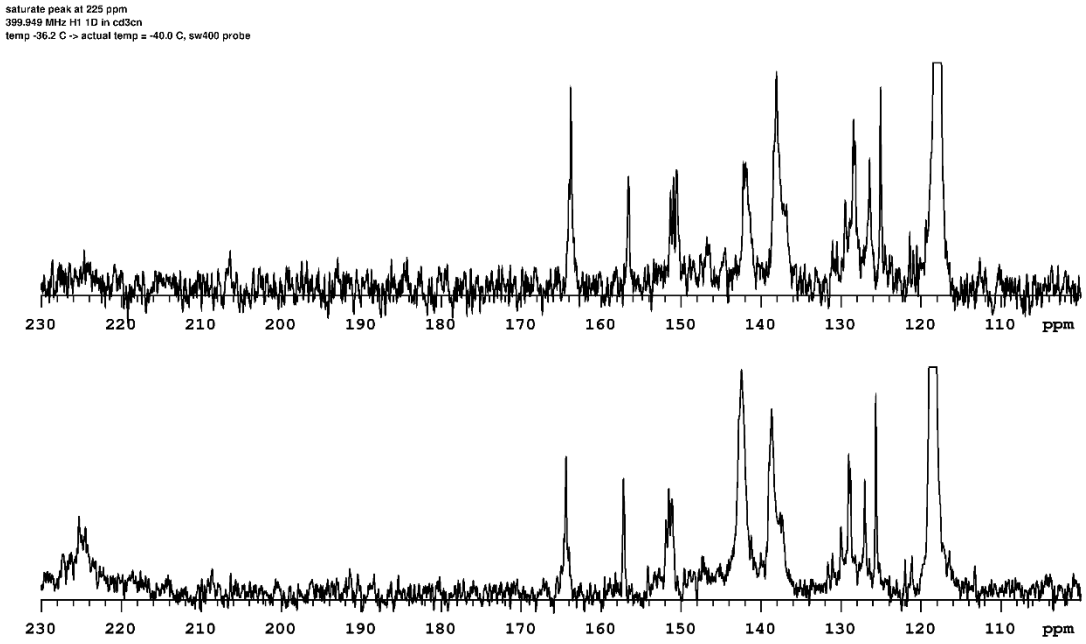

Figure 3-7. Spin saturation transfer experiment. Saturation of peak 225 ppm in ^{13}C after addition of KO^{t}Bu.

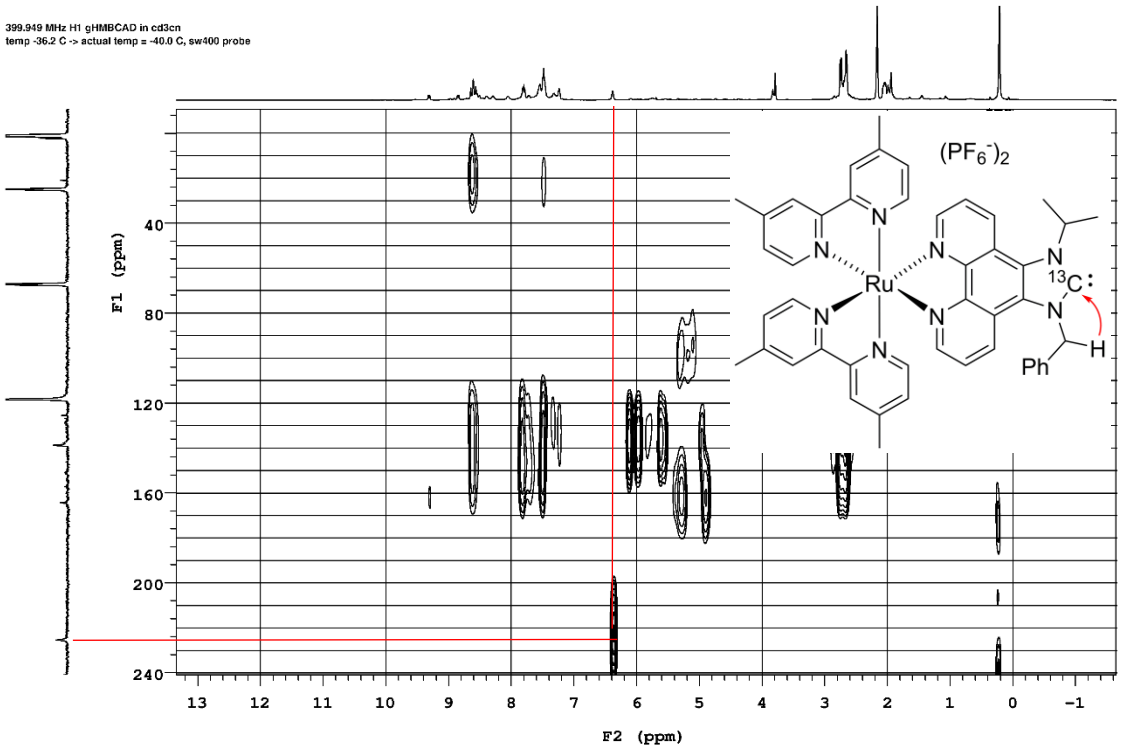

Figure 3-8. ^{1}H-^{13}C gHMBC depicting deprotonation of **12(^{13}C)** with KHMDS at -40 °C.

Chapter 4: Summary and Future Work

4.1 Chapter 1

Chapter 1 outlined the fundamentals of triplet-triplet energy transfer (EnT) and highlighted its recent applications in organic synthesis. Specifically, the use of a metal-polypyridyl complexes or organic dyes as a visible-light photosensitizers to facilitate [2+2] photocycloaddition was discussed and served as the underlying theme for this dissertation.

4.2 Chapter 2

In Chapter 2, introduction of $Sc(OTf)_3$ as Lewis acid enabled the low-cost organic photocatalyst 4CzIPN to facilitate [2+2] photocycloaddition between enolic β-diketones and styrenes (Section 2.2). Unfortunately, attempts to extend these results toward an enantioselective version by addition of a chiral ligand were unsuccessful (Section 2.3). In an attempt to trap the proposed cyclobutanol intermediate formed during photocycloaddition a β-ketoester was converted into a silyl enol ether (Section 2.5). Interestingly, selective Z → E photoisomerization of the silyl enol ether was observed instead of the desired cyclobutane formation (Section 2.5, Scheme 2-9). These results indicated that steric hindrance, introduced by the silyl protecting group (TBDMS), was inhibiting [2+2] photocycloaddition with styrene. Thus, future work will entail subjecting the less sterically hindered enol ether **1** under our standard conditions to generate cyclobutane **2** (Scheme 4-1). Preparation of **1** can be achieved in one step from a Michael addition between ynones and alcohols.[129] We suspect that **1** will be more tolerant to Lewis acids than was observed with the silyl enol ether (section 2.5, Scheme 2-10). Futhermore, the presence of a chiral Lewis acid could afford **2** enatioselectively. Finally, photoluminescence and ^{45}Sc NMR studies will be conducted to better understand the bonding interaction between $Sc(OTf)_3$ and β-diketones.

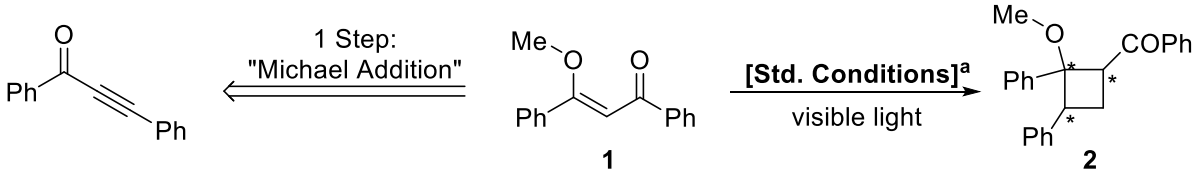

Scheme 4-1. Future work using enol ether **1** in the visible-light promoted De Mayo reaction; Standard conditions: 4CzIPN (4 mol%), $Sc(OTf)_3$ (10 mol%), chiral ligand (15 mol%), styrene (5 equiv.), PhMe [0.02M], blue LEDs, rt.

4.3 Chapter 3

In Chapter 3, synthesis of a photoactive Ru-polypyridyl-NHC species and attempts to characterize its corresponding free NHC was reported (Section 3.2). Low temperature NMR studies determined that the free NHC can be prepared with excess base, but it appears to be unstable at -40 °C (section 3.2, Figure 3-3). These results have been published in *Can J. Chem*.[130] In a new direction, the NHC derivative (**3**) of 4CzIPN has been prepared. Unlike the Ru-polypyridyl-NHC, NMR experiments have indicated the corresponding free NHC **4** is stable at room temperature.[131] As a result, coordination of **3** to a Pd-allyl species to give **5** was achieved (Scheme 4-2a).[132]

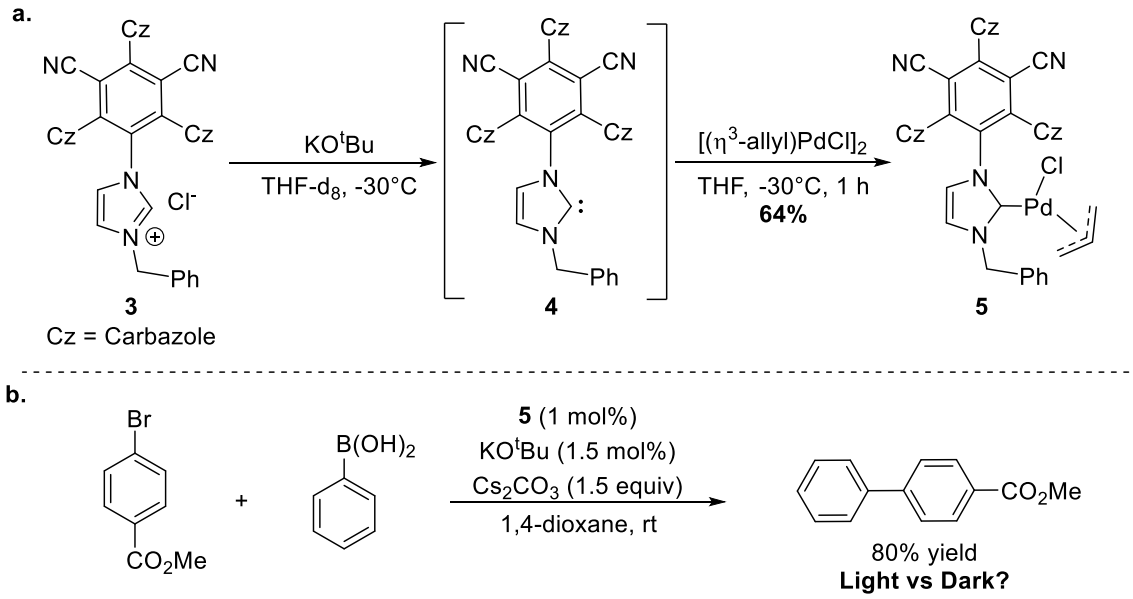

Scheme 4-2. (a) NHC derivative of 4CzIPN and its coordination to a Pd-ally species; (b) Deploying **5** in a preliminary Suzuki-Miyaura cross-coupling reaction.

Preliminary experiments indicated **5** to be a viable catalyst for Suzuki-Miyuara cross-coupling reactions (Scheme 4-2b). Future work will be directed toward obtaining a crystal structure of **5** and determining if the cross-coupling reaction is promoted by light.

References

1) U.S. Energy Information Administration - EIA - Independent Statistics and Analysis. https://www.eia.gov/todayinenergy/detail.php?id=41433# (accessed Feb 20, 2021).

2) IEA. World Energy Outlook 2020 – Analysis. https://www.iea.org/reports/world-energy-outlook-2020 (accessed Feb 20, 2021).

3) Our Energy Needs: World Energy Consumption & Demand. https://www.capp.ca/energy/world-energy-needs/ (accessed Feb 20, 2021).

4) IEA. Energy Technology Perspectives 2017 – Analysis. https://www.iea.org/reports/energy-technology-perspectives-2017 (accessed Feb 20, 2021).

5) Technology Roadmap - Energy and GHG Reductions in the Chemical Industry via Catalytic Processes. https://webstore.iea.org/technology-roadmap-energy-and-ghg-reductions-in-the-chemical-industry-via-catalytic-processes (accessed Feb 20, 2021).

6) Levi, P. G.; Cullen, J. M. *Environ. Sci. Technol.* **2018**, *52* (4), 1725–1734.

7) Nielsen, D. U.; Hu, X.-M.; Daasbjerg, K.; Skrydstrup, T. *Nature Catalysis* **2018**, *1* (4), 244–254.

8) Simmons, M. R.; *Twilight in the Desert*, John Wiley & Sons, Hoboken, NJ, 2005.

9) Olah, G. O.; Goepert, A.; Prakash, G. K. S.; *Beyond Oil and Gas: The Methanol Economy*, Wiley-VCH, Weinheim, 2006.

10) Lewis, N. S.; Nocera, D. G. *Proc. Natl. Acad. Sci.* **2006**, *103* (43), 15729–15735.

11) Morton, O. *Nature* **2006**, *443* (7107), 19–22.

12) Nocera, D. G. *Daedalus* **2006**, *135* (4), 112–115.

13) Lewis, N. S. *Science* **2007**, *315* (5813), 798–801.

14) Ciamician, G. *Science* **1912**, *36* (926), 385–394.

15) Balzani, V.; Credi, A. *ChemSusChem* **2008**, *1* (1-2), 26–58.

16) Kalyanasundaram, K.; Photochemistry of Polypyridine and Porphyrin Complexes (Academic Press, London, 1992).

17) Balzani, V.; Credi, A.; *ChemSusChem* **2008**, *1* (1-2), 26–58.

18) Nocera, D. G. *Acc. Chem. Res.* **2017**, *50* (3), 616–619.

19) Protti, S.; Manzini, S.; Fagnoni, M.; Albini, A. *Green Chem.* **2009**, *2* (7), 80–111.

20) Esser, P.; Pohlmann, B.; Scharf, H.-D. *Angew. Chem. Int. Ed. Engl.* **1994**, *33* (20), 2009–2023.

21) Bach, T.; Hehn, J. P. *Angew. Chem. Int. Ed.* **2011**, *50* (5), 1000–1045.

22) Hoffmann, N. *Chem. Rev.* **2008**, *108* (3), 1052–1103.

23) Thekaekara, M. P. *Sol. Energy* **1976**, *18* (4), 309–325.

24) Oelgemöller, M.; Jung, C.; Mattay, J. *Pure Appl. Chem.* **2007**, *79* (11), 1939–1947.

25) Gensch, T.; Teders, M.; Glorius, F. *J. Org. Chem.* **2017**, *82* (17), 9154–9159.

26) Yoon, T. P.; Ischay, M. A.; Du, J. *Nat. Chem.* **2010**, *2* (7), 527–532.

27) Schultz, D. M.; Yoon, T. P. *Science* **2014**, *343* (6174), 1239176-1-1239176-8.

28) Narayanam, J. M.; Stephenson, C. R. *Chem. Soc. Rev.* **2011**, *40* (1), 102–113.

29) Prier, C. K.; Rankic, D. A.; MacMillan, D. W. *Chem. Rev.* **2013**, *113* (7), 5322–5363.

30) Shaw, M. H.; Twilton, J.; MacMillan, D. W. *J. Org. Chem.* **2016**, *81* (16), 6898–6926.

31) Pirtsch, M.; Paria, S.; Matsuno, T.; Isobe, H.; Reiser, O. *Chem. Eur. J.* **2012**, *18* (24), 7336–7340.

32) Kainz, Q. M.; Matier, C. D.; Bartoszewicz, A.; Zultanski, S. L.; Peters, J. C.; Fu, G. C. *Science* **2016**, *351* (6274), 681–684.

33) Hernandez-Perez, A. C.; Collins, S. K. *Acc. Chem. Res.* **2016**, *49* (8), 1557–1565.

34) Revol, G.; McCallum, T.; Morin, M.; Gagosz, F.; Barriault, L. *Angew. Chem. Int. Ed.* **2013**, *52* (50), 13342–13345.

35) Meyer, T. J. *Acc. Chem. Rese.* **1989**, *22* (5), 163–170.

36) Takeda, H.; Ishitani, O. *Coord. Chem. Rev.* **2010**, *254* (3-4), 346–354.

37) Kalyanasundaram, K. *Coord. Chem. Rev.* **1998**, *177* (1), 347–414.

38) Ulbricht, C.; Beyer, B.; Friebe, C.; Winter, A.; Schubert, U. S. *Adv. Mater.* **2009**, *21* (44), 4418–4441.

39) Fors, B. P.; Hawker, C. J. *Angew. Chem. Int. Ed.* **2012**, *51* (35), 8850–8853.

40) Howerton, B. S.; Heidary, D. K.; Glazer, E. C. *J. Am. Chem. Soc.* **2012**, *134* (20), 8324–8327.

41) Kalyanasundaram, K. *Coord. Chem. Rev.* **1982**, *46 (2)*, 159–244.

42) Juris, A.; Balzani, V.; Barigelletti, F.; Campagna, S.; Belser, P.; von Zelewsky, A. *Coord. Chem. Rev.* **1988**, *84 (7)*, 85–277.

43) Juris, A.; Balzani, V.; Belser, P.; von Zelewsky, A. *Helv. Chim. Acta* **1981**, *64* (7), 2175–2182.

44) Tucker, J. W.; Stephenson, C. R. *J. Org. Chem.* **2012**, *77* (4), 1617–1622.

45) Romero, N. A.; Nicewicz, D. A. *Chem. Rev.* **2016**, *116* (17), 10075–10166.

46) Campagna, S.; Puntoriero, F.; Nastasi, F.; Bergamini, G.; Balzani, V. *Photochemistry and Photophysics of Coordination Compounds I* 117–214.

47) McCusker, J. K. *Acc. Chem. Res.* **2003**, *36* (12), 876–887.

48) Bock, C. R.; Connor, J. A.; Gutierrez, A. R.; Meyer, T. J.; Whitten, D. G.; Sullivan, B. P.; Nagle, J. K. *J. Am. Chem. Soc.* **1979**, *101* (17), 4815–4824.

49) Pavlishchuk, V. V.; Addison, A. W. *Inorg. Chim. Acta* **2000**, *298* (1), 97–102.

50) Lu, Z.; Yoon, T. P. *Angew. Chem. Int. Ed.* **2012**, *51* (41), 10329–10332.

51) Strieth-Kalthoff, F.; James, M. J.; Teders, M.; Pitzer, L.; Glorius, F. *Chem. Soc. Rev.* **2018**, *47* (19), 7190–7202.

52) Zhou, Q. Q.; Zou, Y. Q.; Lu, L. Q.; Xiao, W. J. *Angew. Chem. Int. Ed.* **2018**, *58* (6), 1586–1604.

53) Förster, T. *Ann. Phys.* **1948**, *437* (1-2), 55–75.

54) Dexter, D. L. *J. Chem. Phys.* **1953**, *21* (5), 836–850.

55) Turro, N. J.; Ramamurthy, V.; Scaiano, J. C. *Photochem. Photobiol.* **2012**, *88* (4), 1033–1033.

56) Turro, N. J. *J. Chem. Educ.* **1966**, *43* (1), 13-17.

57) Dilling, W. L. *Chem. Rev.* **1969**, *69* (6), 845–877.

58) Albini, A. *Synthesis* **1981**, (4), 249–264.

59) Wigner E., *Nachr. Akad. Wiss. Goettingen, Math.–Phys. Kl*. **1927**, 375–381.

60) Birks, J. B.; *Nature* **1967**, *214* (5094), 1187–1190.

61) Balzani, V.; Ceroni, P.; Juris, A.; *Photochemistry and Photophysics: Concepts, Research, Applications*, Wiley-VCH, Weinheim, **2014**.

62) Herkstroeter, W. G.; Jones, L. B.; Hammond, G. S. *J. Am. Chem. Soc.* **1966**, *88* (21), 4777–4780.

63) Marcus, R. A. *Rev. Mod. Phys.* **1993**, *65* (3), 599–610.

64) Murov, S. L.; Charmichael, I.; Hug, G. L.; Handbook of Photochemistry, Marcel Dekker Inc., New York, **1993.**

65) Singh, A.; Fennell, C. J.; Weaver, J. D. *Chem. Sci.* **2016**, *7* (11), 6796–6802.

66) Peach, M. J.; Benfield, P.; Helgaker, T.; Tozer, D. J. *J. Chem. Phys.* **2008**, *128* (4), 044118.

67) Tamayo, A. B.; Alleyne, B. D.; Djurovich, P. I.; Lamansky, S.; Tsyba, I.; Ho, N. N.; Bau, R.; Thompson, M. E. *J. Am. Chem. Soc.* **2003**, *125* (24), 7377–7387.

68) Slinker, J. D.; Gorodetsky, A. A.; Lowry, M. S.; Wang, J.; Parker, S.; Rohl, R.; Bernhard, S.; Malliaras, G. G. *J. Am. Chem. Soc.* **2004**, *126* (9), 2763–2767.

69) Lowry, M. S.; Goldsmith, J. I.; Slinker, J. D.; Rohl, R.; Pascal, R. A.; Malliaras, G. G.; Bernhard, S. *Chem. Mater.* **2005**, *17* (23), 5712–5719.

70) Bach, T.; Hehn, J. P. *Angew. Chem. Int. Ed.* **2011**, *50* (5), 1000–1045.

71) Inoue, Y. *Chem. Rev.* **1992**, *92* (5), 741–770.

72) Poplata, S.; Tröster, A.; Zou, Y.-Q.; Bach, T. *Chem. Rev.* **2016**, *116* (17), 9748–9815.

73) Wu, Q.-A.; Chen, F.; Ren, C.-C.; Liu, X.-F.; Chen, H.; Xu, L.-X.; Yu, X.-C.; Luo, S.-P. *Org. Biomol. Chem.* **2020**, *18* (19), 3707–3716.

74) Helms, A. M.; Caldwell, R. A. *J. Am. Chem. Soc.* **1995**, *117* (1), 358–361.

75) Takahashi, Y.; Ando, M.; Miyashi, T. *J. Chem. Soc., Chem. Commun.* **1995**, 5, 521-522.

76) Ikezawa, H.; Kutal, C.; Yasufuku, K.; Yamazaki, H. *J. Am. Chem. Soc.* **1986**, *108* (7), 1589–1594.

77) Lu, Z.; Yoon, T. P. *Angew. Chem. Int. Ed.* **2012**, *51* (41), 10329–10332.

78) Ischay, M. A.; Lu, Z.; Yoon, T. P. *J. Am. Chem. Soc.* **2010**, *132* (25), 8572–8574.

79) Mojr, V.; Svobodová, E.; Straková, K.; Neveselý, T.; Chudoba, J.; Dvořáková, H.; Cibulka, R. *Chem. Commun.* **2015**, *51* (60), 12036–12039.

80) Jirásek, M.; Straková, K.; Neveselý, T.; Svobodová, E.; Rottnerová, Z.; Cibulka, R. *Eur. J. Org. Chem.* **2017**, 15, 2139–2146.

81) Hurtley, A. E.; Lu, Z.; Yoon, T. P. *Angew. Chem. Int. Ed.* **2014**, *53* (34), 8991–8994.

82) Lei, T.; Zhou, C.; Huang, M.-Y.; Zhao, L.-M.; Yang, B.; Ye, C.; Xiao, H.; Meng, Q.-Y.; Ramamurthy, V.; Tung, C.-H.; Wu, L.-Z. *Angew. Chem. Int. Ed.* **2017**, *56* (48), 15407–15410.

83) Wang, C.; Lu, Z. *Org. Lett.* **2017**, *19* (21), 5888–5891.

84) Blum, T. R.; Miller, Z. D.; Bates, D. M.; Guzei, I. A.; Yoon, T. P. *Science* **2016**, *354* (6318), 1391–1395.

85) Miller, Z. D.; Lee, B. J.; Yoon, T. P. *Angew. Chem. Int. Ed.* **2017**, *129* (39), 12053–12057.

86) Huang, X.; Quinn, T. R.; Harms, K.; Webster, R. D.; Zhang, L.; Wiest, O.; Meggers, E. *J. Am. Chem. Soc.* **2017**, *139* (27), 9120–9123.

87) Müller, C.; Bauer, A.; Bach, T. *Angew. Chem. Int. Ed.* **2009**, *48* (36), 6640–6642.

88) Alonso, R.; Bach, T. *Angew. Chem. Int. Ed.* **2014**, *53* (17), 4368–4371.

89) Tröster, A.; Alonso, R.; Bauer, A.; Bach, T. *J. Am. Chem. Soc.* **2016**, *138* (25), 7808–7811.

90) Farney, E. P.; Yoon, T. P. *Angew. Chem. Int. Ed.* **2013**, *53* (3), 793–797.

91) Nicewicz, D. A.; MacMillan, D. W. *Science* **2008**, *322* (5898), 77–80.

92) Ischay, M. A.; Anzovino, M. E.; Du, J.; Yoon, T. P. *J. Am. Chem. Soc.* **2008**, *130* (39), 12886–12887.

93) Uoyama, H.; Goushi, K.; Shizu, K.; Nomura, H.; Adachi, C. *Nature* **2012**, *492* (7428), 234–238.

94) Romero, N. A.; Nicewicz, D. A. *Chem. Rev.* **2016**, *116* (17), 10075–10166.

95) Xu, W.; Dai, X.; Xu, H.; Weng, J. *Chin. J. Org. Chem.* **2018**, *38* (11), 2807.

96) Luo, J.; Zhang, J. *ACS Catal.* **2020**, *10* (23), 14302–14303.

97) Shang, T.-Y.; Lu, L.-H.; Cao, Z.; Liu, Y.; He, W.-M.; Yu, B. *Chem. Comm.* **2019**, *55* (38), 5408–5419.

98) Yokoyama, M.; Inada, K.; Tsuchiya, Y.; Nakanotani, H.; Adachi, C. *Chem. Comm.* **2018**, *54* (59), 8261–8264.

99) Lu, J.; Pattengale, B.; Liu, Q.; Yang, S.; Shi, W.; Li, S.; Huang, J.; Zhang, J. *J. Am. Chem. Soc.* **2018**, *140* (42), 13719–13725.

100) Speckmeier, E.; Fischer, T. G.; Zeitler, K. *J. Am. Chem. Soc.* **2018**, *140* (45), 15353–15365.

101) Mayo, P. D.; Takeshita. *Can. J. Chem.* **1963**, *41* (2), 440–449.

102) Winkler, J. D.; Rouse, M. B.; Greaney, M. F.; Harrison, S. J.; Jeon, Y. T. *J. Am. Chem. Soc.* **2002**, *124* (33), 9726–9728.

103) Winkler, J. D.; Scott, R. D.; Williard, P. G. *J. Am. Chem. Soc.* **1990**, *112* (24), 8971–8975.

104) Martinez-Haya, R.; Marzo, L.; König, B. *Chem. Comm.* **2018**, *54* (82), 11602–11605.

105) Kikuchi, A.; Oguchi, N.; Yagi, M. *J. Phys. Chem. A.* **2009**, *113* (48), 13492–13497.

106) Hanss, D.; Freys, J. C.; Bernardinelli, G.; Wenger, O. S. *Eur. J. Inorg. Chem.* **2009**, *2009* (32), 4850–4859.

107) Flamigni, L.; Ventura, B.; Tasior, M.; Gryko, D. T. *Inorg. Chim. Acta.* **2007**, *360* (3), 803–813.

108) Fukuzumi, S.; Ohkubo, K. *Org. Biomol. Chem.* **2014**, *12* (32), 6059–6071.

109) Luo, J.; Zhang, J. *ACS Catal.* **2016**, *6* (2), 873–877.

110) Lewis, F. D.; Barancyk, S. V. *J. Am. Chem. Soc.* **1989**, *111* (23), 8653–8661.

111) Lewis, F. D.; Howard, D. K.; Oxman, J. D. *J. Am. Chem. Soc.* **1983**, *105* (10), 3344–3345.

112) Evans, D. A.; Fandrick, K. R.; Song, H.-J. *J. Am. Chem. Soc.* **2005**, *127* (25), 8942–8943.

113) Evans, D. A.; Aye, Y. *J. Am. Chem. Soc.* **2006**, *128* (34), 11034–11035.

114) Nakane, S.; Yoshinaka, S.; Iwase, S.; Shuto, Y.; Bunse, P.; Wünsch, B.; Tanaka, S.; Kitamura, M. *Tetrahedron* **2018**, *74* (38), 5069–5084.

115) Metternich, J. B.; Gilmour, R. *J. Am. Chem. Soc.* **2015**, *137* (35), 11254–11257.

116) Metternich, J. B.; Gilmour, R. *J. Am. Chem. Soc.* **2016**, *138* (3), 1040–1045.

117) Rasu, L.; Amiri, M.; Bergens, S. H. *ACS Appl. Mater. & Inter.* **2021**, *13* (15), 17745–17752.

118) Inagaki, A.; Akita, M. *Coord. Chem. Rev.* **2010**, *254* (11-12), 1220–1239.

119) Osawa, M.; Hoshino, M.; Wakatsuki, Y. *Angew. Chem., Int. Ed.* **2001**, *40* (18), 3472–3474.

120) Inagaki, A.; Edure, S.; Yatsuda, S.; Akita, M. *Chem. Comm.* **2005**, 43, 5468-5470.

121) Inagaki, A.; Yatsuda, S.; Edure, S.; Suzuki, A.; Takahashi, T.; Akita, M. *Inorg. Chem.* **2007**, *46* (7), 2432–2445.

122) Inagaki, A.; Nakagawa, H.; Akita, M.; Inoue, K.; Sakai, M.; Fujii, M. *Dalton Trans.* **2008**, 47, 6709-6723.

123) Osawa, M.; Nagai, H.; Akita, M. *Dalton Trans.* **2007**, 8, 827-829.

124) Peuntinger, K.; Pilz, T. D.; Staehle, R.; Schaub, M.; Kaufhold, S.; Petermann, L.; Wunderlin, M.; Görls, H.; Heinemann, F. W.; Li, J.; Drewello, T.; Vos, J. G.; Guldi, D. M.; Rau, S. *Dalton Trans.* **2014**, *43* (36), 13683-13695.

125) Crudden, C. M.; Horton, J. H.; Ebralidze, I. I.; Zenkina, O. V.; McLean, A. B.;Drevniok, B.; She, Z.; Kraatz, H.-B.; Mosey, N. J.; Seki, T.; Keske, E. C.; Leake, J. D.; Rousina-Webb, A.; Wu, G. *Nat. Chem.* **2014**, *6* (5), 409-414.

126) Tapu, D.; Dixon, D. A.; Roe, C. *Chem. Rev.* **2009**, *109* (8), 3385-3407.

127) Arduengo, A. J., III; Gamper, S. F.; Tamm, M.; Calabrese, J. C.; Davidson, F.; Craig, H. A. *J. Am. Chem. Soc.* **1995**, *117* (1), 572-573.

128) Ashford, D. L.; Brennaman, M. K.; Brown, R. J.; Keinan, S.; Concepcion, J. J.; Papanikolas, J. M.; Templeton, J. L.; Meyer, T. J. *Inorg. Chem.* **2015**, *54* (2), 460-469.

129) Li, Z.; He, J.; Chen, X.; Cheng, Y.; Yang, J. *Tetrahedron* **2018**, *74* (45), 6612–6619.

130) Pearson, J. W.; Endean, R. T.; Rasu, L.; Bergens, S. H. *Can. J. Chem.* **2021**, *99* (2), 230–235.

131) Unpublished results by Dr. Loorthuraja Rasu

132) Unpublished results by J. Pearson